12-2011

Pitch-Based Activated Carbon Fibers: The Effect of Precursor Composition on Pore Structure

Halil Tekinalp
Clemson University, ltekinalp@hotmail.com

Follow this and additional works at: https://tigerprints.clemson.edu/all_dissertations

 Part of the Chemical Engineering Commons

PITCH-BASED ACTIVATED CARBON FIBERS:
THE EFFECT OF PRECURSOR COMPOSITION ON PORE STRUCTURE

A Dissertation
Presented to
the Graduate School of
Clemson University

In Partial Fulfillment
of the Requirements for the Degree
Doctor of Philosophy
Chemical Engineering

---

by
Halil Levent Tekinalp
December 2011

Accepted by:
Dr. Mark C. Thies, Committee Chair
Dr. Dan D. Edie
Dr. David A. Bruce
Dr. Christopher L. Kitchens
Dr. Gary C. Lickfield

ABSTRACT

Although researchers have previously investigated the effect of precursor differences on the final properties of activated carbon fibers (ACFs), those precursors were not well-characterized. In particular, detailed information about their molecular composition and anisotropy was not available.

In this study, seven oligomeric fractions, each of well-defined composition and molecular weight (mol wt) distribution, were isolated from a commercially produced isotropic petroleum pitch (i.e., Marathon M-50) and used for the production of ACFs. Four of these precursors of varying oligomeric composition were fully isotropic and three contained different levels of mesophase, so that the effects of molecular composition and molecular order were successfully isolated from each other. After the precursors were melt-spun into fibers and stabilized, they were processed by so-called "direct activation", whereby carbonization and activation occurred simultaneously. Separate carbonization tests were also carried out in order to separate out the effects of carbonization vs. activation.

Carbonization weight loss was found to be higher for fibers prepared from lower average mol wt (480-550 Da) precursors. The presence of mesophase per se did not affect weight loss during carbonization. On the other hand, activation weight loss (~28%) was found to be essentially independent of precursor mol wt for all isotropic fibers. (Activation weight loss for mesophase-containing fibers was much lower.)

The micropore volume of the ACFs was found to increase with decreasing precursor mol wt. However, the ratio of pores smaller than 7 Å (i.e., the desired pore size for hydrogen storage) to the total pore volume (3.9-30 Å) was found to be essentially constant for all isotropic precursors, suggesting that a similar activation mechanism occurred for all of these materials, with both new pore formation and pore widening proceeding at similar rates. For mesophase-containing precursors, on the other hand, this pore volume ratio significantly decreased with increasing mesophase content, indicating that pore widening dominates over new pore formation for this morphology.

In conclusion, this study showed that the lowest mol wt precursor (i.e., a 99% dimer cut with a mol wt of 480 Da) attained the highest narrow micropore (<7 Å) volume required for hydrogen storage.

DEDICATION

I dedicate this work to my parents, Suleyman Tekinalp and Iclal Tekinalp, and my sister, Demet Tekinalp Kaplan.

ACKNOWLEDGMENTS

TABLE OF CONTENTS

Table of Contents (Continued)

Table of Contents (Continued)

Table of Contents (Continued)

Table of Contents (Continued)

LIST OF TABLES

LIST OF FIGURES

List of Figures (Continued)

List of Figures (Continued)

List of Figures (Continued)

Figure

List of Figures (Continued)

List of Figures (Continued)

List of Figures (Continued)

Figure

1 INTRODUCTION

1.1 Carbon Materials

Carbon is the basic element that constitutes all organic matter and is the fourth most abundant element in the solar system (Pierson, 1993). On earth, it is mostly found in compounds in bituminous and anthracite coals, hydrocarbons (such as petroleum, asphalt, and tar), and gaseous hydrocarbons (such as methane). Also, natural graphite and diamond are two allotropes of carbon that are present on earth as minerals (Pierson, 1993).

1.1.1 The Element Carbon and its Allotropes

Carbon has an atomic number of 6, and its electron configuration enables carbon to form different types of hybrid bonding, including sp^1, sp^2, and sp^3. Carbon can form linear, ring-shaped, and 3-dimensional (tetrahedral like in diamond) molecules (**Fig. 1.1a**). Depending on the chemical nature, structure, and arrangements of these molecules, a material has different bulk properties. While amorphous carbon, graphite, and diamond are among the better-known and more common allotropes of carbon, there are other allotropes such as fullerenes (buckyballs, carbon nanotubes, etc.), lonsdaleite, and glassy carbon.

A single sheet of graphite is called graphene (Rand et al., 1998). The most ordered sp^2 type of carbon is single-crystal graphite. In perfect stacking the distance between graphene sheets of graphite is 0.3354 nm (**Fig. 1.1b**). While graphite is the most

1
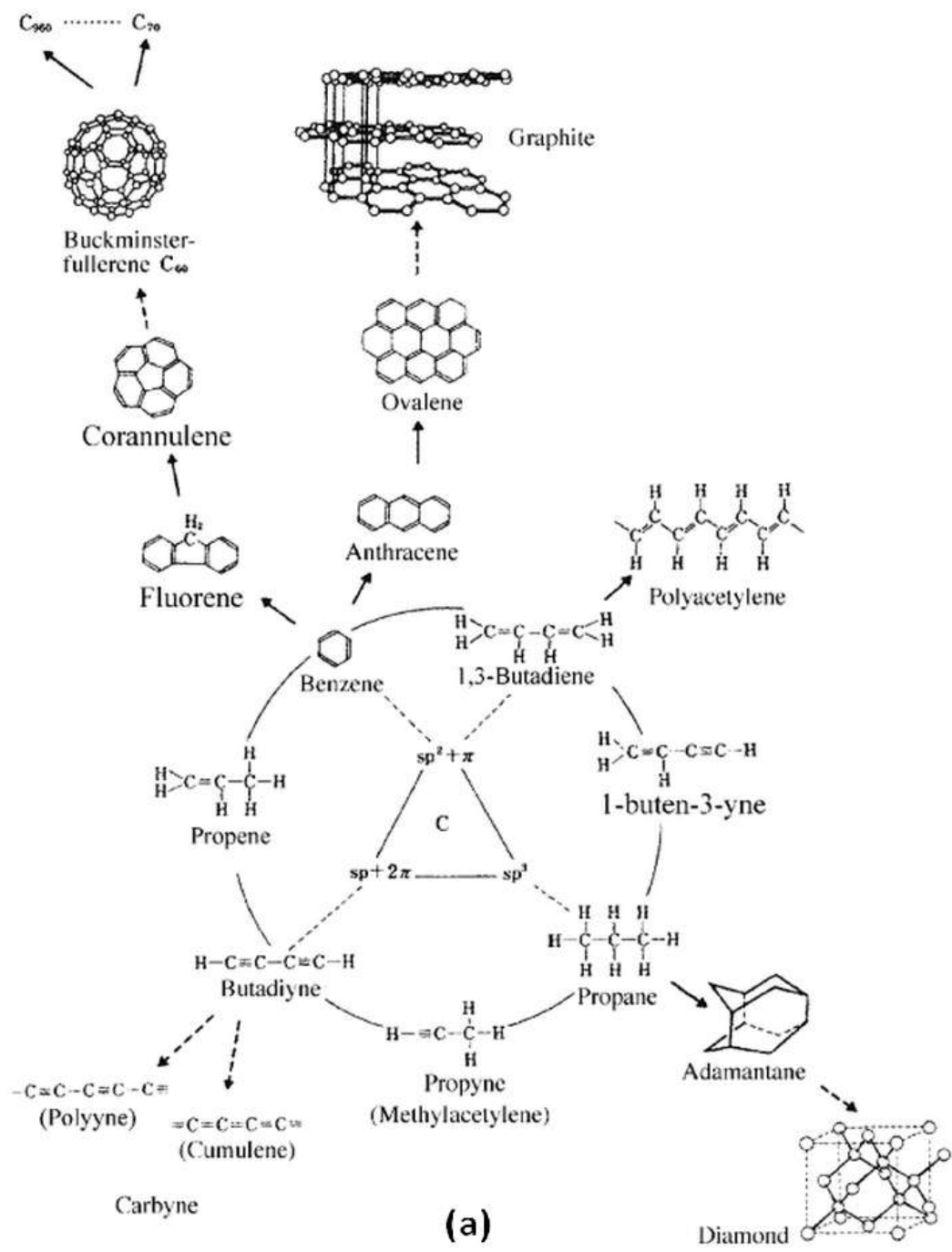
Fig. 1.1 The element Carbon: (a) sp^1, sp^2, and sp^3 hybrid bonding and carbon materials (Reprinted from Yasuda et al, 2003. Copyright 2003 Elsevier. Permission requested); (b) the structure of graphite (Reprinted with permission from Marsh and Reinoso, 2006. Copyright 2006 Elsevier).

Graphene layers

C-axis

Basal plane

Edge plane

B

0.3354 nm

A

0.142 nm

0.246 nm

Outline of unit cell

(b)
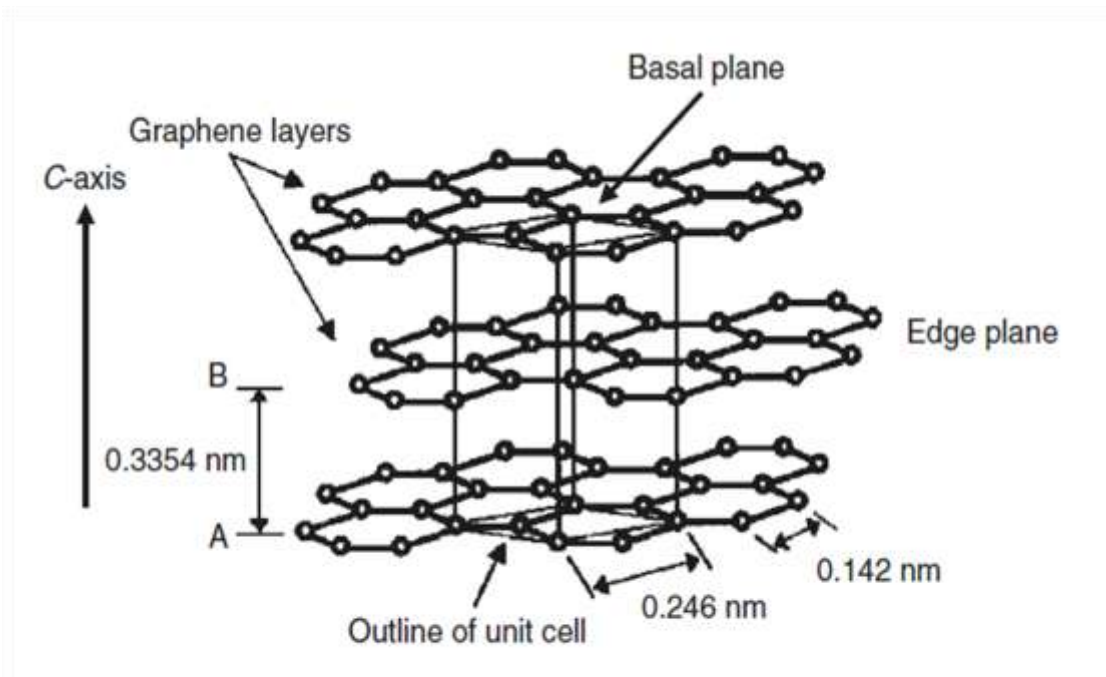
Fig. 1.1 (Contonued).

ordered sp^2-type carbon, amorphous carbons are also composed of sp^2-type bonded molecules without any significant structural order, caused by the existence of crystalline defects, curvatures, and heteroatoms, i.e., atoms other than C, such as O, H, N, and S. Examples of such amorphous carbons include coal, anthracite, pitch, and lignite. When there is no structural order that can be detected by X-ray diffraction, a carbon material is considered to be isotropic. It is important to understand that these materials are not totally disorganized, but disordered. To explain this concept better, consider the structural models for graphitizable vs. non-graphitizable carbons as proposed by Franklin in 1950 and 1951 (Marsh and Reinoso, 2006). **Fig 1.2** shows the arrangement of the graphene

layers based on her model, in which non-graphitizable (isotropic) carbon is composed of short graphene layers, with not all being parallel to each other as is the case with graphitizable carbons.

Although materials close to a perfect graphite structure are achievable, they can be obtained only with a heat treatment process above 2000 ˚C, and not all carbon materials will graphitize upon high-temperature heat treatment. It is the movement of single atoms that causes graphitization, and not the bulk movement.

Depending on the chemical nature and structure, carbon materials can be used to produce all kinds of different products, such as high thermal conductivity carbons (Beauharnois et al., 2001), and activated carbons (Derbyshire et al., 2001). Among these, activated carbons are the focus of this dissertation.
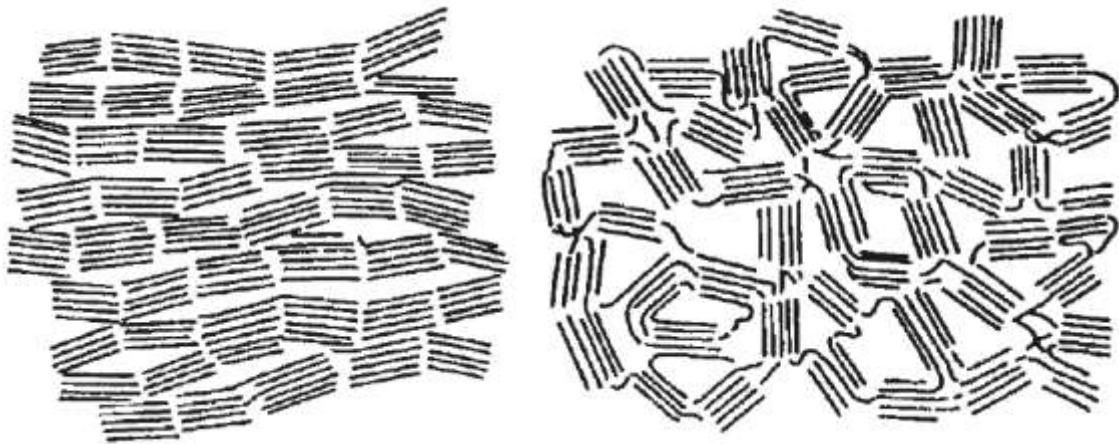
Fig. 1.2 Franklin's model for graphitizable (left) and non-graphitizable (right) carbon. (Adapted with permission from Franklin, 1951. Copyright 1951 The Royal Society.)

1.1.2 Preparation of Carbon Materials

All parent materials for the preparation of carbon come from organic sources; thus, each of these precursors needs to be heat-treated in an inert atmosphere in order to increase the carbon content of the precursor by removing some of the heteroatoms (S, O, N, H, etc.) (Marsh and Reinoso, 2006). This step is called carbonization: Carbonization can be carried out in the solid, liquid, or gas phase, with the solid- and liquid-phase carbonizations being of interest in this dissertation.

In solid-phase carbonization, the solid lattice remains rigid throughout the whole process during which all the structural changes occur; thus, there is no bulk movement. On the other hand, atoms can move short distances in order to move to a more stable position or to form a six-membered ring (Marsh and Reinoso, 2006). This type of carbonization is utilized for the production of activated carbon fibers, which is the focus of this dissertation. During the preparation of activated carbon fibers, as-spun fibers from a carbonaceous material such as petroleum pitch are oxidized, or rendered infusible prior to the carbonization process. Because all the constituent molecules are cross-linked during oxidation, carbonization occurs in the solid state.

In liquid-phase carbonization, bulk movement can occur. The polycyclic aromatic molecules that constitute the carbon material can orient themselves into a liquid crystalline phase, and as a result highly organized solids can be formed. The products of liquid-phase carbonization are anisotropic carbons and they are graphitizable; in other words, by heating to temperatures above 2000 ˚C, they will form 3-dimensional graphene layers in a graphite lattice which can be detected by X-ray diffraction (Marsh and

Reinoso, 2006). The formation of these organized solids is initiated by the growth of aromatic nematic discotic liquid crystals, which are also called mesophase. It is important to note that liquid-phase carbonization is used for the preparation of the graphitizable (mesophase) precursors themselves. In order to make highly ordered carbon fibers, the fibers that are spun from these precursors must first be oxidized and then carbonized in the solid phase.

For carbons, the structure and the arrangement of the carbon atoms in the graphite lattice is crucial to their final properties. Activated carbons are produced from non-graphitizable carbons. They are structurally disordered materials, but they are not amorphous.

1.2 Activated Carbon

Carbonaceous materials that are prepared by carbonization and activation of organic materials are called activated carbons, and their highly porous nature makes them attractive for many applications. The first use of activated carbons goes back to about 1500BC, when ancient Egyptians used them for medicinal purposes and ancient Greeks used wood chars to treat a host of ailments. Later, they were used for removing odors from gangrene and as decolorizing agent for sugar. The first substantial industrial interest in activated carbon was at the beginning of 20th century, when Raphael von Ostrajko obtained British and German patents for the use of activated carbon in gas masks to remove chlorine gas during World War I (Yehaskel, 1978). Today, activated carbons are used in many areas such as filtration, purification, gas adsorption, dry cleaning, alcoholic

beverages, and solvent recovery; the different forms of activated carbons include granular, powder or fiber forms.

The functionality of activated carbons (ACs) arises from the fact that the sizes of their pores are comparable to the size of molecules. These small holes give rise to intense van der Waals forces because of carbon atoms in near proximity; thus, they are suitable materials for applications where adsorption and desorption are important (Marsh and Reinoso, 2006). Pore sizes in ACs are generally classified into three groups: Pores smaller than 2.0 nm are called micropores; those ranging in size from 2.0 nm to 50 nm are called mesopores; and pores bigger than 50 nm are called macropores. Controlling the pore size of ACs can enable one to tailor such carbons for different specific applications. In this sense, activated carbon fibers (ACFs) are more advantageous than other forms of AC, as fibers have more uniform size and shape as a precursor to begin with. Also, better diffusion between the fibers makes ACFs more suitable for adsorption applications (Suzuki, 1994).

ACs can be produced from non-graphitic and non-graphitizable precursors, such as coals, pitches, peat, woods, fruit stones, coconut shells, and lignites. The final properties of ACFs depend on the precursor used and the activation treatment to prepare them (Menendez-Diaz and Martin-Gullon, 2006). In this study, in order to obtain a better understanding of the effect of precursor structure and composition on final pore structure, ACFs were produced from controlled molecular weight (mol wt) fractions of a commercially available petroleum pitch.

1.2.1 Pitch as an Activated Carbon Precursor

There are two common types of pitch that can be used for AC production: petroleum pitch and coal-tar pitch. In brief, petroleum pitch is produced as a residue of crude oil distillation, and coal-tar pitch is a liquid product from the production of metallurgical coke. In general, coal-tar pitches have more aromatic content than petroleum pitches; however, the lower benzene- and quinoline-insoluble content of petroleum pitches makes them preferable for fiber applications (Chung and Deborah, 1994). The insoluble portions of coal-tar pitch cause faster coke formation during processing at high temperatures, and as a result more fiber breakage.

Because of its thermoplastic nature, pitch can be used for the production of all forms of ACs, including fibers, powders and granules. To produce ACFs, pitch is first melt-spun into small-diameter fibers. The resultant green fibers are then rendered infusible via oxidation to prevent them from melting and losing their shape during subsequent, higher-temperature, heat treatment steps. This process is called stabilization, or infusibilization, and is also used for the production of other forms of ACs. Following this stabilization process, the fibers are carbonized under an inert atmosphere at temperatures up to 1000 ˚C. After this step the carbon content of the fibers approaches 100% and the fibers are truly "carbon" fibers. At this point, depending on the composition of the pitch precursor, the fibers may be suitable for the production of high-performance carbon fibers or for the production of ACFs. High-performance carbon fibers are produced by further heat treatments above 2000 ˚C in an inert atmosphere, whereas ACFs are produced by activating the carbon fibers by either chemical or

physical (thermal) means, typically at temperatures between 800 ˚C and 900˚C. Details of these processes are given later in this chapter.

1.2.2 Advantages of Activated Carbon Fibers vs. Other Forms of Activated Carbons

ACs are used in many separation and purification applications. Common forms of ACs available are powdered, pelletized, granular and molded forms. The introduction of ACFs brought new perspectives to the AC concept in terms of design and applications. Carbon fibers were introduced to the market at the beginning of the 1960s and today are relatively common. They have been used for the production of high-performance composite materials for the transportation industry, primarily for aerospace applications. In 1972, ACFs were introduced to the market in both fiber and fabric form by Arons and McNair (Suzuki, 1994). The use of viscose textiles and phenol-formaldehyde (Novolak) fibers as precursors for AC textiles and high surface area ACFs has been patented (Rodgers, 1965; Doying, 1966; Peters, 1966).

ACFs have important advantages over ACs in powder or granular form. Because of their small diameter, ACFs have better intraparticle adsorption kinetics than pelletized and granular ACs (Suzuki, 1994). Furthermore, their fiber form is more suitable for many applications, for example, for fabrics and filters (Thwaities et al., 1993). It is the opinion of the author of this dissertation that because of their uniform size, ACFs can generate a more uniform pore structure compared to other forms of ACs. Thus, ACFs are advantageous for adsorption applications where the rate of adsorption and desorption are critical.

1.3 Preparation of Activated Carbon Fibers

1.3.1 Spinning

Spinning is the first step of the ACF production process; here the precursor in powder or granular form is melted and converted into fibers. The melt-spinning process can be broken down into three stages: melting of the precursor, extruding through the die, and drawing of the fibers. Successful spinning of the precursor strongly depends on the viscosity of the molten material, and the viscosity of the pitch is a strong function of temperature. Thus, there is only a limited temperature range over which the precursor can be spun. This temperature range is called the spin window and is dependent on the properties of the precursor material. If spinning temperatures are too low, even if the material is molten, the resultant fibers can be brittle, causing excessive fiber breakage during drawdown. If spinning temperatures are too high, both low viscosity and degradation of the source material can become a concern, making the production of continuous fibers impractical.

1.3.2 Stabilization

Stabilization is the process that makes the as-spun fibers infusible in preparation for subsequent heat treatments (Chung and Deborah, 1994). Once stabilized, the fibers will not melt and lose their shape or stick to each other. This oxidative thermosetting step is the most time-consuming step in ACF production and can take days to complete. Thus, choosing relatively high softening point precursors is important to speed up the stabilization reaction to the extent possible. The most common stabilization method is

heating fibers under an oxygen (or air) atmosphere; that is why this process is often referred to as oxidation. Air-convection ovens are usually employed for this process. The stabilization step mainly consists of oxygen uptake (Stevens and Diefendorf, 1986), resulting in cross-linking of the molecules in the fibers. The oxidation process is a simultaneous combination of diffusion and reaction. Generally fibers are initially heated to a temperature ~50-60 °C below the softening point of the precursor, and then the temperature is gradually increased to the range of 230 °C to 280 °C.

The rate of stabilization depends on several parameters, including the temperature, the oxygen concentration, and the chemical nature of the precursor molecules (Miura et al., 1995; Drbohlav and Stevenson, 1995; Lavin, 1992). Typically, fibers gain 6-15% weight when they are fully stabilized (Lin, 1991). The main mechanism of oxidation is believed to be dehydrogenation and the attachment of oxygen to the aliphatic side chains at the early stages of oxidation process, during which water is given off, forming compounds such as carboxylic acids, aldehydes, and ketones (Miura et al., 1995; Drbohlav and Stevenson, 1995). During the later stages of the oxidation process, the fibers lose weight as CO_2 is formed.

1.3.3 Carbonization

After the fibers have been stabilized, they are then ready for carbonization. During this step, the stabilized fibers are heat-treated at temperatures up to 1000 °C under an inert atmosphere. Above 1000 °C, the carbon structure becomes more ordered and starts to graphitize. Thus, for the production of ACFs, temperatures of only 1000 °C, at which

most of the elimination of the non-carbon elements occur, are preferred. (Incidentally, carbonization temperatures as high as 3000 ˚C are used if highly graphitic, high-performance carbon fibers are being made from mesophase pitch).

Carbonization is mainly based on growth and polymerization of aromatic molecules, and at the beginning of the process, nonaromatic compounds are aromatized first (Lewis, 1982). Although the overall mechanism of carbonization process is complex, the major reactions can be summarized as follows (Lewis, 1982): (1) cleavage of aromatic C-C and C-H bonds to form free radicals, (2) molecular rearrangement, (3) thermal polymerization, (4) aromatic condensation, and (5) elimination of side chains and hydrogen.

During these reactions, non-carbon elements are volatilized in the form of gases, such as hydrogen, carbon dioxide, carbon monoxide, methane, and water (Edie, 1998), yielding fibers with 92% or more carbon content. In the literature it has also been shown that at temperatures between 300 ˚C and 500 ˚C, hydroxyl, carbonyl, and saturated aliphatic hydrocarbons are eliminated, while between 500 ˚C and 800 ˚C hydrogen is eliminated and aromatic condensation takes place (Yang and Simms, 1993). At around 800˚C, the weight of the fibers stabilizes, showing that the carbonization process is complete (Wu et al., 2008). The net carbonization yield can vary between 60-85%, depending on the nature of the pitch precursor used. After the carbonization process, the fibers are cooled down to room temperature, resulting in thermal contraction and densification of the fibers.

1.3.4 Activation

Most of the carbonized fibers develop some porosity during the carbonization step; however, the pores are too small and the pore volume is too low for most applications. Because of this, a formal activation process must be applied to the carbonized fibers in order to improve their porous structure and adsorption potential. There are two principal types of activation, physical and chemical activation. In physical (also called thermal) activation, the fibers are reacted with either CO_2 or steam at temperatures between 800 and 900 ˚C. In chemical activation, reactants such as phosphoric acid, zinc chloride, potassium hydroxide, or potassium carbonate are used as activating agents to modify the pore structure of the fibers. In some cases, a combination of the two processes is employed.

The main mechanism of physical activation is the removal of carbon atoms in the form of carbon monoxide via gasification reactions using the activating agents steam or CO_2. The use of steam or CO_2 as an activating agent results in different pore structures. The main reactions can be shown as follows:

$$C + CO_2 = 2CO$$

$$C + H_2O = CO + H_2$$
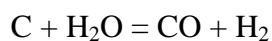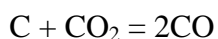
When CO_2 is used as the activating agent, it reacts with the free carbon atoms to give off CO molecules. However, during this process, chemisorption of oxygen atoms also occurs. That is, during the reaction of CO_2 with a carbon atom, an oxygen atom from the CO_2 molecule is chemisorbed on the carbon surface and forms surface oxygen complexes (Harry and Marsh, 2006). These complexes have broad chemical

functionalities. They can act as reaction intermediates and go on to form free CO gas, or they can act as inhibitors for the activation reaction by blocking the reaction sites. In addition, the reaction products CO and H_2 can inhibit the gasification reaction by a reverse reaction with surface oxygen complexes.

When steam is used as an activating agent, it reacts with the free carbon atoms to give off CO and H_2 molecules. Similar to the CO_2 gasification reactions, hydrogen can be chemisorbed on the carbon surface and block the reaction sites. The inhibition effect of chemisorbed hydrogen is more pronounced, because surface carbon–hydrogen complexes are much more stable than surface carbon–oxygen complexes.

During gasification reactions, activating agents do not randomly react with any carbon atom that they encounter; instead, they are highly selective, with the reactivity of the carbon atoms in the fiber microstructure being strongly dependent on the chemical nature of the precursor. Carbon atoms in a precursor are assembled into five, six or seven-membered rings (Marsh and Reinoso, 2006). These polycyclic aromatic molecules form the defective micro-graphene layers and are bonded to each other. Due to atom vacancies and the presence of hydrogen and heteroatoms [e.g., sulphur, nitrogen, oxygen and phosphorus], which cause bending and curvature, these graphene layers are not well-ordered. Instead, they form a 3-dimensional disordered network in which the spaces between layers form porosities. Such is the nature of the non-graphitizable carbonaceous materials that are used in the production of ACFs. Non-graphitizable materials are required because graphitizable carbonaceous materials would form graphene layers

similar to 3-dimensional crystalline graphite, and activating agents would not be able to access the internal carbon atoms.

Non-graphitizing carbons also exhibit some degree of molecular order; however, it is far from that of perfect graphite. The distance between layers is much larger than that found in graphite; furthermore, the layers are not completely parallel to each other. Also, the extent of organization among the layers (on the order of nanometers) is much smaller than that of graphitizable carbons, where crystallite sizes might be as high as hundreds of nanometers and even micrometers.

1.4 Activated Carbon Models

In order to understand the activation process better, understanding the carbon microstructure and the porosity in ACs is very important. Although none of the proposed models for porous, ACs are completely correct, they can be helpful for the insights that they provide. Marsh and Reinoso have included a detailed discussion about different models and approaches in their book (2006). Some of those models are summarized here.

Ideally, in order for a model to be realistic and acceptable, it should address several issues about the structure and should also be consistent with experimental results such as X-ray diffraction (XRD), small angle X-ray diffraction (SAXD), and adsorption isotherms.

First, the model should relate the microstructure of the parent carbon material to the porosity. The walls of the pores should be consistent with the structure of the molecules constituting the precursor material. Also, the molecules that form the AC

should be interconnected to form a network and to address the hardness of the material. The chemical composition and nature of the precursor material should be considered, and heteroatoms such as oxygen, nitrogen, and sulfur should be included in the model.

Second, different aspects of pore structure should be addressed. Pores are not all uniform and independent. Therefore, a complete model has to consider the interconnectivity of pores, pore size distribution, the simultaneous existence of both micropores and mesopores, and the shape of pores.

Third, the model should address the activation process and relate the carbon structure before the activation process to the final carbon structure and the pore network.

Finally, it should be consistent with experimental observations such as the ratio of carbon atoms to adsorbate atoms, isotropy, and density. A more detailed list of the preferences for a model is given by Marsh and Reinoso (2006). In the next two sections, first some of the simpler visual models and then some of the more advanced simulation models are discussed.

1.4.1 Visual Models

The first models that attempted to describe porosity in ACs were simple and assumed porosity to be similar to macro objects that are easy to visualize.

Drilled-hole models (**Fig. 1.3**) are an attempt to illustrate the different sizes and shapes (round or slit) of pores, but obviously don't take the structure of carbon into account at all. Another simple model is a branched-tree model, which consists of a high-contrast image of a branched tree (**Fig. 1.4**), and in which the tree is considered as the

16

pore network. This model shows the interconnectivity of the porosity as a network. It also

addresses the size variation of the pores. However, like the previous model it doesn't

address the structure of carbon at all, and it limits the distribution of microporosity and

mesoporosity.
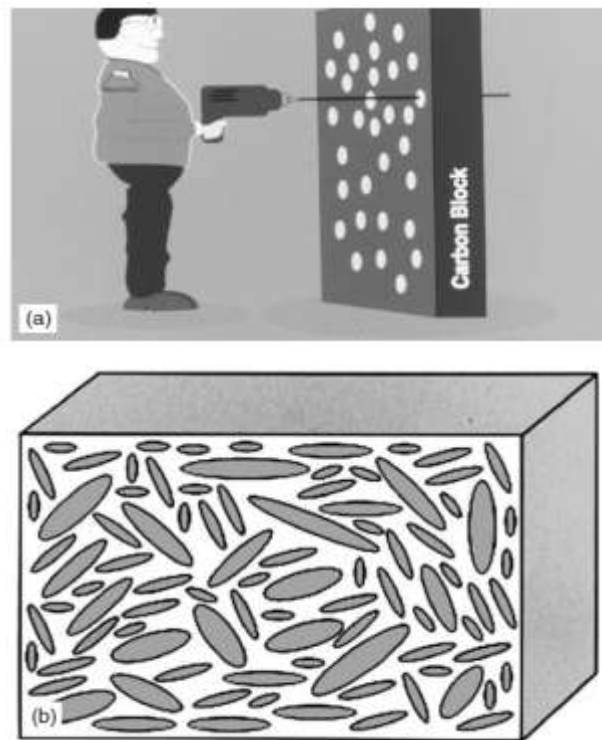
Fig. 1.3   Drilled-hole model with (a) round-shaped pores, or (b) oval (slit-like)-
shaped pores. (Reprinted with permission from Marsh and Reinoso, 2006.
Copyright 2006 Elsevier.)

Fig. 1.4   Branched-tree model: high-contrast image of a branched tree. (Reprinted in part with permission from Marsh and Reinoso, 2006. Copyright 2006 Elsevier.)

The potato-chip model (**Fig. 1.5**) is a simple visual model that attempts to explain the porosity based on the carbon structure itself. Each potato chip can be considered to be a defective micrographene layer, and the spaces between the chips can be thought of as the pores. The connectivity of the pores to each other, and the non-planarity of the micrographene layers are also taken into account by this model. Note that the use of smaller- or larger-sized potato chips would give a different pore structure – an observation that is directly related to the main focus of this dissertation. Among the weaknesses of the model are that the potato chips are too uniform and that there is no interconnectivity between the micrographene layers.
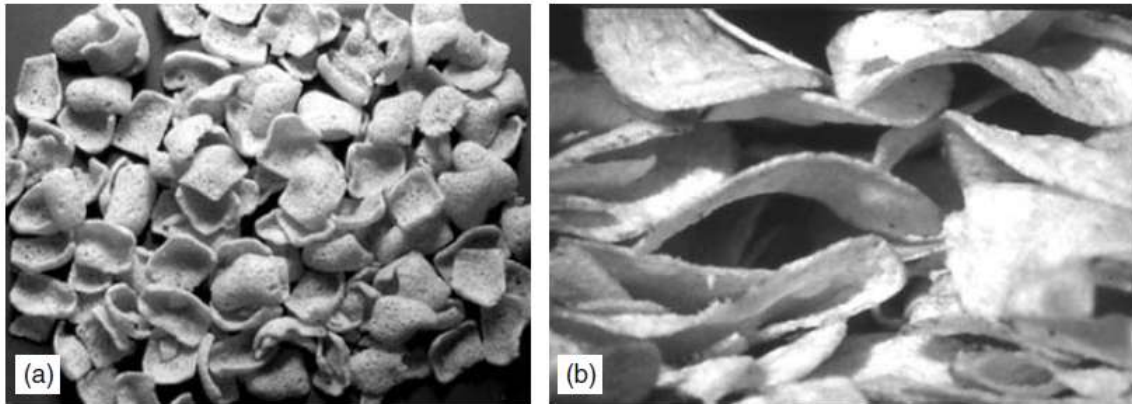
Fig. 1.5　　Potato-chip model with (a) smaller-sized chips with more curvature, and with (b) bigger-sized chips. (Reprinted with permission from Marsh and Reinoso, 2006. Copyright 2006 Elsevier.)

The Norit model (**Fig. 1.6**) resembles Franklin's model (Franklin, 1951) that was mentioned before in this chapter. Similarly, this model is composed of planar layers, and the distance between these layers is defined as the porosity. As a result of activation, some of these layers are removed either partially or as a group to form bigger pores (**Fig. 1.6b**). The model has the advantage of defining the pores based on carbon structure and in modeling the activation process by the removal of carbon atoms; however, the graphene layers introduced are too planar and homogenous, and there is no bonding between these layers, which is necessary for explaining the hardness of the material.

Fig. 1.6   The Norit model: (a) structure before activation; (b) removal of some of the graphene layers (as indicated by the lighter color) either individually or in groups as a result of activation. (Reprinted with permission from Marsh and Reinoso, 2006. Copyright 2006 Elsevier.)

In addition to simpler visual models, Marsh and Reinoso (2006) suggested that scanning electron micrographs (SEM) of exfoliated graphite (**Fig. 1.7a-d**) and of montmorillinite (**Fig. 1.7e**) could serve as useful visual models for the structures of ACs. Exfoliated graphite is formed by the rapid heating of graphite intercalation compounds, which are formed as a result of the reaction of graphite with oxidizing agents, such as SO_3. Once the graphite intercalation compound is heated rapidly, the intercalated substances vaporize and force the graphene layers to separate. Also, although montmorillinite is not a carbon material, it has a similar structure to exfoliated graphite. All these figures (**Fig. 1.7a-e**) can illustrate the carbon network, the interconnectivity of
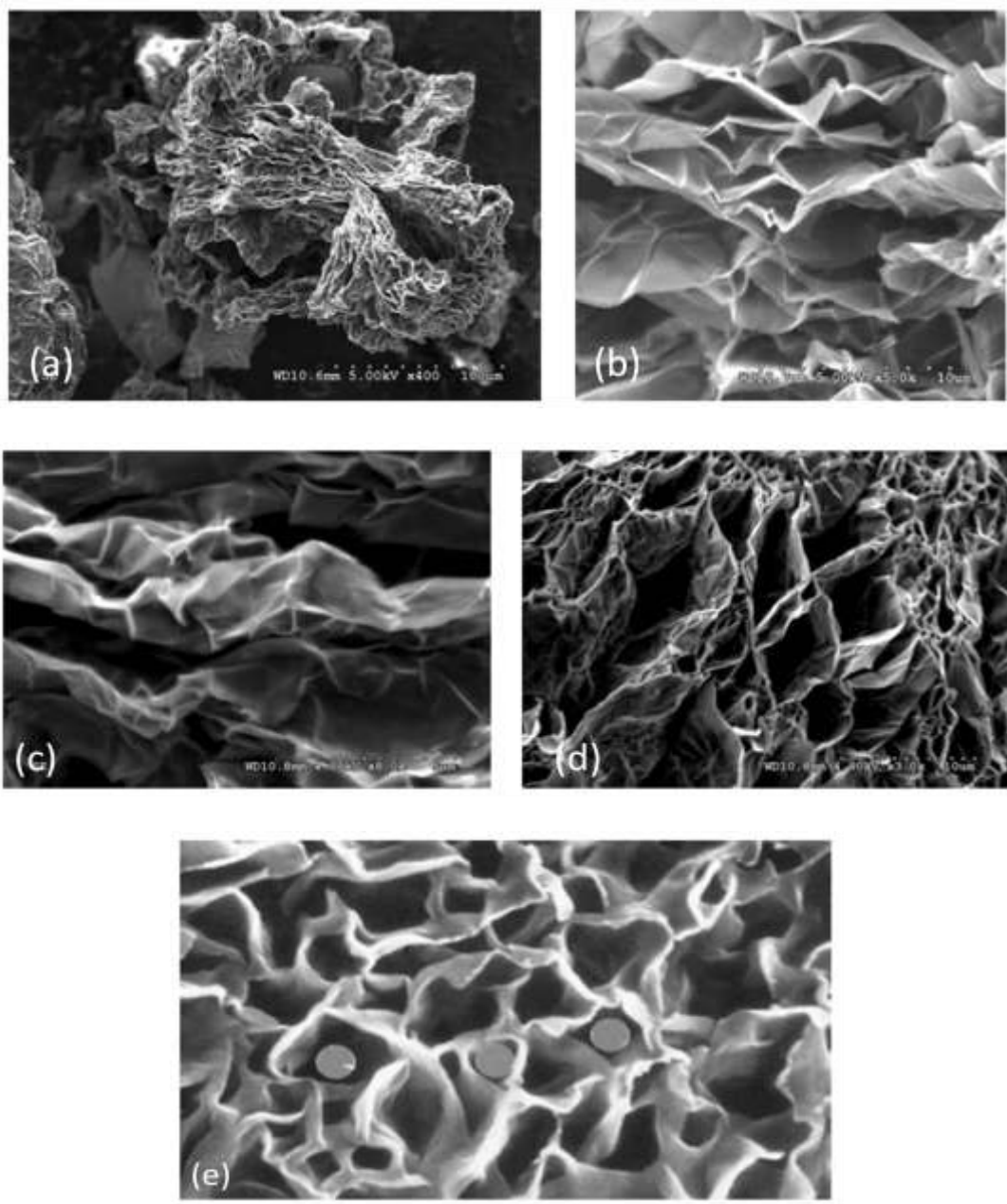
Fig. 1.7 Scanning electron micrographs of surfaces of exfoliated graphite and montmorillonite (a clay mineral). ACs are believed to have similar structures to these materials. (a-d) SEM micrographs of surface of exfoliated graphite at different magnifications; (e) SEM micrographs of surface of montmorillonite (grey spheres represents the theoretical adsorbate molecules adsorbed in microporosity in ACs). (Reprinted with permission from Marsh and Reinoso, 2006. Copyright 2006 Elsevier.)

the pores, and the co-existence of micropores and mesopores. They also help us to visualize slit-shaped pores. However, in actual microporous carbons, the size (thickness) of the pore walls is comparable to the size of the pores.

In addition, Marsh and Crawford in 1982 and Rouzaud and Clinard in 2002 used high resolution transmission electron microscopy (TEM) to investigate the structure within porous carbons. Note that the micrographs (**Fig. 1.8**) consist of cross-sections, so they essentially show the 2-dimensional structure of the porous carbons at a given depth. **Fig. 1.8a-c** show TEM pictures of porous carbons produced from polyvinylidene chloride, saccharose-based carbon, and soot nanoparticle carbon, respectively. Note that all micrographs show non-planar, defective, micro-graphene layers.

1.4.2 Mathematical and Molecular Simulation Models

Before moving to a discussion of some of the more detailed molecular simulation models for activated, porous carbons, it is worth mentioning the studies of Kaneko et al. (1992), who related the high surface area of ACs to the geometric area of graphitic microcrystallites of polycyclic aromatic hydrocarbon (PAH) molecules. Calculations were made on molecules containing from 56 to 212 carbons. Both sides and edges were considered, and the available geometric area was also calculated for stacks of three microcrystallites. The calculated geometric areas were from 4100 m^2/g to 6000 m^2/g for single microcrystallites and from 1900 m^2/g to 3200 m^2/g for a stack of three microcrystallites. Although area calculations in the latter case were reasonable, the

formation of such big structures (i.e., PAH containing 212 C atoms) at relatively low carbonization and activation temperatures, which are typically less than 1000 ˚C, contradicts XRD results for isotropic precursors. Nevertheless, their approach was important as it related the surface area of AC directly to molecular structure.
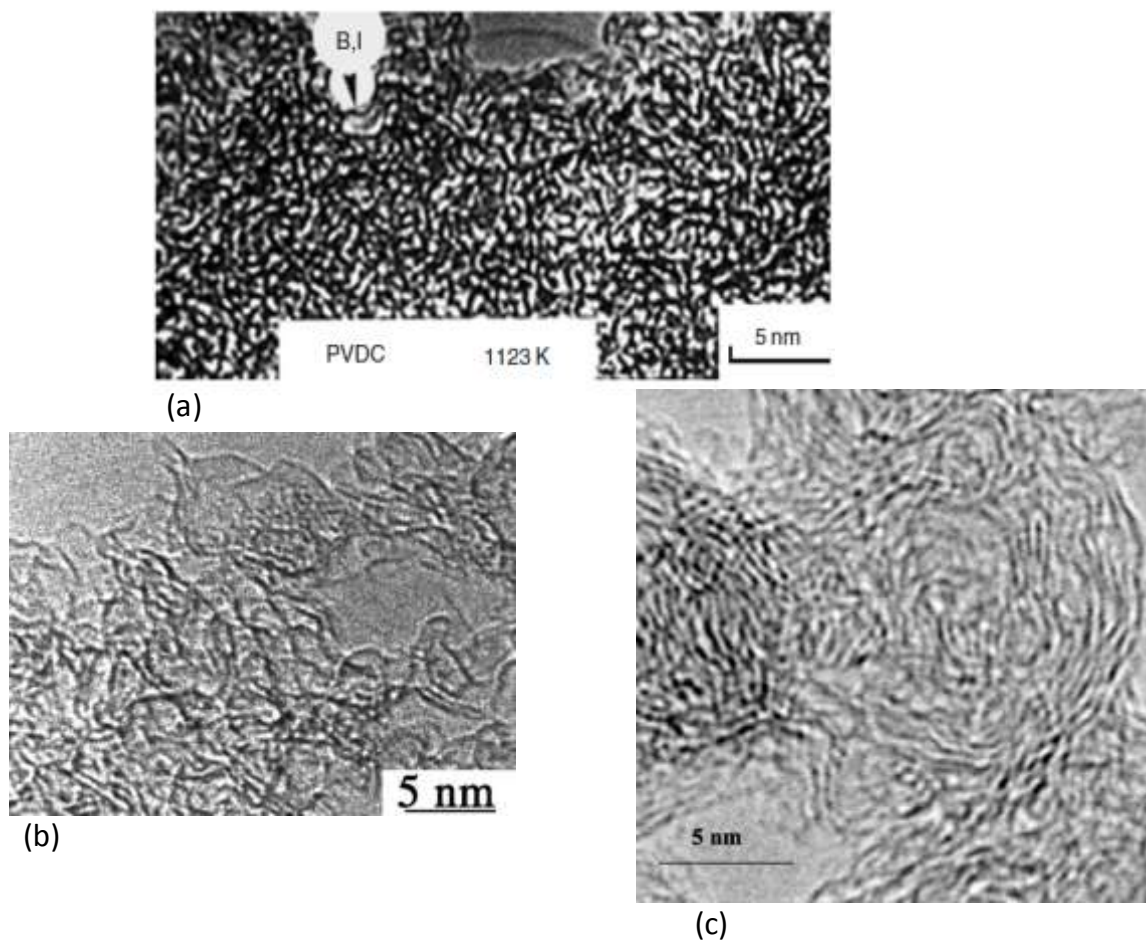
Fig. 1.8   TEM micrographs of a cross-section of (a) a heat-treated polyvinylidene chloride carbon (Reprinted with permission from Marsh et al., 1982. Copyright 1982 Elsevier), (b) an activated saccharose-based carbon, and (c) a soot nanoparticle carbon. (Reprinted with permission from Rouzaud and Clinard, 2002. Copyright 2002 Elsevier.)

Among the molecular simulation models, several of the proposed models are based on the assumption that ACs have similarities to glassy carbon. Glassy carbon is a disordered carbon material that contains individual cage-like pores, so its porosity is "closed" to the surface. It is prepared by carbonization in a closed system to prevent the escape of volatile materials. Before starting with the molecular simulation models on glassy carbon, having a look at the study of Yoshida et al. (1991) will help one imagine the structure of glassy carbon. Their study was based on their observations of the surface texture of glassy carbon that was heat-treated at 2000-3000 ˚C and then crushed into 2-3mm particles. Field-emission electron gun type SEM micrographs showed that the fracture surfaces of these particles were granular. Yoshida et al. (1991) suggested that the microstructure of glassy carbon samples could be similar to the model for the microtexture of phenol resin char heat-treated at 2800 ˚C (**Fig. 1.9**) as proposed by Shiraishi et al. (Yoshida et al., 1991), and adopted this model for glassy carbon. The model of Yoshida et al. shows the cage-like structure of the pores of ACs where adsorption occurs, with the walls of the structure being made of defective micro-graphene layers.
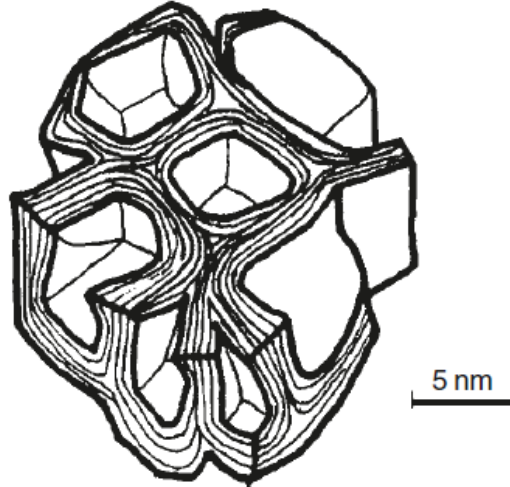
Fig. 1.9   Granular glassy carbon model. (Reprinted with permission from Yoshida et al., 1991. Copyright 1991 Elsevier.)

One of the first molecular simulation models for glassy carbon was proposed by O'Malley et al. (1998). They used reverse Monte Carlo (RMC) computer simulation to propose molecular structures for glassy carbons heat-treated at 1000 and 2500 ˚C. (With the reverse Monte Carlo method, the structure of a material is adjusted until it produces results that are most consistent with experimental data.) O'Malley et al. used TEM electron diffraction patterns and density values as experimental data, and their proposed structures consisted of a non-planar, buckled, defective graphene layer with different-sized ring systems and vacancies (**Fig. 1.10)** (O'Malley et al., 1998). As the proposed structure is non-planar with defects, true stacking of two similar structures is not possible, leaving a molecular space between them. Both sufficiently large ring systems and the molecular spaces between such structures can be considered to be adsorption sites, and thus the "source" of porosity.

Following the work of O'Malley et al., similar studies using RMC were carried out by Pikunic et al. (2001) and Petersen et al. (2003) on glassy carbons that were heat-treated at 2500 °C. Petersen et al. used a modified RMC in which they used a neutron diffraction pattern in addition to an electron diffraction pattern as experimental data. The molecular structures proposed by these two groups are shown in **Fig. 1.11** and **Fig. 1.12**. Their studies confirmed the results of O'Malley, that the glassy carbon network is composed of bent, multi-sized ring systems. Both the simultaneous existence of micropores and mesopores and their interconnectivity were addressed in these two models. It should be noted that the glassy carbons investigated were heat-treated at 2500°C and did not have an accessible porosity. Thus, although these models are important for helping us understand the structure of porous carbons heat-treated at lower temperatures, their structures are not completely representative of porous, ACs.
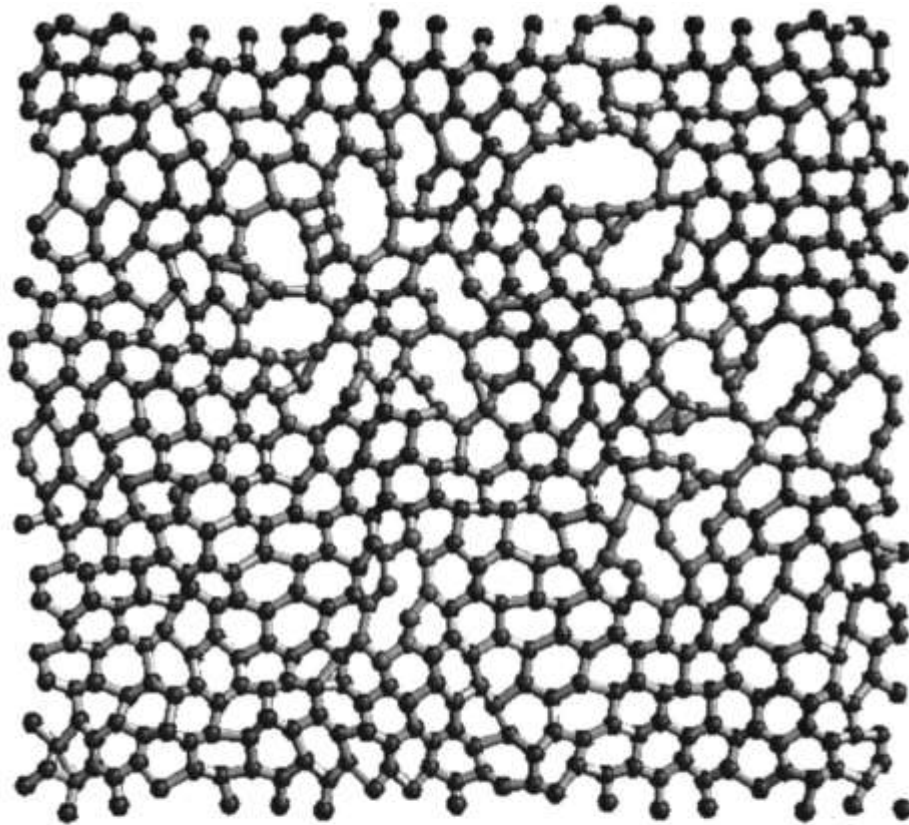
Fig. 1.10 A model structure of a glassy carbon heat-treated at 1000 ˚C proposed from the study of O'Malley et al.; (a) top view of a proposed basal plane; (b) side view of a proposed basal plane. (Reprinted with permission from O'Malley et al., 1998. Copyright 1998 American Physical Society.)
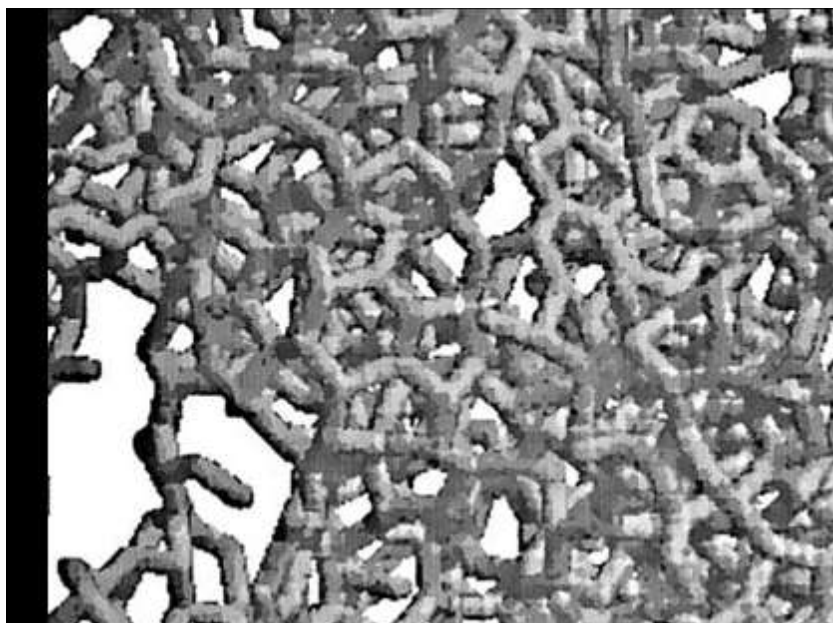
Fig. 1.11   Glassy carbon structure proposed by Pikunic et al. (2001) (Reprinted from Marsh and Reinoso, 2006. Copyright 2006 Elsevier. Permission requested).

Another molecular model, "The Chemically Constrained Model", was proposed by Acharya et al. (1999). Their model for nanoporous carbon consisted of graphene layer fragments having only sp^2 type bonding and composed only of carbon and hydrogen atoms. They used a bond-making algorithm that determines the structures starting from small fragments and bonding them together. Structures with the minimum internal energy and the right H/C ratio for the desired material to be simulated were chosen. The carbonization of poly-furfuryl alcohol at 400-800 ˚C was simulated. Among the proposed structures, the ones that matched the known density of poly-furfuryl alcohol heat-treated at a specified temperature were chosen. Several copies of one of their proposed structures were randomly put together by Marsh and Reinoso (2006) to help us imagine the porosity

(**Fig. 1.13**). This model shows the interconnectivity of pores, the existence of different-sized pores, and the bending of the layers due to the strain caused by five-membered rings. The model of Acharya et al. predicts the existence of fragments that are too graphitic for the low heat-treatment temperatures (HTT) carried out experimentally. In microporous carbons, these layers are expected to be smaller and contain more defects. Nevertheless, the model is still helpful in furthering our understanding of the structure of porous carbons.
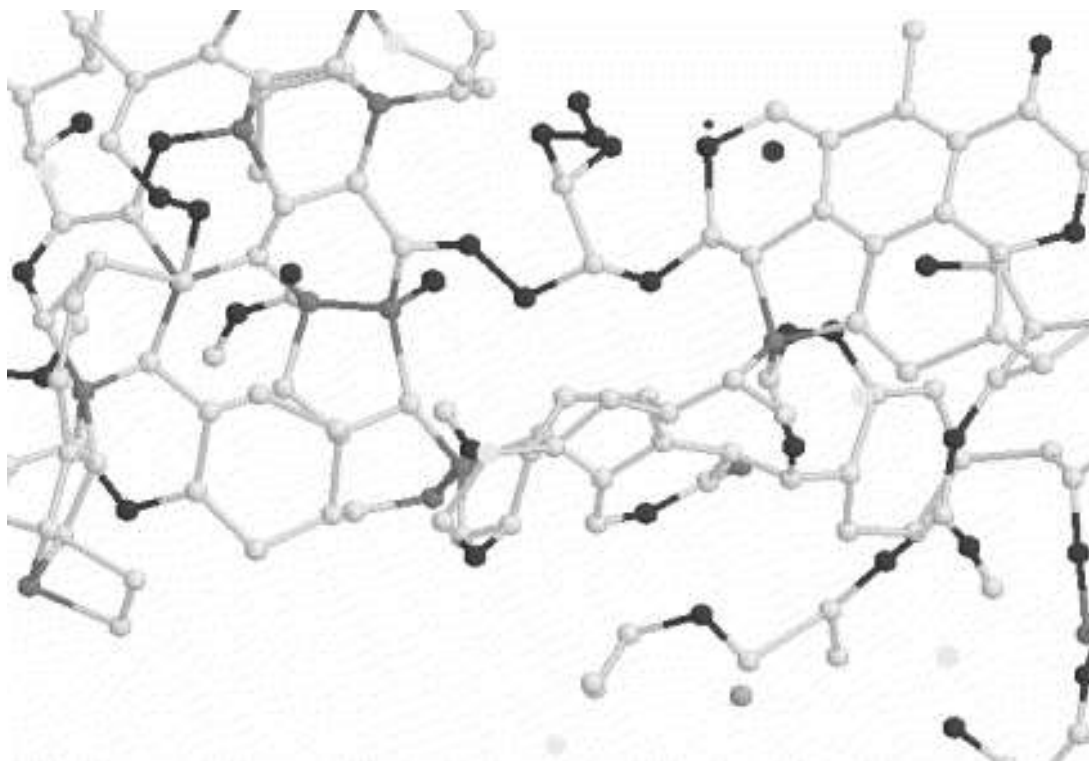
Fig. 1.12   Glassy carbon structure proposed by Petersen et al. (Reprinted with permission from Petersen et al., 2003. Copyright 2003 Elsevier.)

.

In the above discussion, we have seen that models based on both experimental findings and advanced computations have been proposed, but the structures that constitute porous carbons have yet to be precisely determined. However, we do have enough knowledge of the characteristics of porous carbons to help us to anticipate the general structures. For example, we know that the carbon atom network is composed of defective micro-graphene layers, instead of graphitic micro-crystallites. These graphene layers are composed of non-planar layer fragments with defects, five- to seven-member rings, vacancies, and bending. These layers are known to be short fragments, and there is no real stacking between these layers. All of these layers are interconnected to give the carbon material its hardness. The porosity is also a network where different sizes of pores (micropores and mesopores) co-exist interconnected in close proximity. Although these micrographene layers are not completely parallel to each other, the micropores are known to be mainly made up of basal planes, i.e., they are slit-shaped (Ehrburger et al., 1992).
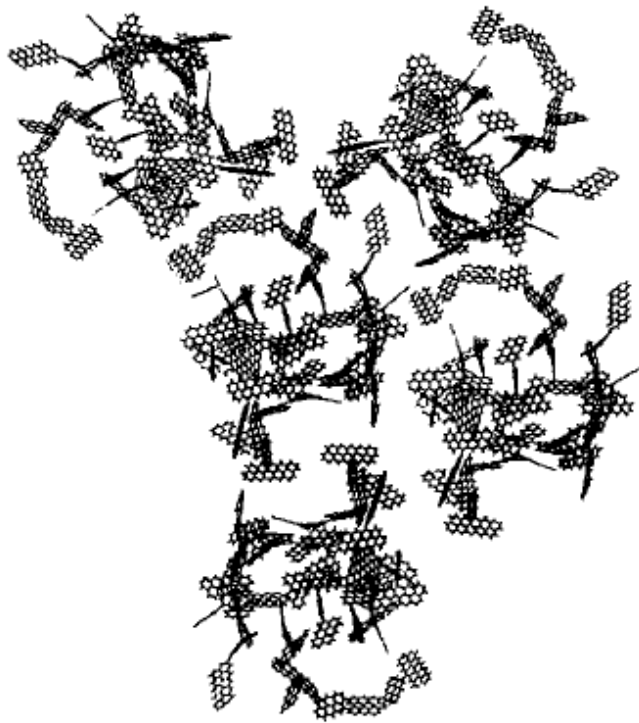
Fig. 1.13   "The Chemically Constrained Model" for modeling carbonized nanoporous poly-furfuryl alcohol by Acharya et al. (1999) (Reprinted with permission from Marsh and Reinoso, 2006. Copyright 2006 Elsevier.)

The cage-like molecular spaces between these defective micro-graphene layers, created as a result of the activation process, are the adsorption sites. In a microporous carbon that has a surface area of 1000 m^2/g (assuming single-layer adsorption), it is a good approximation that eight carbon atoms are employed for the adsorption of one nitrogen molecule (Marsh and Reinoso, 2006). This shows that the walls of the pores cannot be more than 2 or 3 layers thick.

It is the opinion of the author of this dissertation that among the models discussed above, the exfoliated graphite (**Fig. 1.7**) and the TEM images of non graphitizing carbons

(**Fig. 1.8**) (similar to the Norit model (**Fig. 1.6**) before activation but with a more disordered structure) are the most helpful models to envision the AC structure.

In the work of this dissertation, the seven precursors that were used to prepare ACFs were prepared from the same mother petroleum pitch that had an oligomeric character. A comprehensive analytical characterization study by the Thies group (Burgess and Thies, 2011) indicates that the dominant molecules present in these precursors are dimer and trimer species, with some monomer present in only one of the precursors and some tetramer present in several of the precursors (see **Fig. 1.14**). Furthermore, each oligomeric unit is joined by a single, five-membered connectivity ring. Thus, in our case the molecules that form the defective micrographene layers are typically composed of at least nine rings, including at least one five-membered ring.

Also, it is important to point out that four of the seven precursors studied in this work were isotropic, while three of them had mesophase contents at different levels. This enabled us to see the effect of increasing mesophase content (anisotropy) and, more importantly, to isolate the effect of molecular composition (i.e., oligomeric content) on oxidation, carbonization, and activation behavior, and on the final porosity of the ACFs.
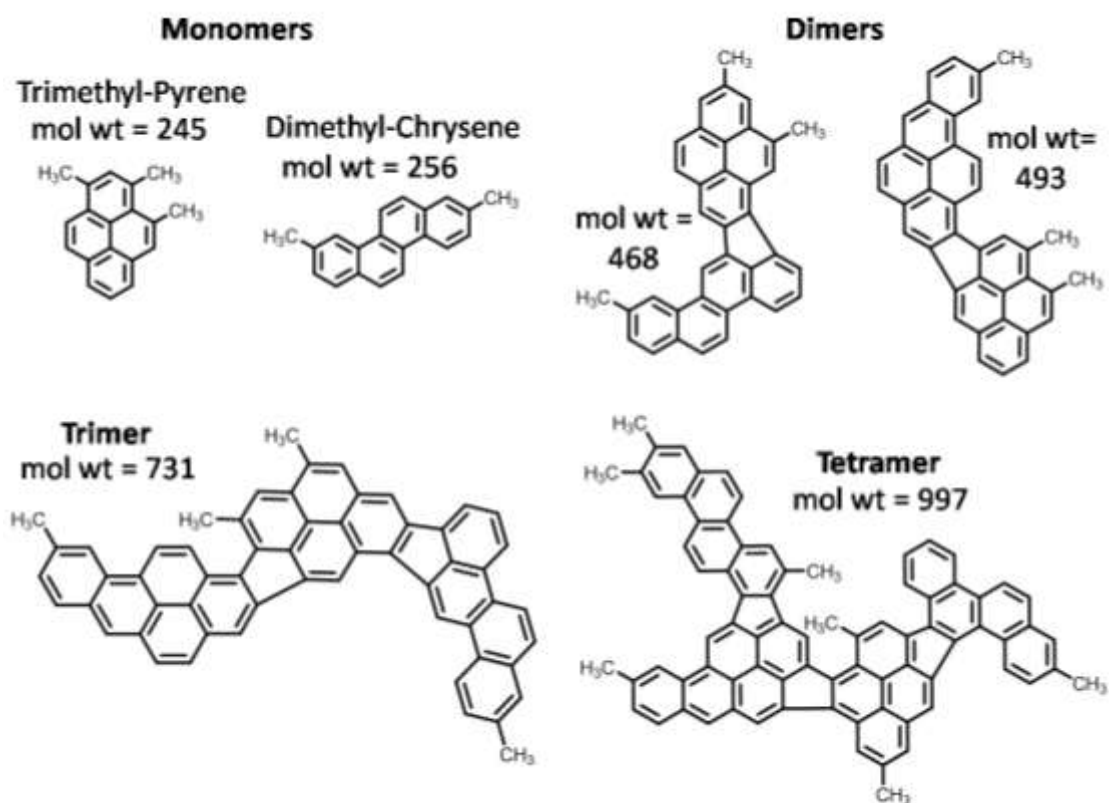
Fig. 1.14   Representative molecular structures present in the precursors used in this study (Cervo, 2010a, Burgess et al., 2010; Burgess and Thies, 2011). (Reprinted with permission from Cervo, 2010a. Copyright 2010 Dr. Eduardo Cervo.)

The molecules shown in **Fig. 1.14** are typical of the basic structural units that cross-link during the oxidation process to form extended carbon network. Therefore, changing the composition (and thus the molecular weight) of the precursor changed the size of the basic structural units, that is, of the defective micrographene layers.

A key hypothesis of this study was that a knowledge of the molecular structure of the pitch precursor, and the ability to control that structure, would help us better

understand the activation process, the effect of precursor structure and composition on final pore structure, and the effectiveness of the adsorption process itself.

In the next part of the "Introduction" section, previous studies on physical and chemical activation are presented as background information, and studies on ACs and ACFs prepared from different precursors are discussed.

1.5 Literature Review

1.5.1 Physical Activation: Steam vs. CO_2

The use of the two different activation agents, steam and carbon dioxide, generally results in quite different activation rates and pore structures. Several studies (Alcaniz-Monge et al., 1994; Walker, 1996; Molin-Sabio et al., 1996) have compared the effects of the activating gas on the pore structure of the ACs and ACFs.

Alcaniz-Monge et al. (1994) used commercially available, isotropic, petroleum-based pitch as a precursor and prepared ACFs. They carried out the activation processes at 887˚C under steam and CO_2 flow. Their detailed analysis of pore structure, tensile strength, and pore diameter clearly showed that there is a significant difference in activation mechanisms. According to their studies, although steam has a higher activation rate than carbon dioxide, carbon dioxide creates narrower micropores.

In their study Alcaniz-Monge et al. (1994) showed that at low burn-off levels (14-15%), steam activation creates a more narrow microporosity than CO_2 activation, whereas it is the opposite above 30% burn-off. This change occurs because of the difference in activation mechanism with two different agents. In steam activation, the

34

volume of narrow micropores remains almost constant at their value at ~15% burn-off, and significant pore widening occurs at higher burn-offs (above 36% in their case), resulting in the formation of super micropores and mesopores. On the other hand, during CO_2 activation the narrow porosity continuously increases with increasing burn-off level, showing that the formation of narrow pores continues even at high burn-off levels.

It is also of interest to look at the effect of the two activation gases on fiber diameter. After the initial stages, steam activation causes a continuous decrease in fiber diameter, whereas in CO_2 activation the fiber diameter remains almost constant after a small initial decrease. However, fibers activated with CO_2 exhibit larger decreases in tensile strength vs. those activated with steam.

In summary, steam activation creates larger-sized pores, causing a decrease in fiber diameter and keeping the tensile strength higher due to more external burn-off, while CO_2 activation generates a narrower pore distribution by penetrating deeper into the fiber core, with a more significant loss in tensile strength.

Alcaniz-Monge et al. (1994) explained that the more uniform pore formation of CO_2 activation was a result of CO_2 having a higher configurational diffusion (diffusion in narrow micropososity) coefficient. However, Walker (1996) disagreed with this reasoning. He pointed out that Koresh et al. (1980) showed that steam has a smaller critical molecular dimension than CO_2 through diffusion in molecular-sieve carbons. Thus, steam would be expected to diffuse faster through narrow micropores. Also in larger pores, steam would also have a higher Knudsen diffusivity because of its lower molecular weight (Wheeler, 1951). Walker (1996) claimed that the more uniform pore

35

formation during CO_2 activation is caused by (i) the lower activation rate and (ii) the higher product inhibition effect of H_2 vs. CO, and thus concluded that the intentional addition of the activation reaction products (CO or H_2) into the activation process might lead to a more uniform gasification reaction and superior microporosity development. However, in 1997 Alcaniz-Monge et al. showed that the activation rate does not cause any significant change in pore formation, and that the inhibition effects of CO and H_2 are not so different as to cause the observed differences in porosity using CO_2 vs. steam. Furthermore, they did some activation experiments in the presence of 5% CO or H_2 as suggested by Walker (1996), and they did not observe any change in porosity. They thus concluded that the difference in porosity most probably was because of the difference in configurational diffusivities between CO_2 and steam.

Molin-Sabio et al. (1996) also did a study on carbon activation using steam and CO_2 as activating agents. They used char made from olive stones as a precursor and did not make fibers. However, their findings in terms of pore formation and widening were similar to the results of Alcaniz-Monge et al. (1994) on ACFs.

Lozano-Castello et al. (2002) also conducted a similar study, in which they investigated porosity in commercial petroleum pitch-based isotropic carbon fibers activated both via CO_2 activation and steam activation. They carried out single-fiber tests using microbeam small-angle X-ray scattering for the investigation of pore formation along the fiber diameter. Their findings supported the previous studies, in which CO_2 activation creates more homogenous porosity throughout the fiber core, whereas steam activation creates pores mostly in the external regions of the fibers.

36

All fibers used in this dissertation were prepared using CO_2 as an activating agent; thus, the above studies are important because they provide information about the CO_2 activation mechanism and the importance of diffusivity of the activating agent inside the pores.

1.5.2 Chemical activation

Because the mechanism of physical activation is based on widening of the rudimentary pores already existing in the parent precursor (Rodriguez-Reinoso et al., 1989; Rodriguez-Reinoso and Linares-Solano, 1989), and because variables such as temperature, pressure, and heating rate have a limited effect on the micropore structure (Gonzales et al., 1997), chemical activation is an alternative for controlling pore size distribution. However, only a few of the studies with chemical activation are based on ACs in the fiber form. For the chemical activation of precursors with a specific shape such as granular or fiber, impregnation of the activating reagent into the precursor is very important (Marsh and Reinoso, 2006). This step is usually carried out by dissolving the reagent in water, mixing with the precursor, and keeping the mixture at approximately 85 ˚C (Marsh and Reinoso, 2006). This process helps the reagent reach the interior regions of the precursor. After the impregnation step, the precursor is carbonized under nitrogen flow, during which the activation occurs. Following this step, samples are typically washed in order to remove any remaining chemicals.

Agullo et al. (2004) studied the preparation of pitch-based ACFs using chemical activation. They compared the effect of physical activation vs. chemical activation on

milled carbon fibers (i.e., carbon fibers that were cut into short pieces) made from coal-tar pitch, using NaOH and KOH as chemical activating agents. Then, for comparison they used CO_2 as a physical activating agent. Agullo et al. (2004) concluded that chemically ACFs gave higher yields with narrower pore distributions (using KOH as activating agent) or similar pores with higher pore volume (using NaOH as activating agent). Also, they discovered that the surface of the fibers activated using chemical agents was smoother and less damaged.

In 2004, Kim et al. compared the pore structure of mesophase and isotropic pitch-based carbon fibers that were subjected to chemical activation using KOH as the activating agent. Similar to Agullo et al. (2004), they also milled the fibers prior to the impregnation process with KOH. They investigated the effect of increasing KOH/precursor ratio on pore development. Results indicated that with increasing ratio, the size of the pores of isotropic ACFs increased gradually, whereas the size of the pores of mesophase ACFs increased in a stepwise manner. Also, although isotropic ACFs had higher specific surface areas and nitrogen uptake, Kim et al. found that mesophase ACFs had narrower pore size distributions.

Lozano-Castello et al. (2006) conducted a similar study, in which they investigated pore formation in both pitch-based isotropic carbon fibers and anisotropic PAN fibers during chemical activation. However, unlike the above-mentioned studies, they did not used milled fibers. Instead, they carried out single-fiber tests using microbeam small-angle X-ray scattering. Using this method, they investigated pore formation for a single fiber diameter. They found that activating agents reached the center

of the anisotropic fibers, as well as the isotropic fibers, and caused the formation of porosity. They, also concluded that porosity was developed more homogenously along the fiber diameter of the isotropic fibers via chemical (Lozano-Castello et al., 2006) vs. physical (with CO_2) activation (Lozano-Castello et al., 2002).

S. J. Park et al. (2003) prepared ACFs using a combination of physical and chemical activation. They used nitric acid to improve surface functionality of the ACFs initially prepared by steam (physical) activation. Although the specific surface area and pore volume of the steam-activated carbon fibers dropped upon nitric acid treatment, they observed that carboxyl groups were created on pore surface. Therefore, their results show that the chemical nature of the pore surface can be modified via chemical activation.

In summary, these studies showed that chemical activation can create more homogenous and narrower porosity than physical activation, and can also be used for activating anisotropic pitches. Therefore, it might be a good alternative for future studies that would investigate the porosity formation of fibers produced from precursors similar to the ones used in this dissertation.

1.5.3 The Effect of Precursor Type on the Preparation Process and Final Properties of Pitch-Based ACFs

Compared to conventional powder and granular ACs, activated carbon in the fiber form exhibits higher adsorption/desorption rates and capacities, which makes it attractive for adsorption applications (Vilaplana-Ortego et al., 2008). However, the spinnability requirement of ACFs limits the precursors that can be used and also increases production

costs. Therefore, there is still a search for better precursors and preparation methods (Suzuki, 1994; Vilaplana-Ortego et al., 2003 and 2007; Park et al., 2003).

Among the different materials that have been evaluated as precursors for ACFs (such as rayon (Huidobro et al., 2001), nomex (Blanco-Lopez, 2000), phenolic resin (Worasuwannarak et al., 2003), and pitches (Alcaniz-Monge et al., 1994; Uraki et al., 2001; Derbyshire et al., 2001; Alcaniz-Monge et al., 1997), pitch appears to be the most attractive because of its low cost and high carbonization yield (Alcaniz-Monge et al., 1994 and 1997).

In 1992, Ehrburger et al. investigated ACs that were prepared from three different precursors: mesophase microbeads with a 10-µm mean particle diameter, pre-oxidized polyacrylonitrile (PAN) fibers with a mean fiber diameter of 12 µm, and phenolic (PH) fibers with a mean fiber diameter of 14 µm. The precursors were investigated by optical microscopy prior to the carbonization and activation processes. While the mesophase microbeads were found to be highly anisotropic, the PAN fibers had a slightly oriented texture and the PH fibers were isotropic. Precursors were activated using CO_2 as an activating gas. Ehrburger et al. (1992) calculated the narrow micropore volumes of activated samples from their CO_2 adsorption isotherms measured at 0 ˚C and found that activated PH fibers created the highest micropore volume (i.e., 0.49 cm^3/g at 54% burn-off), while PAN fibers created 0.18 cm^3/g at 51% burn-off, and activated mesophase microbeads created 0.07 cm^3/g at 47% burn-off. Although all precursors were from different origins, these results are an indication of the negative effect of anisotropy on physical (CO_2) activation and pore formation. Ehrburger et al. (1992) not only

investigated micropore volume, but they also investigated the change in active surface area with increasing extent of activation. The ratio of the active surface area to the micropore volume was essentially the same for all three activated samples, and was very low (just a few % of the total area). Because active surface area (ASA) is directly related to the edge planes, where most of the atom vacancies, dislocations, and stacking faults are present, and because this ratio of ASA/micropore volume was very low and was the same for all three precursors, Ehrburger et al. (1992) concluded that the micropore walls are mainly made up of basal planes (i.e., lateral surfaces of defective micrographene layers). They also showed that isotropic (i.e., PH) fibers were the best among the three precursors in terms of high micropore volume.

In 2000, Daguerre et al. prepared ACs from toluene-insoluble fractions of heat-treated A-240 petroleum pitch, using carbon dioxide as an activating agent. The precursor preparation part of their work was conceptually similar to our work at Clemson. In both studies, precursors were prepared by fractionation of petroleum pitch using toluene as a solvent, although in our study the solvent was employed at dense-gas conditions. Because solvent density and temperature can be controlled in addition to solvent/pitch ratio in dense-gas extraction, we had better control over the fractionation process in this study. Also, Daguerre et al. (2000) analyzed their pitch fractions only for toluene- and quinoline-soluble contents, whereas in our study detailed mol wt distributions, and softening points of the fractions were determined. Furthermore, they prepared their ACs in powder form instead of fiber form. Because the motivation of their study was the use

41

of ACs for refrigerating machines, they used high-pressure carbon dioxide for the adsorption analysis and determined pore structure information from that data.

In their experiments, Daguerre et al. removed the toluene solubles (TS) via mixed-solvent extraction (Riggs and Diefendorf, 1980), using two different solvent/pitch ratios to obtain precursor precipitates consisting primarily of toluene insolubles. In particular, they obtained two precursors: one with 12% TS and the other with 5% TS. It should also be noted that both precursors had a ~20% quinoline-insoluble fraction, which was identified as having mesophase domains by polarized-light microscopy (Brooks and Taylor, 1968). The 5% TS showed a higher activation rate. Daguerre et al. concluded that this was the result of smaller mean particle diameters of the 5% TS precursor ($<20\mu m$ vs. $<40\mu m$), induced by the extraction process, and the possible differences in reactivities induced by the TS. When the ACs from the two precursors at similar burn-off levels were compared, the fibers produced using the precursor with lower TS content had significantly higher micropore volumes without a significant increase in mean pore size.

Although Daguerre et al. (2000) did not determine any mol wt information for the two precursors, based on extraction conditions (solvent/pitch ratio) and TS content one would expect the 5% TS precursor to have a higher average mol wt than the 12% TS. Based on this assumption, their results indicate that the higher mol wt precursor created higher micropore volume — which is completely the opposite of our findings in this dissertation (see Chapter 3 Results and Discussion).

In their pioneering work in this area, Derbyshire et al. (2001) showed that the precursor used to prepare the ACFs has an important effect on both the preparation

process and the final properties of the ACFs. The group investigated carbon fibers from isotropic non-conventional precursors, such as coal-tar pitch, coal solutions (i.e., solvent extracts of a bituminous and sub-bituminous coal), shale oil, and petroleum pitch. They characterized precursors for elemental analysis, mol wt distribution, and aromaticity, and studied the effect of precursor composition on the stabilization process, carbonization yield, activation rate, and final-fiber properties. To render the precursors more suitable for the production of ACFs, they removed the quinoline insolubles (QI) by filtration if the precursor had more than 0.5% QI by weight; they also carried out distillation, if needed, to increase the softening point of precursors to the range of 230-260 ˚C, temperatures that are suitable for melt-spinning fibers.

Derbyshire et al. (2001) used gel permeation chromatography (GPC) to analyze the mol wt distribution of the precursors. Therefore, only the THF-soluble portion of each precursor could be analyzed. Since they did not have any calibration standards for the analysis of their precursors, they could not obtain absolute mol wt distributions. They observed that all the precursors that were analyzed for mol wt distribution had a common GPC peak, and this peak was taken as reference. Using this reference peak, they defined peaks before this peak as high mol wt and after this peak as low mol wt, and made a relative comparison between the mol wt of precursors. They only presented mol wt results vs. tensile strength, and not vs. pore volume.

Derbyshire et al. (2001) found that with increasing carbon content of the precursor, both the oxidation weight gain and the carbonization yield increased. The activation rate was also found to increase with increasing heteroatom (i.e., H, O, N and S)

43

content, especially O content of the precursor. The activation rate was also found to be higher for precursors of higher aliphatic content. They didn't reach any significant conclusions on porosity, as all samples had different burn-off levels, and some of the samples were not large enough to obtain reliable surface analysis data. Among the analyzed samples, ACFs prepared from coal-tar pitch, with a 57% burn-off and a high hetero-atom content, were found to have the highest micropore volume.

The work of Derbyshire et al. (2001) is important because it compares ACFs produced from isotropic precursors from different origins with different compositions. Although they provided information about the carbon content, aromaticity, and heteroatom content of the precursors, and the effect of these precursor properties on processing conditions and final properties of the ACFs, their results did not give sufficient information about the pore structure of the ACFs, which is one of the key properties of the ACFs. In our study, unlike Derbyshire et al. (2001), we prepared all precursors from the same mother pitch M-50 with a known molecular composition (Burgess and Thies, 2010, 2011) and focused on the absolute mol wt distributions of the precursors and the porosity of the final ACFs. Also, CO_2 was used as an activating agent in our study, while Derbyshire et al. (2001) used steam. As mentioned before in this chapter, steam and CO_2 have different activation mechanisms, and this difference may result in differences in the effect of precursor composition on final properties.

Edie and coworkers (Basova et al., 2004) compared two isotropic petroleum pitches, one from Chungham National University, Korea, and one from Conoco-Philips Inc., Oklahoma. They prepared ACFs from both precursors and from their mixtures with

silver nitrate. They used matrix-assisted laser desorption/ionization time of flight (MALDI-TOF) and gas chromatography (GC) mass spectroscopy (MS) to determine the mol wt distributions of the precursors, and the composition of the lower mol wt (<300 Da) species, respectively. MALDI showed that the Korean pitch had a broad mol wt distribution (~200-1250 Da), with a maximum at ~400 Da, while Conoco pitch had a polymer-like oligomeric distribution (~200-1150 Da), with maxima at 250, 500, 750, and 1000 Da for each oligomeric group. GC-MS showed that the Korean pitch had a higher concentration of disc-shaped polycyclic aromatic hydrocarbons (PAH), while the Conoco pitch had more (linear) open PAH structures.

Their study (Basova et al., 2004) showed that the Korean pitch fibers could be activated significantly faster than the Conoco pitch fibers. Also silver particles catalyzed the activation process for both precursors, increasing both the activation rate and the mesopore ratio. Even at similar burn-off levels, silver-containing fibers had a significantly higher mesopore ratio. The effect of silver particles on the pore structure was less pronounced for the Conoco vs. the Korean fibers. This shows that precursor composition plays an important role in determining the final pore structure of the ACFs prepared from different pitches.

Vilaplana-Ortego et al. (2008) conducted a detailed study of the effect of precursor on the pore structure of ACFs, using CO_2 as the activating gas. They compared four isotropic coal-tar pitches to four isotropic petroleum pitches. Each precursor was subjected to elemental analysis, and the toluene insolubles, quinoline insolubles, and softening point of each precursor were measured. The main differences between coal-tar

and petroleum pitches used in their study were that the petroleum pitches had higher H/C ratios and slightly higher C content (2-3%), while coal-tar pitches had significant S + O content and higher toluene-insoluble content.

As a result of reactivity experiments conducted with a microbalance, Vilaplana-Ortego et al. (2008) observed that the CO_2 activation rate of coal-tar pitch-based fibers was higher. They claimed that the difference in the reactivity could have been caused by the carbon microstructure that exists after carbonization. The carbonization yield of petroleum-pitch-based carbon fibers was 60-70%, while that of coal-tar-based carbon fibers was around 85%. According to Vilaplana-Ortego et al. (2008), this difference could have been caused by the higher content of alkyl groups in the petroleum pitch carbon fibers. These alkyl groups would likely generate more radicals during the carbonization process and result in subsequent condensation reactions. As a result, better-packed graphene layers could form (Lewis, 1982) during carbonization, causing less reactivity during the activation process. Although Vilaplana-Ortego et al. did not mention it in their discussions, the higher activation rate of coal-tar pitches could be attributable to their higher hetero-atom content of ~8% vs. the ~5% in petroleum pitches.

Vilaplana-Ortego (2008) did not focus on the differences among ACFs from the same type of pitch (i.e., petroleum pitch or coal-tar pitch), but the differences between petroleum and coal-tar pitch. They observed some differences in activation rates as mentioned above. Also, they concluded that ACFs prepared from both precursor types exhibited comparable micropore volumes based on total weight loss (carbonization + activation), whereas petroleum pitches, which had a higher H/C ratio, developed a higher

46

proportion of narrow microporosity. In our studies, on the other hand, we have shown that ACFs with similar direct activation (carbonization + activation) weight losses not only have differences in their narrow micropore volume, but also in their total micropore volume. Details of these studies are given in Chapter 3, Results and Discussion.

1.6 Synopsis and Dissertation Outline

Although researchers have investigated the effect of the precursor on the final properties of ACs, or ACFs, the precursors used and compared in those studies were from different origins, for example coal-tar pitch vs. petroleum pitch, and were not well characterized. In particular, detailed information about the molecular composition and anisotropy of those precursors was not available.

The objective of this study was to compare ACFs prepared from precursors with a well-defined composition coming from the same origin (i.e., mother pitch), in order to investigate the effect of molecular composition and molecular order on pore structure (i.e., pore size distribution).

Therefore, seven selected fractions of a commercially produced isotropic petroleum pitch (i.e., Marathon M-50), each of relatively well-defined composition and mol wt distribution, were prepared and used for the production of ACFs. Four of these fractions were chosen as fully isotropic, and three of them were chosen with different levels of mesophase; thus, the effects of both molecular composition and molecular order (i.e., mesophase content) could be isolated from each other.

In Chapter 2, the procedure for the preparation of the precursors is explained. Five precursors were prepared using single-column dense-gas extraction (DGE), while other two, middle-cut, dimer precursors were prepared via the combination of single-column DGE with either low-pressure stripping or vacuum evaporation. Next, the procedures for the conversion of these precursors into ACFs via spinning, stabilization, carbonization and direct activation are described. Finally, the analytical techniques used to determine the properties of the precursors and the fibers, such as molecular weight distribution, softening point, molecular order, and pore size distribution, are given.

In Chapter 3, the properties of all precursors are presented. Their softening points and molecular weight distributions are compared. Also, polarized-light photomicrographs are presented, and the mesophase area percentage of the mesophase-containing precursors is given. The weight gains of the fibers during oxidation, and their weight loss during carbonization and direct-activation, are compared, and the effects of molecular composition and molecular order on the weight change of the fibers are discussed. Nitrogen isotherms at -196 ˚C and pore size distributions (PSD) of the direct-activated fibers interpreted from these isotherms using density functional theory assuming slit-shaped pores are compared. The change in PSD with mol wt distribution and presence of mesophase is discussed. Finally, the change in burn-off and PSD with activation time is discussed.

In Chapter 4, conclusions from this study are given, and recommendations for future work are made.

2 EXPERIMENTAL

In this study, an isotropic petroleum pitch was fractionated in order to obtain seven precursors with different compositions. These fractions were analyzed for Mettler softening point (MSP), optical anisotropy, and mol wt distribution. Activated carbon fibers (ACF) were prepared from these seven different precursors. During preparation (oxidation, carbonization, and direct activation) weight changes were recorded, and nitrogen adsorption isotherms of ACFs were obtained for porosity analysis.

In our early studies in Clemson University in collaboration with Oak Ridge National Laboratory (ORNL), we worked on Pd-containing, pitch-based ACFs. The goal of that work was to investigate and improve the hydrogen-storage capabilities of ACFs by both controlling the pore size distribution and by the addition of Pd metal complexes to the precursor prior to the spinning process. It was observed that Pd particles were well-distributed in green fibers; however, they traveled and agglomerated during the high-temperature processes of carbonization and activation. In order to minimize this sintering problem, we decided to minimize the exposure temperature and time. Therefore, we started to direct-activate (i.e., simultaneous carbonization and activation) the stabilized fibers, and also decreased the activation temperature from 900°C down to 840°C. After observing that we obtained ACFs with similar porosity as in the conventional two-step carbonization and activation process at 900 °C, we adopted the direct-activation method at 840 °C for the preparation of all ACFs used in this study.

2.1 Precursor Preparation

2.1.1 Materials

In order to produce ACFs, isotropic petroleum pitch with a reported softening point of 104–124 °C (the MSP was measured to be 116 °C in our labs) was obtained from Marathon Petroleum Company LLC (CAS 68187-58-6). The pitch, known as M-50, was received in pellet form and used without further modification. HPLC-grade toluene (CAS 108-88-3) with a stated purity of 99.9% was obtained from Fisher Scientific and used for the DGE fractionation of M-50 pitch. For MALDI analysis, 7,7,8,8-tetracyanoquinodimethane (TCNQ, CAS 1518-16-7) was obtained from TCI America. TCNQ was used as a matrix for MALDI samples. For preparation of Pd-containing fibers, $Pd(acac)_2$ (Palladium(II) 2,4 – pentanedionate, Pd 34.7%) (CAS 14024-61-4) was obtained from Alfa Aesar. Coleman Grade carbon dioxide gas (UN1013, 114041) for activation experiments and UHP Helium gas for free space measurement during porosity analysis was supplied by National Welders. Nitrogen was also supplied by National Welders as liquid nitrogen (99.99% purity) in a central tank, where it was distributed to the labs. Nitrogen gas was used for both carbonization experiments and adsorption isotherm measurements.

2.1.2 Precursor Production via Single-Column DGE

Several petroleum-pitch precursors, each with a different molecular weight distribution and composition, were used for the preparation of ACF. These precursors were produced from the fractionation of M-50 pitch by dense-gas/supercritical extraction

(DGE). For production of one of the precursors (Dimer-2), further fractionation was carried out using a vacuum oven, as explained later in this chapter. A brief description of the DGE process is given here; a detailed description of the apparatus and procedure is given elsewhere (Edwards and Thies, 2006, Cervo and Thies, 2010).

For production of the first five precursors, referred to as 750psig, 760psig, 780psig, 800psig, and 830psig (the extraction pressures were used to name the precursors), a single packed column was used as shown in Fig. 2.1. The extraction apparatus consists of a stainless steel column with an i.d. of 1.8 cm and a height of 2.0 m, with random stainless steel packing (Cannon Instrument Co., part no. 3947-A20). The packed height of the column is 1.5 m. Pitch is fed to the top of the column in molten form (at ~300 °C) at a flow rate of ~120 g/h via a single-screw extruder (Alex James and Assoc., model no. AJA 58) and a metering pump (Zenith Pumps, Model HPB, 0.160 ml/rev). An HPLC pump is used to deliver the extraction solvent, in this case toluene (P_c = 41.1 bar, T_c = 318.6 °C), to the bottom of the column at ~600 g/h. Pressurized toluene is preheated before being fed to the column.
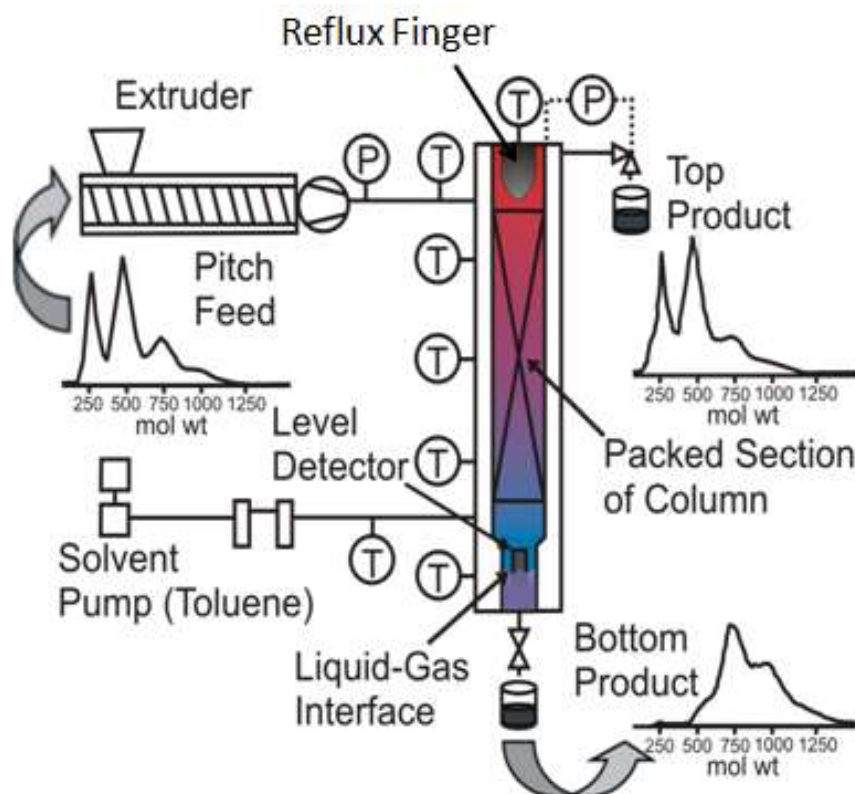
Fig. 2.1 Single-column, dense-gas/supercritical extraction (DGE) apparatus for continuous fractionation of M-50 petroleum pitch. 750psig, 760psig, 780psig, 800psig and 830psig precursors were produced using this setup. Typical normalized MALDI mass spectra for the feed pitch and outlet products are also shown. (Reprinted with permission from Cervo, 2010a. Copyright 2010 Dr. Eduardo Cervo.)

During the process, the dense-gas toluene flows upward through the packing and the molten pitch downwards due to density differences. During contact, the lower molecular weight (mol wt) species are stripped from the pitch into the solvent-rich phase according to the extraction temperature and pressure, while some of the solvent is absorbed into the pitch-rich phase. The lower mol wt oligomers concentrated in the solvent-rich phase (monomer, dimer, and trimer) are taken off as top product, while the higher mol wt oligomers (dimer, trimer, tetramer and heavier) that are not extracted are

taken off as pitch-rich bottom product. The reflux finger, that is, the bullet-shaped object at the top of the column shown in **Fig. 2.1**, is used to improve product selectivity by being kept at a higher temperature than the rest of the column.

The column temperature was kept at 350 °C throughout the entire column, and the column pressure was kept at the desired pressure for each precursor, i.e., 750, 760, 780, 800, and 830 psig, respectively. The solvent-to-pitch (S/P) ratio was kept constant at 5.1:1, and the bottom products were collected as the desired precursors. For collection, glass jars immersed in an ice bath were used, and 100-150 g of total product were collected. **Table 2.1** summarizes the extraction conditions that were used.

Collected bottom products were dried in order to remove the solvent. First, samples were dried under N_2 at 150 °C and 2 mbar for 30 min in a vacuum oven (Fisher Scientific, model no. 285A). This step evaporated 98 wt% of the toluene. However, in order to spin fibers the remaining solvent had to be removed, or it would volatilize during the spinning process, causing fiber breakage. Thus, a second drying of the samples was carried out at 20-30 °C above their approximate softening points (see below) under N_2 at 267 mbar (which is the min pressure attainable by the oven) for 30 min using a Vacuum Atmospheres Model VTW Vacuum Oven connected to a Model Dri-Lab-08/85 nitrogen glove box. (Typical glove box conditions were 0.5 ppm O_2 and 1 ppm water content.) Because some of the samples had softening points as high as 340 ℃ and had to be dried at 360-370℃, the drying time was limited to 30 min in order to prevent any probable reaction among precursor molecules.

Table 2.1   Summary of the production conditions for all seven precursors.

Precursor	Column 1 (DGE/SCE Column)				Column 2 (High-temperature Stripper)			
Name	Temperature (°C)	Pressure (psig)	S/P	Stream	Temperature (°C)	Pressure (psig)	S/P	Stream
750 psig	350	750	5.1/1	Bottom	-	-	-	-
760 psig	350	760	5.1/1	Bottom	-	-	-	-
780 psig	350	780	5.1/1	Bottom	-	-	-	-
800 psig	350	800	5.1/1	Bottom	-	-	-	-
830 psig	350	830	5.1/1	Bottom	-	-	-	-
Dimer-1	ΔT (330-350-380)	1000	5.1/1	Top	380	22	13.6/1	Bottom
Dimer-2	ΔT (350-380-400)	1000	12.1/1	Top	Vacuum Oven, 30 min	350°C, 0.03 psig	-	-

Approximate softening points were measured using a temperature-monitored hot plate (i.e., Fisher-Johns Melting Point Apparatus, serial no. 1833) in order to establish the second drying temperature. This method was preferred because it was quicker, and easier to use than MSP apparatus, and only approximate softening point values were required at this point.

2.1.3 Production of Dimer-1: Two-Column Extraction:

As discussed above, the first five precursors were fractionated isothermally in a single-stage, isothermal DGE setup. On the other hand, the precursors Dimer-1 and Dimer-2 were generated using a different procedure. Dimer-1 was obtained using two packed columns operating in series (**Fig. 2.2**), with the first column (Col-1) being
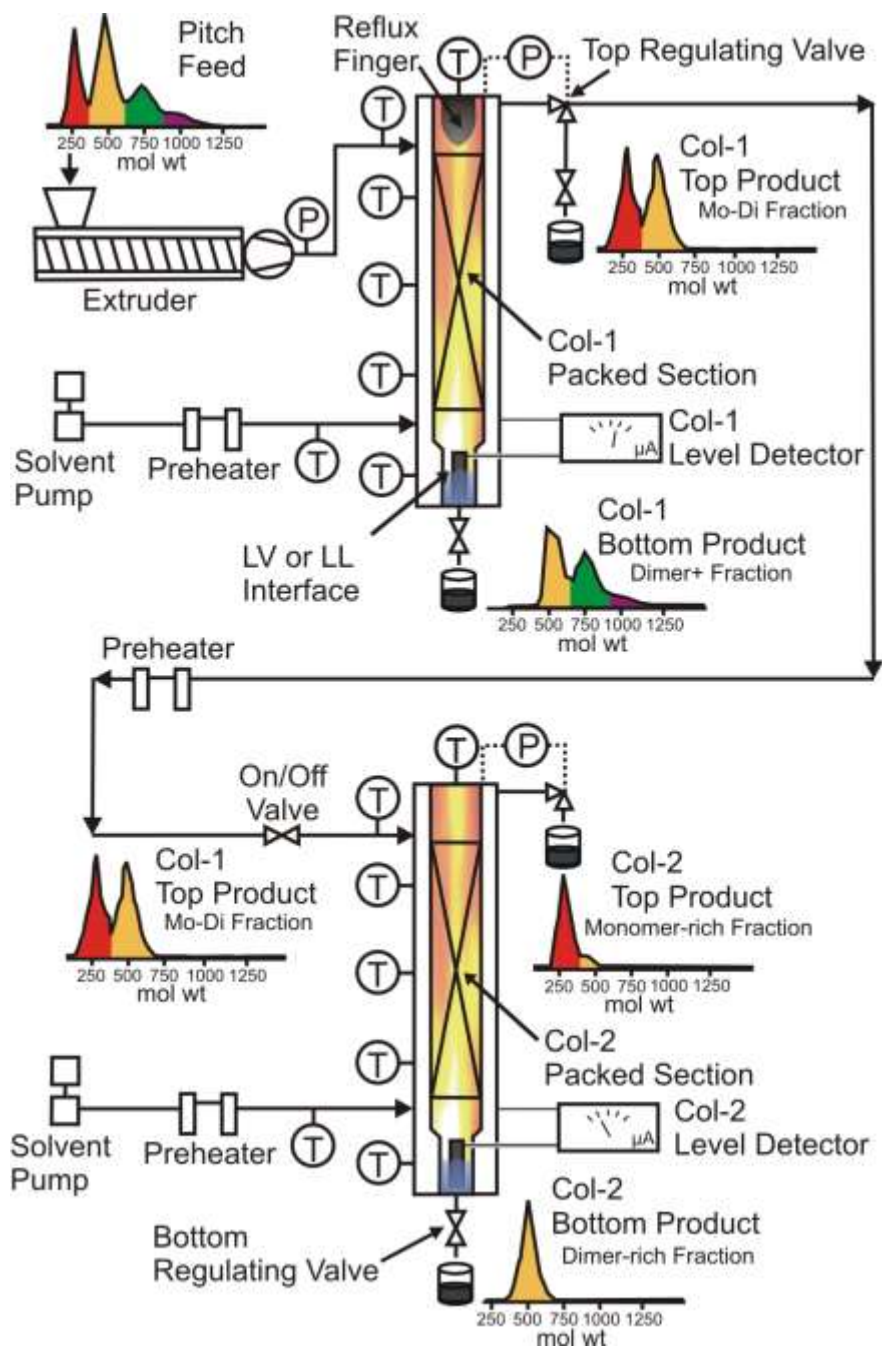
Fig. 2.2   Two-column solvent extraction apparatus for continuous fractionation of M-50 petroleum pitch, with Col-1 operated at dense-gas/supercritical extraction (DGE) conditions and Col-2 as a low-pressure stripper. Dimer-1 precursor was produced using this setup. Normalized MALDI mass spectra shown in the figure are representative of the actual spectra. (Reprinted with permission from Cervo, 2010a. Copyright 2010 Dr. Eduardo Cervo.)

operated under DGE conditions in order to extract a monomer-dimer mixture, and the second column (Col-2) at atmospheric pressure as a high-temperature stripper to remove monomeric species. In particular, Col-1 was operated at 1000 psig and a S/P ratio of 5.1/1 under a positive temperature gradient (ΔT), with the bottom of the column at 330 ˚C, the middle at 350 ˚C, and the top at 380 ˚C. Col-2 was operated at 380 ˚C, at atmospheric pressure, and a S/P ratio of 13.6/1.

As shown in the MALDI cartoon for Col-1 in **Fig. 2.2,** the top product stream from Col-1 is composed of monomer and dimer species. This stream is then reduced to near atmospheric pressure and preheated to 380 ˚C prior to being fed to Col-2. In Col-2, the monomer species are stripped out and a bottom product rich in dimer species is obtained. The stripping agent, hot gaseous toluene, is fed to the bottom of Col-2 at a rate of 544 g/hr. Dimer-1, which is rich in dimer species, was collected as the bottom product of Col-2 at a rate of ~10 g/hr for 5 hr in order to obtain a total of ~50 g of product. It was collected in a glass jar immersed in ice bath, and dried using the same procedure as described above for the first five precursors.

2.1.4 Production of Dimer-2: Single-Column DGE and Vacuum Oven Separation

Dimer-2 was produced by using single-column DGE to obtain a monomer/dimer top product, as was done with Dimer-1. The S/P ratio was 12.1/1, and a different temperature profile was also used, namely a positive temperature gradient with the bottom of the column at 350 ˚C, the middle at 380 ˚C, and the top at 400 ˚C. The dimer-

rich Dimer-2 product was then produced by evaporating the monomer species in the Col-1 top product in a vacuum oven, as is described below

The monomer-dimer mixture from top of Col-1 was first dried in a shallow aluminum tray (9"x15") under N_2 at 150 °C and 2 mbar for 30 min in a vacuum oven (Fisher Scientific, model no. 285A) in order to remove most of the toluene. Because the resultant product was very sticky, a small amount of liquid nitrogen was then poured into the tray in order to solidify the pitch. While the product was still solid and brittle, it was broken into small pieces using a spatula; the pieces were then divided among several aluminum trays into ~30 g increments. Dispensing the pieces into thin layers in this way was important for obtaining a thin film of molten pitch, therefore enhancing the diffusion of monomer species from the surface of the film.

Next, each tray was heated to 350 °C under N_2 at ~2 mbar for 30 min using a Vacuum Atmospheres model VTW vacuum oven connected to a model Dri-Lab-08/85 nitrogen glove box. Here volatilization of any remaining residual toluene and of the monomer fraction of the pitch occurred. The yield was around 10% and the resultant product is what we refer to herein as Dimer-2.

2.2 Conversion of Precursors into Activated Carbon Fibers

To make ACFs, the precursors described above were first spun into "green" fibers. Then these as-spun fibers were stabilized (oxidized) in an air convection oven. Finally, the oxidized fibers were directly activated in order to obtain the desired ACFs. A detailed procedure of these steps is given below.

57

2.2.1 Fiber Spinning

For a given run, one of the precursors shown in **Table 2.1** was ground with mortar and pestle; the resultant powder (~40-60 g) was then loaded into the batch-spinning cartridge shown in **Fig. 2.3**. Before loading the precursor, the spinneret along with a mesh filter (Alex and James Inc., part no. RBD3040148.51) that fit perfectly to the spinneret was installed. Anti-seize lubricant (Permatex, item no. 80078) was applied to the spinneret bolts before attaching to the cartridge.

Next, a graphite seal was prepared using graphite tape (Teadit, part no. 2550). Approximately a 1-m length of graphite tape was rolled around the piston tightly, and with the tape wrapped around the piston the piston was placed into the cartridge. As shown in **Fig. 2.3**, the rolled tape fits into space between the piston and cartridge. The pressure cap was placed into its cavity, and the 4 bolts that attach the pressure cap to the cartridge were tightened in the sequence shown in **Fig 2.4**. The purpose of this process was to press the graphite tape firmly in place and thus create the needed seal.

Following this process, the pressure cap was removed, and the nitrogen purge extender and temperature and pressure probes were screwed into place, and the piston was carefully removed in order to load the precursor inside the cartridge. After loading the precursor powder, first the piston and then the pressure cap were replaced, and finally the bolts attaching the pressure cap to the cartridge were screwed in and re-tightened in the appropriate order. Anti-seize lubricant (Permatex, item no. 80078) was applied to the bolts before installation.
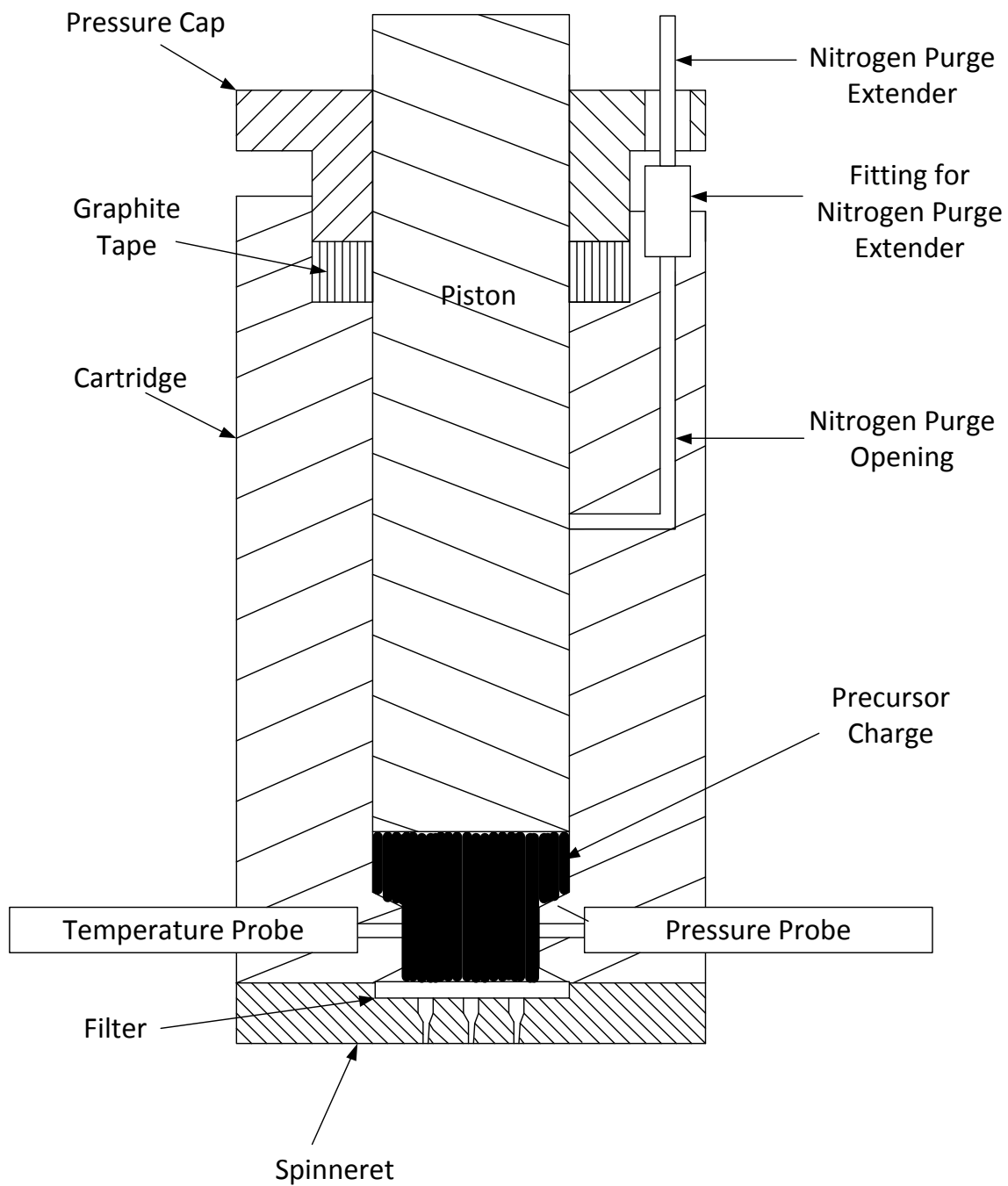
Fig. 2.3   Cross-section of the spinning cartridge used for melt-spinning the precursors shown in **Table 2.1**.
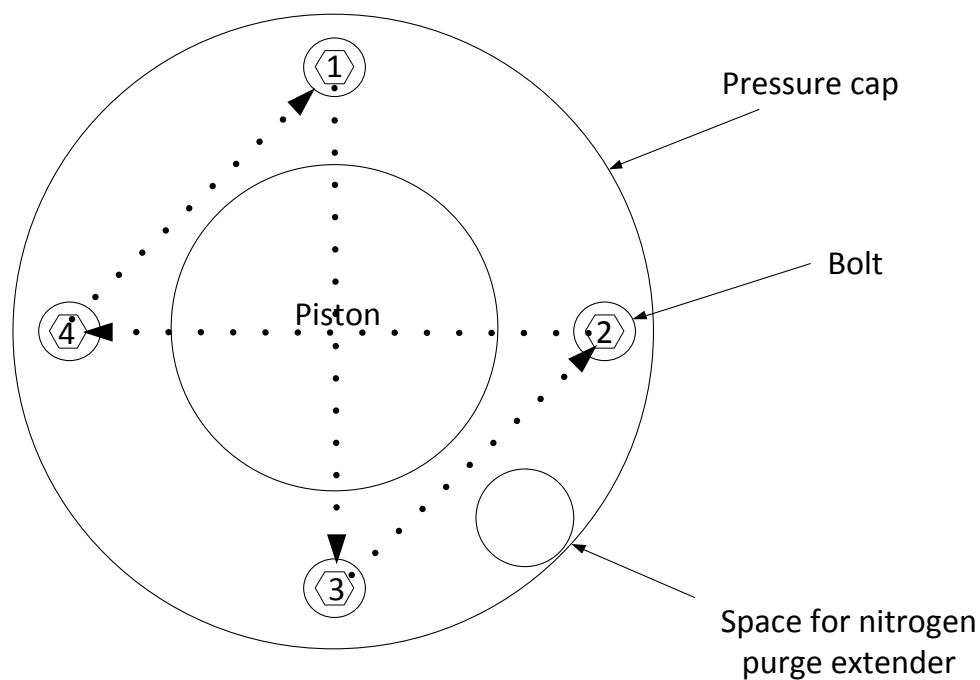
Fig. 2.4 Top view of the spinning cartridge. The arrows show the tightening sequence of the bolts (1,3,2,4,1,3,2,4,…..) necessary to pack the graphite tape evenly for a good seal before loading the precursor.

The loaded cartridge was kept under nitrogen in an antechamber attached to the nitrogen glove box (Vacuum Atmosphere Inc., model no. Dri-Lab-08/85) overnight at room temperature in order to minimize the oxygen level in the cartridge. The gauge attached to the antechamber does not provide a precise pressure reading; however, based on the vacuum level reached by the vacuum oven connected to the same glove box and the same vacuum pump, we can assume it is around 2 mbar. Before leaving the cartridge under vacuum overnight, the antechamber was refilled with nitrogen to atmospheric pressure and then evacuated again. This procedure was repeated 2-3 times in order to minimize any air left inside the antechamber (This is the general procedure used for

transferring any sample or tool into the glove box.) Then the cartridge was attached to the batch-spinning instrument (Alex&James Inc.) (**Fig. 2.5**), and final preparations were made for fiber spinning, as described below.

First the spinning cartridge was placed inside the stationary half of the heating jacket, and the moving half of the jacket was then rotated into place around the cartridge. Using the attached clamps, the halves of the jacket were tightened around the cartridge. Next the temperature and pressure transducers were connected to their respective probes, and the nitrogen line was connected to the extender (**Fig. 2.3**). The nitrogen flow was then started at a regulator outlet pressure of 2 psig, and the jacket temperature was set to the desired temperature (i.e., MSP + 25 ˚C) for a given precursor. (Prior to spinning, the MSP of the precursor was measured; details are given in Section 2.4.2.)

When the melt temperature (as read from the temperature probe embedded inside the cartridge; see **Fig. 2.3**) reached 2-3 ˚C below the set point and the molten pitch started to ooze out of the spinneret, the drive motor was engaged, and the piston was driven by the motor at a constant ram speed of 2 cm^3/min by setting the ram direction to "down" using the switch below the ram speed gauge and switch. Once the cartridge pressure started to build up and molten pitch started to flow out of the spinneret, the winder was set to 400 m/min using the roll speed switch, the filaments were started around the winder with the hands, and fiber collection began. Please note that the winder installed on the instrument (3-15/16 in. diameter) was smaller than the original winder (8-7/8 in. diameter), so the actual winder speed was 177 m/min.
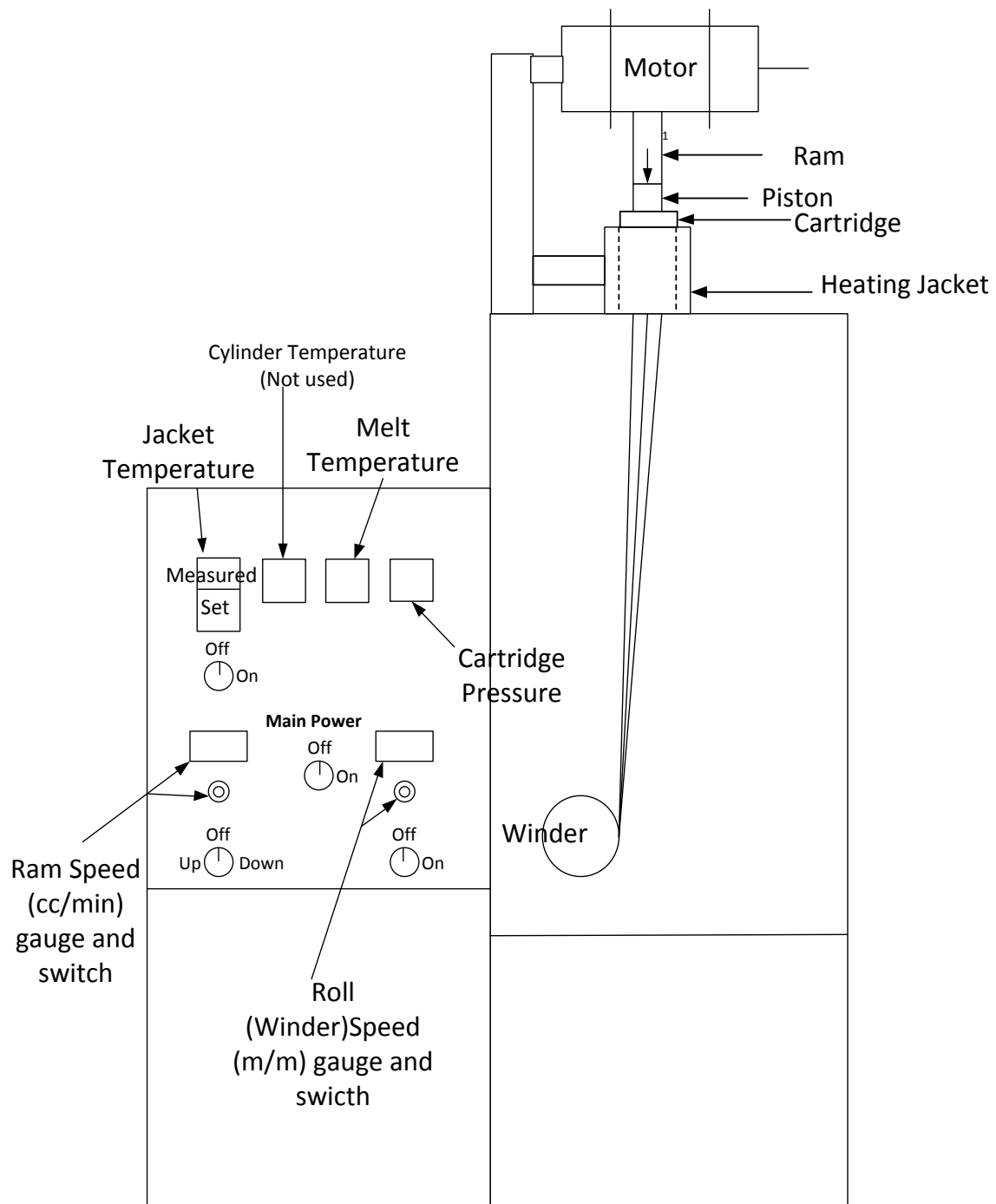
Fig. 2.5 Batch-spinning apparatus. Here the apparatus is shown after the spinning cartridge has been placed under the motor and the heating jackets are enclosed around the cartridge.

Based on visual observation, the temperature for the spinning process was adjusted to obtain minimal fiber breakage and the optimum amount of fibers. All fibers were spun at the same ram and winder speed in order to obtain similar-sized fibers (25-30 μm). After the fibers were collected, they were cut from the bottom part of the winder with a brass spatula, carefully removed, and placed into a tie box in bunches (Yes, tie boxes were used as they were the most suitable boxes for keeping the fibers.) The amount of fibers collected was 2-10 g for different precursors.

2.2.2 Stabilization

Next, the as-spun fibers were stabilized to make them infusible for the subsequent high-temperature heat treatments, so that they would not lose their shape or stick together. First, 2-3 g of fibers were cut into 1-1.5 in.-long pieces and then spread out onto the metal grill in the air convection oven (see **Fig. 2.6**) to allow good air circulation among the fibers. For spreading out the fibers, the bunch was cut and placed onto the metal grill using tweezers to spread them out. If more fibers needed to be oxidized at the same time, an additional metal grill or metal screen was added to the bottom part of the oven. The sides of the metal screen was bent to form 4 in.-long legs so as not to block air flow coming from the bottom part of the oven.

The fibers were then gradually heated up to a final temperature of 264 °C in a Fisher Scientific air convection oven (model no. 825F, **Fig. 2.6**) via a 6-day temperature programming schedule (see **Fig. 2.7**). Because the MSPs of some of the precursors were as low as 202 ˚C, the oxidation process had to start at 150 ˚C, at which the oxidation

reactions are very slow, and the temperature was gradually increased. Therefore, the oxidation process took 6 days. Throughout the stabilization process, sample weights were recorded in order to monitor the weight change that occurred for each temperature level of heat treatment. For this purpose, a 4 in. x 5 in. aluminum sheet (simply made by folding aluminum foil into 3-4 layers) was used. In particular, approximately 0.4-0.5 g of fibers were spread onto this ~2 g aluminum sheet, and the weight of the sheet with the fibers on it was measured at the end of each temperature level shown in **Fig. 2.7** using an Ohaus Corporation AR2140 lab scale.
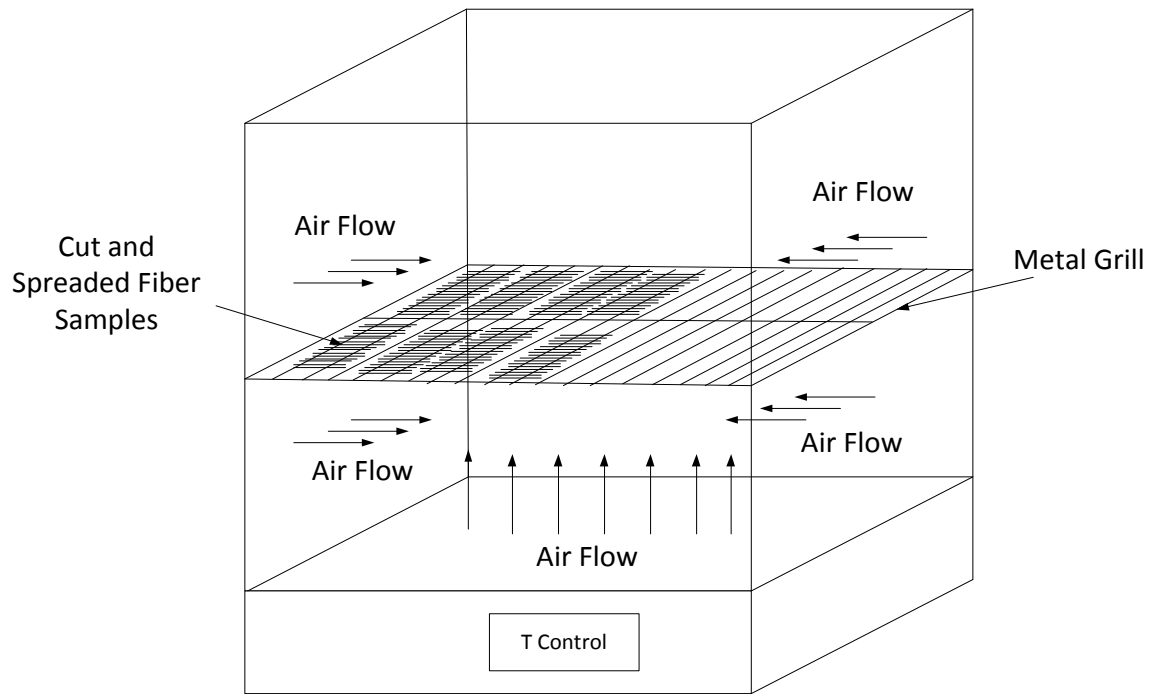
Fig. 2.6   Air convection oven for oxidative stabilization of as-spun fibers.
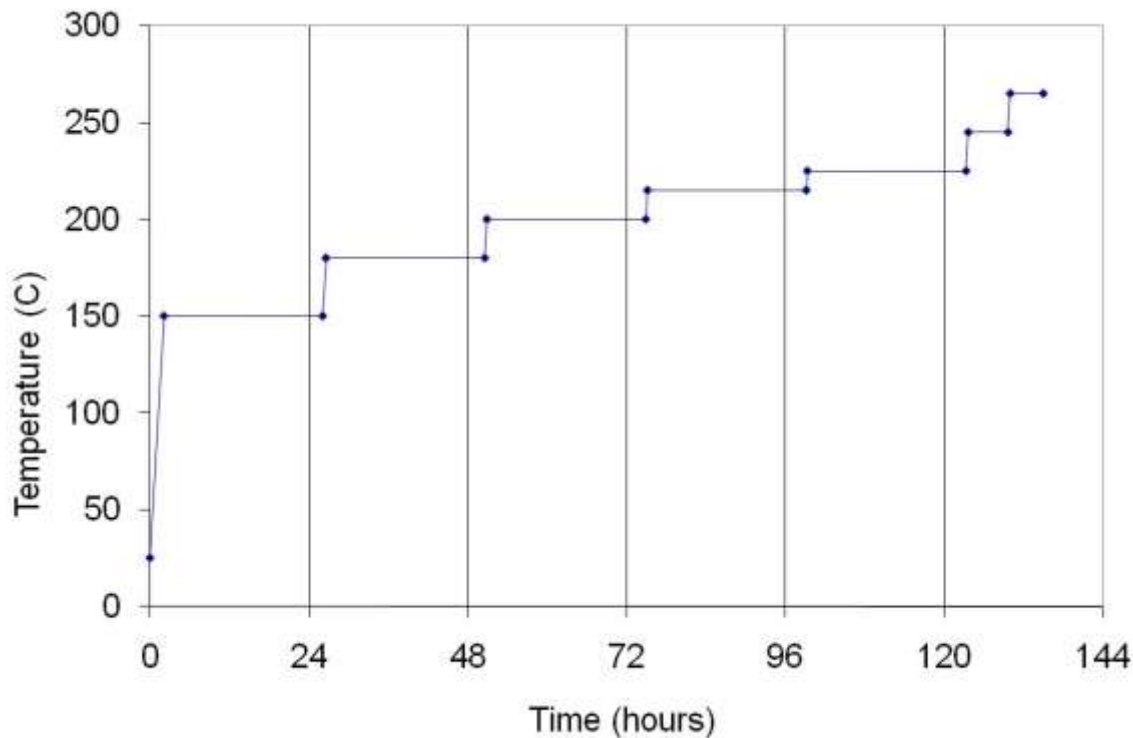
Fig. 2.7   Temperature-programming schedule for the oxidative stabilization of as-
                spun fibers. The same schedule was used for all seven precursors.

2.2.3. Carbonization

Following the stabilization process, 2 sets of fibers (70-75 mg each) from each of

the seven precursors shown in **Table 2.1** were carbonized under a nitrogen flow of 1

L/min in a custom-made Lindberg tubular furnace by General Signal (project no.

9305198); the furnace has an inner diameter of 2.5 in. and a length of 61 in. (**Fig. 2.8**).

The detailed carbonization procedure is given below.

The fiber samples were placed in a quartz boat, or sample holder (Sigma-Aldrich,

model no. Z406627, see **Fig. 2.9**) which is designed for use at high temperatures and can

handle sudden temperature changes. As shown in **Fig. 2.8**, there are three heating zones

(Zone 1, Zone 2, and Zone 3), and they are controlled by temperature controllers T1, T2, and T3, respectively. The temperature in Zone 2 is also measured by using an Omega K-type thermocouple (**Fig. 2.9**). The temperature is set to 875 ˚C in Zone 2 in order to have the 840 ˚C gas temperature as measured by the thermocouple, and is set to 600 ˚C in Zone 1 and Zone 3. Cooling water run through copper tubing wrapped around the ends of the ceramic tube of the tubular furnace was used to keep those (i.e., at points A and B) ends at temperatures below 100 ˚C.
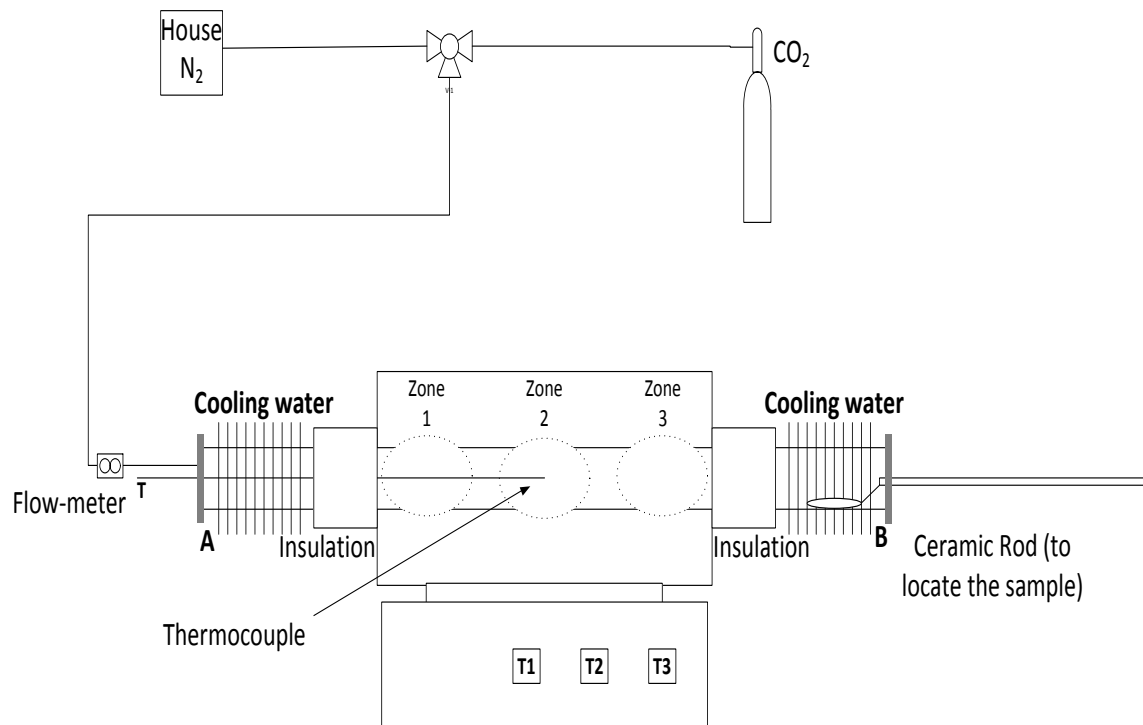
Fig. 2.8   Tubular furnace for carbonization and activation experiments. The furnace can be operated under N_2 or CO_2 flow. The ceramic rod is used to push the quartz boat (with samples) into Zone 2 inside the furnace.
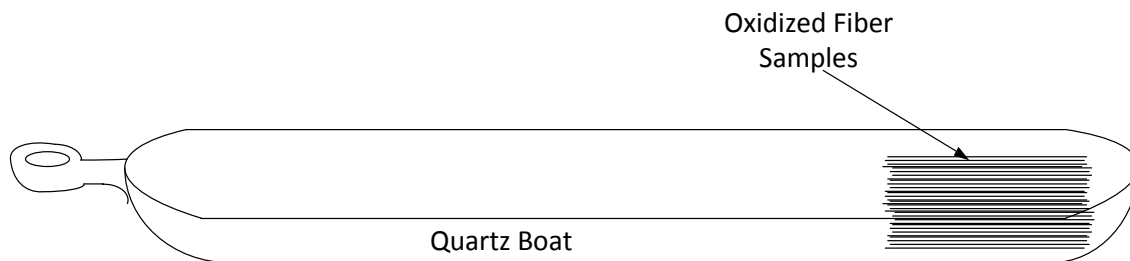
Fig. 2.9   Quartz sample holder (boat) used for high-temperature heat treatments (i.e., carbonization and activation). Fibers are placed at the end of the boat as shown.

Prior to carbonization, the boat with sample is first placed inside the furnace, at the "B" end of the tube, and is kept there under 1 L/min nitrogen flow for 1 hr in order to remove any air (oxygen) left inside the furnace during sample loading by removing the cover. While placing the boat inside the furnace, the boat is attached to a metal hook connected to a thin long ceramic rod, which passes through the small opening in the cover (**Fig. 2.10**). Using the rod, the boat along with the fibers is pushed to the center of the furnace (Zone 2).

After 10 min of exposure at 840 ˚C (where carbonization occurs), the fiber samples are taken back to the "B" end of the furnace for cooling down to below 100 ˚C. After 15-20 min of cooling, the fibers are removed. The weights of the fibers were measured both before and after the carbonization process using an Ohaus Corporation analytical lab scale (model no. AR2140). Using these weight measurements of two sets of fibers, an average carbonization % weight loss was calculated for each precursor.
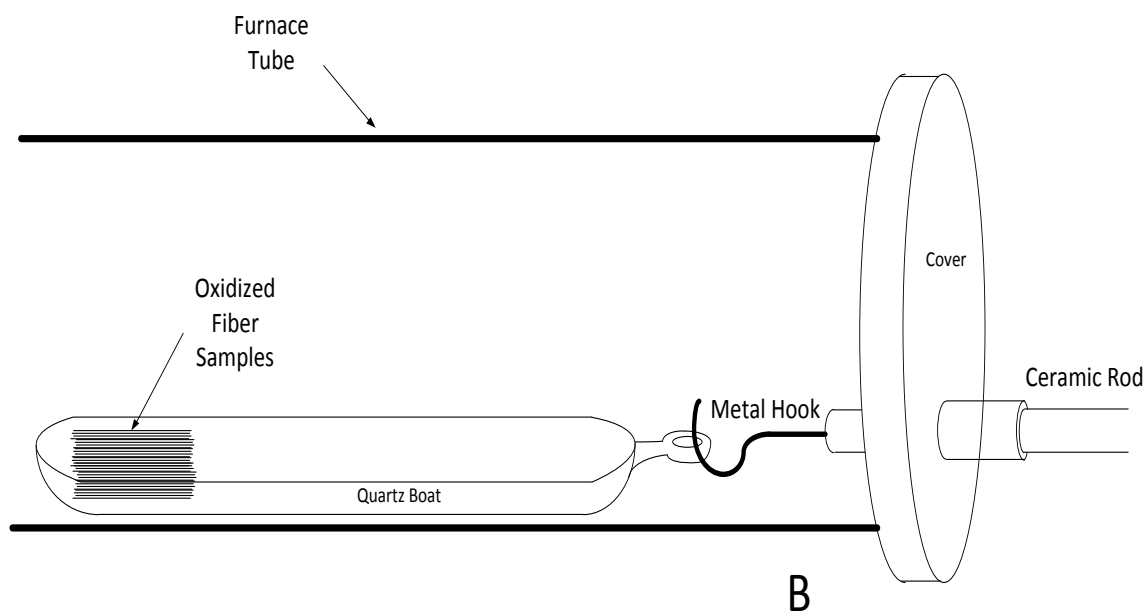
Fig. 2.10   B-edge of the tubular furnace. The boat and samples are placed at the "B" end of the tube during the air-purge process. The figure shows how the quartz boat is connected to the ceramic rod via a metal hook.

2.2.4 Direct-Activation

The conventional method for activating carbon fibers is to activate them after carbonization. However, in this work the carbonization step was skipped and the stabilized fibers were directly activated; this process is referred to as "direct activation". The carbonization process described in the previous section was carried out in order to (1) investigate the effect of precursor composition on the carbonization behavior of the fibers separately from direct activation and (2) determine the portion of the fiber weight loss attributable to carbonization vs. activation.

For our direct-activation work, the same Lindberg Furnace was used as for carbonization. As with carbonization, the fibers were first kept at the "B" end of the tube for 1 hr to remove any air (oxygen) left in the tube during sample loading. Then a ceramic rod was used to push the boat and its fiber contents into the high-temperature zone (Zone 2) of the furnace, where the temperature was kept at 840 ˚C. Instead of nitrogen, carbon dioxide at a flow rate of 0.5 L/min was used for the direct-activation process, and the exposure time was set to 6 hr. In order to keep the gas temperature (as measured in **Fig. 2.8** by the thermocouple) at 840 ˚C, the temperature of Zone 2 was set to 882 ˚C (vs. 875 ˚C for carbonization). Finally, the fibers were moved to the edge of the furnace for 15-20 min in order to cool, and were then removed.

The weights of the fibers were measured both before (initial weight) and after the direct-activation process (final weight), using an analytical lab scale (Ohaus Corporation, model no. AR2140). Because the measured weight loss for a given fiber sample was the combination of carbonization and activation weight losses, in order to calculate the burn-off value (i.e., the weight loss attributable to activation), the average carbonization weight loss value calculated in Section 2.2.3 was used. Carbonization was assumed to be completed at the beginning of the activation process before significant activation reaction occurred, and the fiber weight at the end of carbonization was calculated using the initial weight of the fibers and the average carbonization weight loss. Finally, the burn-off value was calculated using the final weight of the fibers and the calculated weight of the fibers at the end of carbonization.

At least two sets of all seven precursors were direct-activated for 6 hr. In addition to those, two sets of stabilized Dimer-1 fibers were direct-activated for 3 hr, 9 hr and 12 hr, respectively, to observe the effect of activation time on burn-off (i.e., weight loss) and the final pore structure of the ACF. For this additional activation experiments Dimer-1 fibers were chosen because ACFs from Dimer-1 were found to have the highest pore volume.

2.3 Analytical Techniques

2.3.1 MALDI-TOF Analysis of Precursors

All precursors (see **Table 2.1**) were analyzed for their molecular weight (mol wt) distribution with a Bruker Daltonics Autoflex MALDI-TOF mass spectrometer equipped with a 337 nm nitrogen laser. The procedure used is given below.

Samples for MALDI analysis were prepared by mixing 10 mg of precursor analyte and 200 mg of the matrix TCNQ (Tetracyanoquinodimethane) for 5 min in a mini ball mill (Thermo Electron Corp., model no. Wig-L-Bug). A thin film of the mixture was then deposited onto a cell of a MALDI target plate using a solvent-free, "water-spotting" method, which was developed in our laboratories and is explained in detail elsewhere (Edwards, 2003). The instrument operating parameters were as follows: reflectron mode, target plate charged at +19.0 kV, secondary ion source at 16.5 kV, lens at 7.67 kV, reflector at 20.0 kV, pulsed ion extraction at 90 ns, matrix suspension up to 210 Da, detector gain at 5.0x, and a resolution of 2.0. The spectra presented herein are a summation of 200 laser shots carried out at a rate of 20 Hz (Cervo et al., 2008). To

facilitate comparison between different MALDI spectra, many spectra shown in this dissertation were formatted as follows: MALDI data files were (1) compressed to reduce the amount of data generated and subtract the noise from a given spectrum, (2) smoothed, and (3) normalized so that the area under a given spectrum summed to 1 (Edwards, 2005, Appendix C). Whenever comparison between spectra needed to be made, all samples were analyzed at the same time on a given day. The laser power was adjusted based on the initial spectra obtained. For example, as the size of the precursor molecules increases, the signal response decreases; therefore, laser power had to be increased in order to detect the heavier molecules present.

2.3.2 Mettler Softening-Point Measurements

Softening points of all precursors were measured by using a Mettler FP83HT Dropping Point Cell instrument. In preparation for a measurement, samples were first ground with mortar and pestle, and were then packed into the softening point cups with a finger, using a clean weighing paper under the finger to protect the sample. The ground sample was added and pressed into the cup until the sample was hard and well-packed.

The instrument was run inside a chamber under a nitrogen atmosphere and at a heating rate of 2 ˚C/min. The starting temperature for the measurement was chosen as 5-10 ˚C below the approximate softening point as measured with a temperature-monitored hot plate (i.e., Fisher-Johns Melting Point Apparatus, serial no. 1833). Once the material reaches its MSP, with the pressure of the metal ball placed on the top of the sample the molten precursor flows down the softening point cup, forming a drop. Once the drop

reaches the optical detector level, a temperature is automatically recorded, and instrument starts to cool down.

If the difference between the measured MSP and the starting temperature is less than 10 ˚C, then repeating the measurement with a lower starting temperature (to keep the difference around 20 ˚C) is suggested, because when the starting temperature is too close to the MSP of the sample, the measurements tend to give values higher than the correct value. Measurements were repeated for second set of samples for each precursor.

2.3.3 Mesophase Analysis

2.3.3.1 Grinding and Polishing

The precursors are in granular form after being dried; however, for optical microscopy they need to be hard, polished solids. Thus, precursors have to be melted and then cooled down in order to prepare samples for polishing. Drops of molten pitch exiting the Mettler FP83HT Dropping Point Cell instrument after a given softening point measurement was completed were hard solids, and thus were suitable for polishing and were used for optical microscopy analysis. The drops were mounted in cylindrical mounting cups with an i.d. of 1.25 in. using a mixture of epoxy resin (Buehler, item no. 20-8120-009) and hardener (Leco Corporation, item no. 811-164). The epoxy resin and hardener were mixed together in a 5 g epoxy resin:1 drop hardener ratio in a separate beaker and stirred slowly without causing air bubbles until the mixture was homogeneous. For a given sample, in order to keep the molten pitch drop vertical inside the mounting cup, a piece of small epoxy block is taped to the pitch drop as a support.

Then, the sample with the taped block is placed into a mounting cup and a previously prepared mixture of epoxy resin and hardener is slowly poured on them. Each cup was kept at 70 °C for ~12 hr to speed the hardening process in a GCA Precision mechanical convection oven (Precision Scientific Inc., model no. STM135).

The hardened epoxy blocks containing the samples were placed into the sample holder of the Ecomet 2 polisher-grinder with the sample side down. The sample holder can hold up to 6 samples, and it is important to use at least 3 samples for balanced grinding/polishing. [Based on my personal experience, I would recommend filling all 6 sample holes for best results.] Even if 6 samples are not available at that moment, epoxy blocks without embedded samples can be used for this purpose.

While the polishing and the polarized-light microscopy analyses of the precursors used for the ACF production in this study were carried out by Fathollahi and co-workers at the University of California, San Diego (UCSD) (details of his procedure can be found in Fathollahi and White (1994) and Cervo (2008)), that of the heat-treated 780psig samples were carried out at Clemson University using a similar procedure to that was proposed by Kundu (2006). As many scratches were observed on the polished sample surfaces using the exact same procedure proposed by Kundu (2006), the procedure was modified with the addition of the 240- and 400-grit SiC polishing papers to the procedure. Also, as it was observed that minimizing the force set point during polishing helped minimize the scratches, polishing was always performed at the min force (5 lbs) allowed by the instrument instead of the 8 lbs used by Kundu.

In the modified procedure, first the sample holder was attached to the power head, and the 240-grit grinding (Buehler Carbimet SiC) paper was placed on the wheel of the Ecomet 2 polisher-grinder. The force was set to 5 lbs, the cycle time was set to 5 min, and the motor speed was set to 120 rpm; by pressing the green buttons located on the right- and left-hand sides of the power head, the samples were brought in contact with the grinding paper. It is important to run water both before grinding to wet the grinding paper and during the grinding process by moving the water distributer attached to instrument. The process was repeated using 320-, 400-, and 600-grit SiC papers, respectively, while washing the samples under tap water between each run.

After completing grinding, the samples were polished, using the same procedure as described above, with 1200-grit Buehler Carbimet SiC paper for 20 min (The process is called grinding when using lower-grit papers, while it is called polishing when using finer-grit papers.) After this step, the sample surfaces were visually checked, and if they appeared to be well-polished (i.e., reflecting light well), then they were used for optical microscopy analysis.

If further polishing was needed, the samples were first polished for 1 min with white label (Allied High Tech Products Inc., part no. 90-150-500) polishing paper. A 1 µm diamond suspension was sprayed before the process was started, and distilled water was applied intermittently every 15-20 s. After samples were washed under distilled water, they were then polished in a second step using Chem-Pol Black polishing cloth (Allied High Tech Products Inc., part no. 180-10050) for 2 min, with a 0.05 µm alumina suspension being applied intermittently during the process.

At the end of the polishing process, the samples were washed with distilled water. Because some alumina particles could still be on the surface of the samples, the surface was gently rubbed using a cotton swab and 10-15 drops of Micro Organic Soap (Allied High Tech Products Inc.) mixed with distilled water (~100 ml) in a plastic cup. Then the samples were dried using canned compressed air (Miller-Stephenson Allied High Tech Products Inc.) and taken for microstructure analysis.

2.3.3.2 Optical Microscopy

Microstructure analysis was performed using an Olympus BX60 Microscope with cross-polarized light and a first-order red plate. Here, only a brief procedure of the process is given; details of the instrument configuration and settings are given elsewhere (Kundu, 2006).

The microscope was operated in the reflective light mode. To assure the flatness of the investigated surface, a small piece of soft clay was placed on the microscope slide, and the epoxy block was placed on top of it, with the sample surface facing up. Then, a sample flattener was used to press the block to obtain a horizontal sample surface on the top.

Next, the sample was placed on the rotating microscope stage and brought into focus by using focusing knobs. To do the focusing faster, one can externally observe the circle of light reflecting on the sample surface, and then using the focusing knobs, adjust it when the circle is the smallest. Then, fine focusing can be performed by looking through the eye pieces. To take pictures, 20x and 50x lenses were used.

Once focusing was completed, one of the eye pieces was removed and replaced with a Sony DSC-S70 digital camera with a camera adaptor (Martin Microscope Company, model no. MM3XS). For consistency, the camera was operated at its maximum zoom during the taking of all pictures, and the flash was turned off. While taking pictures, the light level was adjusted to 8/12 while using the 20x lens, and to 12/12 while using the 50x lens in order to obtain the clearest pictures using the light-level switch on the right-hand side of the microscope. It needs to be noted that every time the lens is switched, the sample again needs to be brought in focus.

In order to improve color contrast and observe yellow, blue, and magenta colors more clearly, color enhancement was used on some of the pictures (photomicrographs) using Photoshop 6.0 software. The photomicrograph of interest was opened, and by clicking through "Image > Adjust > Auto Levels" the photomicrographs was significantly enhanced. Details of this procedure can be found elsewhere (Kundu, 2006). Also, the mesophase area percentages of the mesophase-containing precursors were measured from the photomicrographs using the procedure proposed by Kundu (2006).

2.3.4 ^{1}H NMR Analysis of Dimer-1 and Dimer-2 Precursors

^{1}H NMR analyses of the Dimer-1 and Dimer-2 precursors were carried out with the help of Ha Nguyen, a PhD candidate in Chemical Engineering at Clemson University. The spectra were obtained by using a 300 MHz Bruker Avance System (Chemistry Department, Clemson University). The samples were prepared by dissolving

approximately 5 mg of material in 0.75 ml of $CDCl_3$ (99.8% atom D, Acros Organics), and then filtering through a 0.45 μm filter.

2.3.5 Heat Treatment Tests on 780psig Precursor

In order to better understand the effect of exposure to elevated temperatures on the possible formation of mesophase in a precursor, a portion of the 780psig precursor was heat-treated under inert atmosphere. The same quartz boat and tubular furnace that were described above for carbonization and direct-activation experiments were used, along with the same procedure under 1 L/min N_2 flow. The only difference was that the precursor in powder form was placed inside the quartz boat instead of oxidized fibers. Approximately 1.0 g of sample was used for each run, and samples were heat treated for 30 min, 1 hr, 3 hr, and 5 hr, respectively. Samples were weighed using Ohaus Corporation AR2140 lab scale both before and after heat treatment, and the % weight loss was calculated. MSPs of the collected samples were measured, and they were polished and analyzed by optical microscopy as described above.

2.3.6 Wide Angle X-ray Diffraction Analysis on Carbonized Fibers

As was described above, optical microscopy was used to estimate the percentage of mesophase present in our starting precursors. The extent of orientation in the carbonized fibers made from each precursor was also determined by wide angle X-ray diffraction (WAXD). A PhD candidate in Chemical Engineering at Clemson University, Marlon Morales, assisted in this work. An osmic Micromax CuK_α X-ray source was used

to obtain azimuthal intensity distribution. The collimator pinhole size was 0.5 mm, and samples were set 12 cm apart from the detector. Samples were exposed for approximately one hr per image, and 2D image plates were used to capture diffracted patterns. The image plates were scanned using a Fuji BAS 1800 scanner, and diffractograms were Fraser-corrected and analyzed using Polar® 2.6.7 software. Measurements were repeated for a duplicate set of fibers made from the same precursors that were spun and oxidized together with the first set, but were carbonized separately. Details of the WAXD measurement procedure can be found at Lee et al. (2005).

2.3.7 Surface Characterization of Activated Carbon Fibers

Surface characterization of all ACF was carried out using a Micromeritics Accelerated Surface and Porosity Analyzer (Micromeritics Instrument Corporation. Model no. 2020). Nitrogen was used as an adsorbent at a bath temperature of 77 K. Test tubes with a ½ inch in. diameter were used with a seal frit assembly (Micromeritics, part no. 260-25890-00), that is, a top cover with a valve that prevents a sample from inadvertently coming out during the evacuation process (see **Fig. 2.11**).
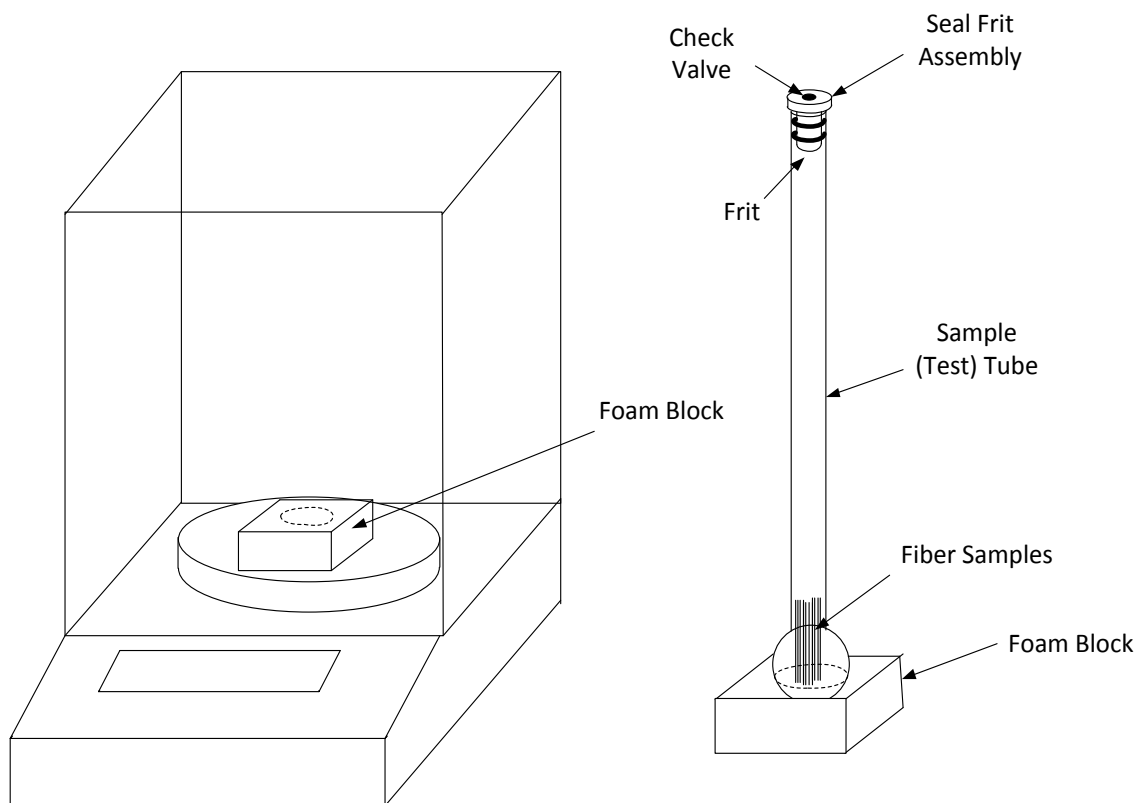
Fig. 2.11 The scale used for weighing the sample test tube for surface characterization. A foam block with a spherical hole was used to keep the test tube vertical in order to obtain accurate weight measurements.

In order to initiate the procedure, first a clean and dried empty test tube with a seal frit assembly was weighed using the Ohaus Corporation AR2140 lab scale. As the sample test tubes are taller than the scale, the scale was used while its top window was open. To keep the sample tube vertical during measurement, a foam block with a hole was used (**Fig. 2.11**). Because a typical sample weight (~30 mg) was much smaller than the weight of the test tube (~37 g), extra care had to be taken. Every measurement was

repeated three times, an antistatic gun was applied to the test tube before placing it into the foam block on the scale, and an average of these measurements was taken.

Next, the sample was weighed on weighing paper, and was then placed into the test tube by using another weighing paper that had been rolled and inserted into the top of the tube. (This sample weighing was made to ensure that consistent results were being obtained with the balance for the laboratory conditions present at the time.) The purpose of the rolled weighing paper is to prevent fibers from sticking to the walls of the test tube close to the top, where they might not be immersed in liquid nitrogen bath during micropore analysis.

After the fibers were loaded into the test tube and the seal frit assembly was replaced, the sample was degassed in order to remove any gas or moisture adsorbed by the fibers. Before degassing, the test tube with the fiber samples was re-weighed, as was done above, to ensure consistent weighing could be made. Then, the test tube was attached to one of the degassing ports of the Micromeritics ASAP 2020 instrument as shown in **Fig. 2.12**, and the heating jacket assigned to that port was put on to the bottom part of the test tube. Next, the degassing schematic was opened from the Micromeritics software in the connected PC, and manual control was enabled from the degassing menu. The valves between the pump and the desired degassing port were opened, and the temperature of the heating jacket was set to 300 ˚C. After degassing for 4 hours at 300 ˚C, the heating jacket was removed, and the pressure was brought back to atmospheric pressure by nitrogen flow. Once the test tube and fiber sample within had cooled down to room temperature, it was removed from the degassing port and weighed as described

before. Then, the actual fiber sample weight was calculated by subtracting the initially obtained, empty weight of the test tube (with seal frit assembly) from this final weight.

The fiber sample was then ready for "free-space" (i.e., the space in the tube not taken by the sample) analysis. The test tube was attached to the analysis port (**Fig 2.12a**) after it was inserted into an isothermal jacket (**Fig 2.12b**). To perform the free-space analysis, from the "sample analysis" menu "analysis conditions" dialog was chosen, and only two relative pressure (p/p^0) points were entered for data collection; 0.1 and 0.2 in order to keep the analysis short, and under the free space dialog box the "measure" option was chosen. After the file was saved, the analysis was started. The purpose of the free space analysis was to measure warm and cold free spaces for this test tube with this sample in it. This volume information was required for calculation of adsorbed N_2 amounts from measured pressure values during adsorption analysis.

During free-space analysis, He molecules can be trapped in narrow micropores (<7 Å). Therefore, the fiber sample needs to be re-degassed after free-space measurement in order to remove any trapped He molecules, and to allow access to these narrow micropores during micropore analysis with the adsorbent N_2.

Re-degassing was carried out at the analysis port by placing the test tube and sample under vacuum for 3 hr at 300 ˚C. For heating the sample, one of the two available heating jackets was used. Following this second degassing process in the analysis port, the heating jacket was removed, and the fiber sample was allowed to cool down to ambient temperature. Detailed micropore analysis was now ready to be carried out.

For micropore analysis, measurements as obtained from free-space analysis were entered. Relative pressures from 0.05 to 0.3 at increments of 0.05 were chosen, and the incremental dosing option was selected. The use of incremental dosing option is a part of standard procedure for detailed micropore analysis. As suggested by the manufacturer, the incremental dosing amount was chosen as 1/50 of the N_2 adsorbed at a relative
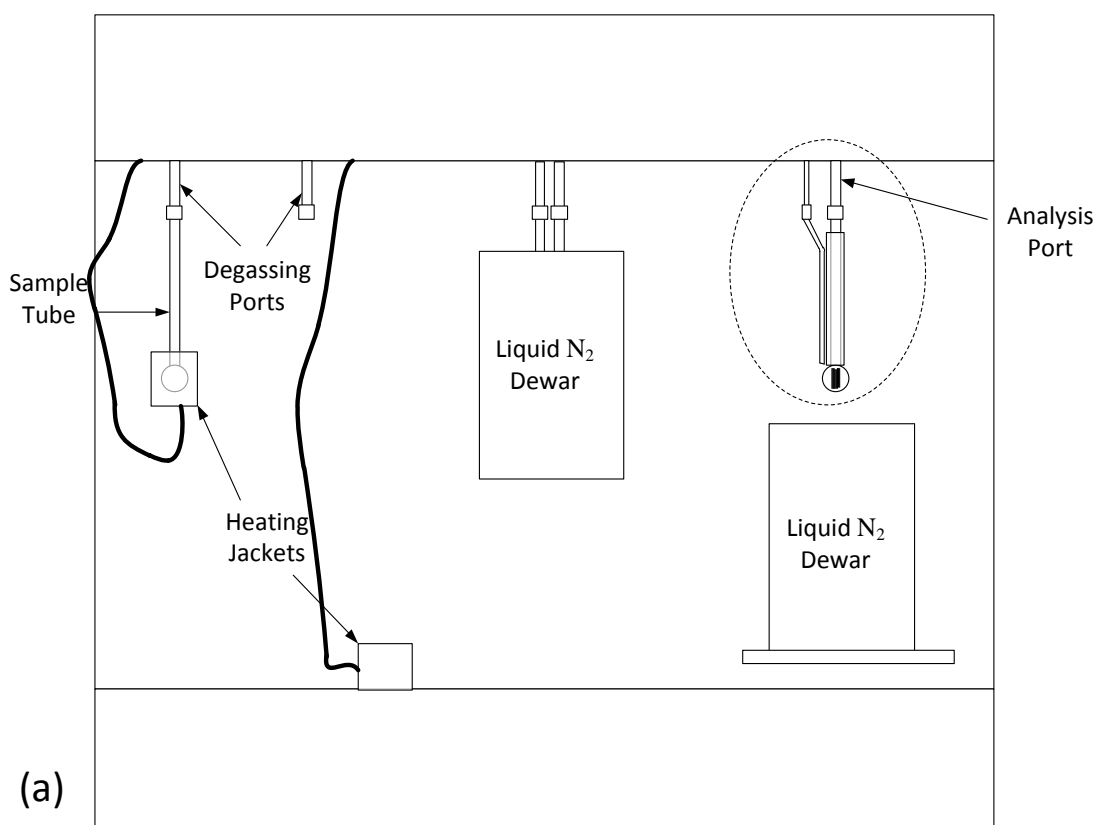
Fig. 2.12   Micromeritics ASAP 2020, Surface Analyzer. (a) Shows the instrument with one sample at the degassing port and one sample at the analysis port; (b) shows a zoomed-in version of the analysis port.

Fiber
Samples

Reference
Tube

Analysis Port

Isothermal
Jacket
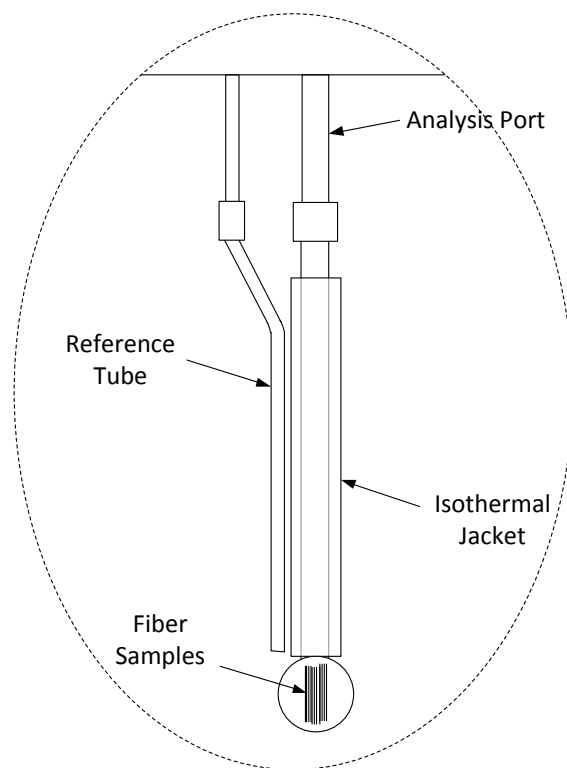
(b)

Fig. 2.12   Continued.

pressure (p/p^0) of 0.1 during the free-space analysis. By using this option, data (adsorbed N_2 amount (cm^3 (STP)/gram sample)) at relative pressures as low as 10^{-7} was collected. Following the analysis, pore size distribution data were obtained using the Micromeritics ASAP 2020 instrument software based on Density Functional Theory, assuming slit-shaped pores.

3 RESULTS AND DISCUSSION

In this research, the effect of precursor composition on the final pore structure of activated carbon fibers produced from petroleum pitch was investigated. The pore structure of the activated carbon fibers were successfully controlled by manipulating the composition and molecular weight distribution of the precursors. All precursors were from the same origin; in other words, they were all produced from the same mother material. Unlike previous studies, a detailed mol wt distribution and the mesophase content (molecular order) of each precursor were determined prior to the fiber production process. The final activated carbon fibers were then analyzed for nitrogen adsorption isotherms to obtain pore size distribution information. Details of all production processes and analysis methods are given in this chapter.

3.1 Production of 750psig, 760psig, 780psig, 800psig, and 830psig Precursors

The precursors used to prepare activated carbon fibers (ACFs) in this study were obtained by fractionation of a low softening point, commercial petroleum pitch (M-50, Marathon Oil Company LLC.). Details of the dense-gas extraction (DGE) fractionation process were given in Chapter 2. Production of all precursors from the same starting material gave us the opportunity to isolate the effect of the mol wt distribution of the precursor on the final pore structure of ACFs. Furthermore, detailed studies by Burgess and Thies (2011) had elucidated the dominant molecular structures present in M-50 pitch.

3.1.1 Mettler Softening Points and Bottom Product Yields

Five precursors with different molecular compositions were produced from M-50 pitch using single-column DGE at 350 ˚C. Precursors with softening points above 200 ˚C were desired, as the slowest step of ACF production is the temperature-dependent oxidation step. The use of precursors with softening points below 200˚C would make the oxidation process impractically long. Mettler softening points (MSP) of these five fractions of M-50 pitch are given in **Table 3.1**.

Table 3.1   Mettler Softening Points of five ACF precursors produced using single-column DGE at 350 ˚C.

	MSP(˚C)[a]
750psig	210
760psig	257
780psig	297
800psig	312
830psig	339

[a] MSPs are accurate to ±2 ˚C.

The increase in softening points with increasing extraction pressure (at 350 ˚C isothermal operation) is an indication of an increase in molecular weight of the precursors. Bottom product yields were also found to decrease with increasing operating pressure (**Fig. 3.1**). With isothermal DGE operation, bottom product yields are seen to drop if a higher mol wt material is obtained. Cervo and Thies (2007) have previously

documented this effect, which is due to the increased solvent power of the supercritical fluid at high pressures for a given supercritical temperature. On the other hand, we also see from **Table 3.1** and **Fig. 3.1** that much higher bottom yields (and commensurately lower softening points) are obtained if the extraction pressure is decreased below 750psig (~52 bar), due to a significant decrease in solvent power. As we desired precursors with softening points greater than 200 °C, 750psig and higher extraction pressures were used for the isolation of all five precursors produced via DGE.
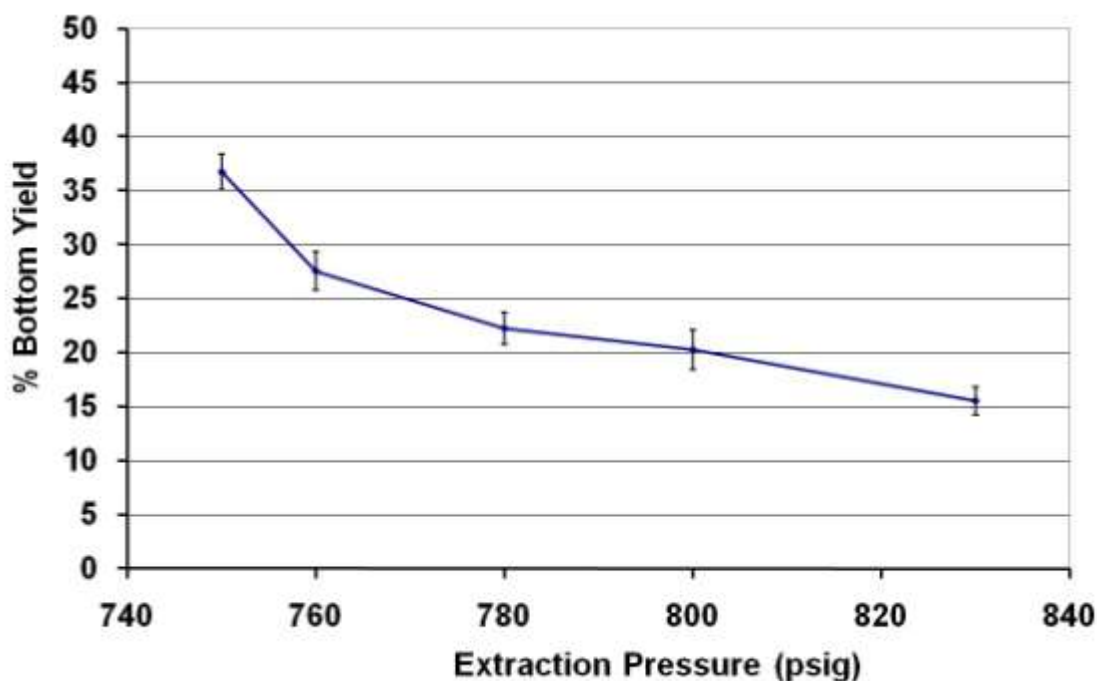
Fig. 3.1   DGE bottom-product yields for the five precursors shown in **Table 3.1** (error bars = ± 1 std dev).

3.1.2 MALDI Spectra

The raw MALDI spectra of these five precursors are given in **Fig. 3.2**. Although the detailed operating procedure for MALDI was given in Chapter 2, we remind the
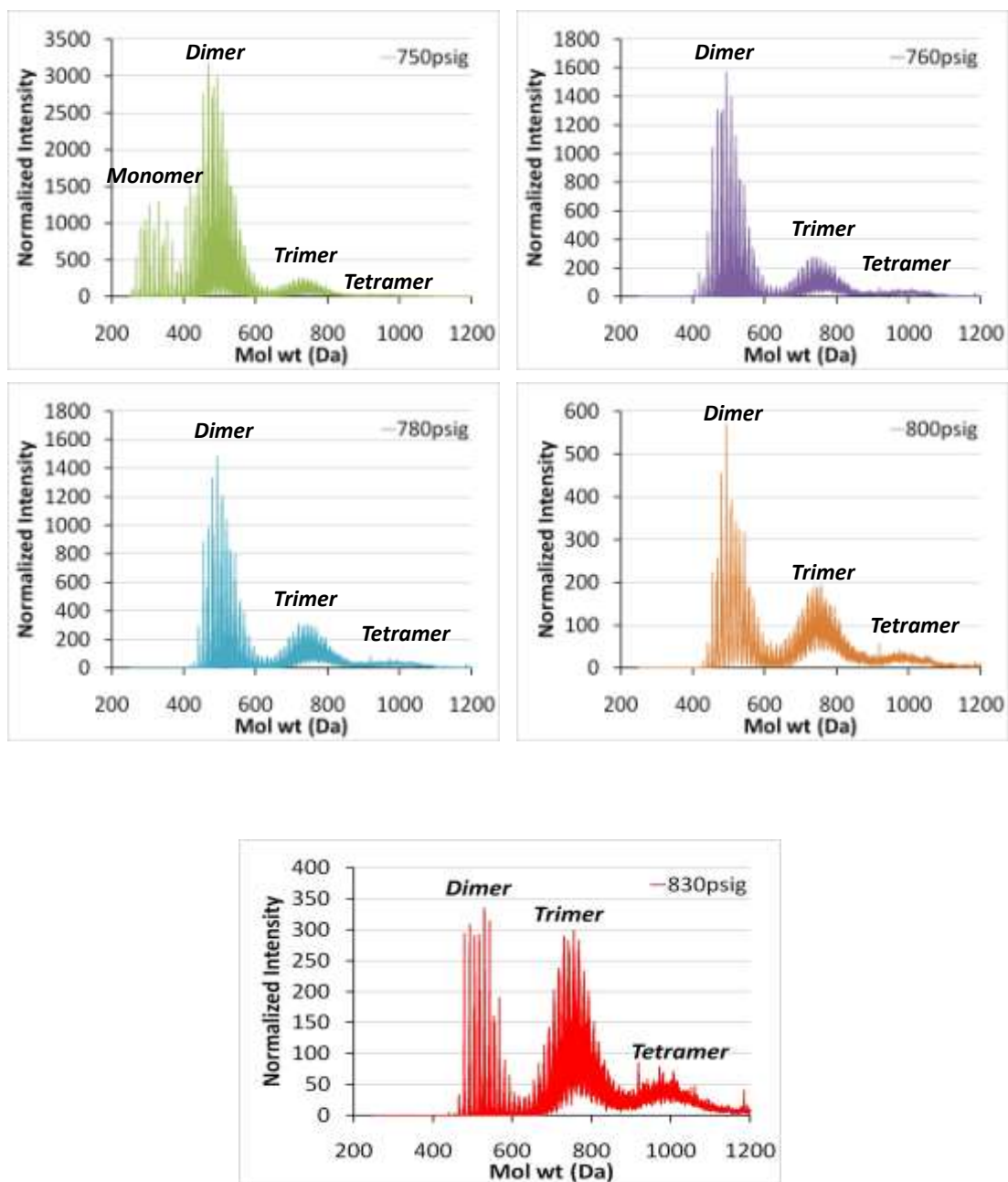
Fig. 3.2   Raw MALDI spectra for the five precursors produced using single-column DGE at 350 ˚C and the pressures noted above. All spectra were obtained on the same day to ensure consistency.

reader here that for consistency the laser power was chosen to keep the intensity baseline

increase below 100 units for each sample.

MALDI spectra for the different precursors are also compared on a normalized

intensity basis in **Fig. 3.3**, so that we are able to better compare the spectra. Per the work

of Edwards (2005), the spectra from **Fig. 3.2** were processed using a smoothing function

and were then normalized such that the area under each spectra summed to 1.0.
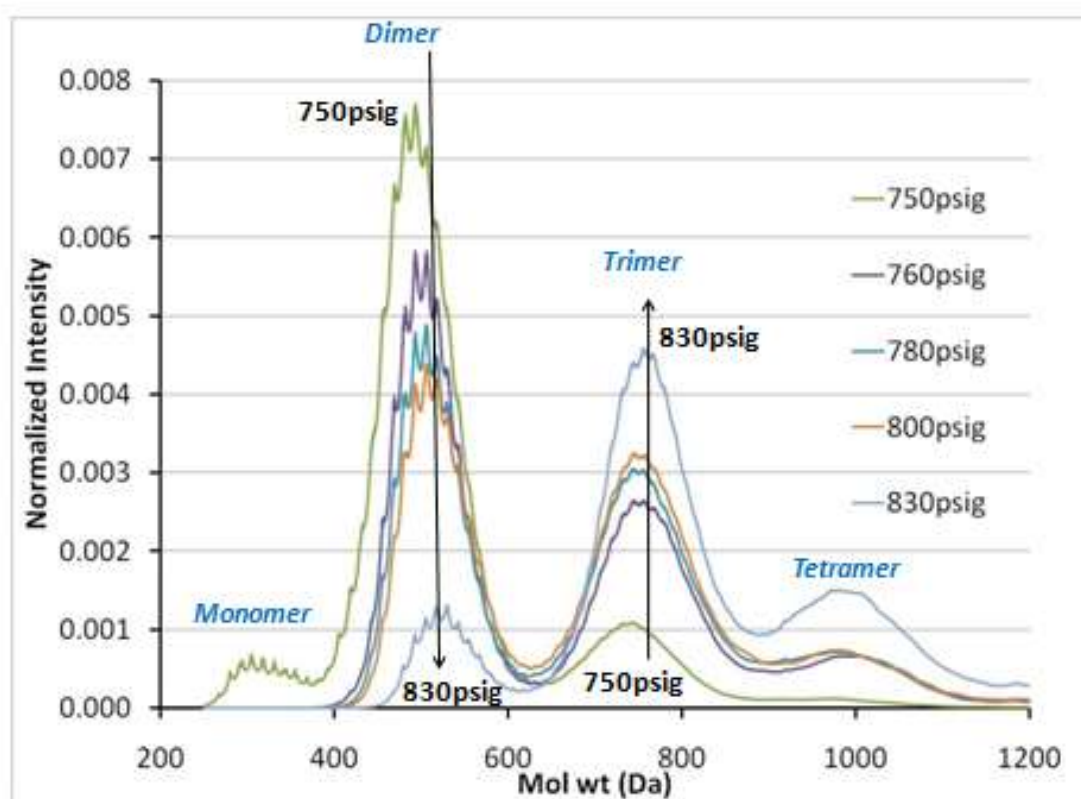
Fig. 3.3   Smoothed and normalized MALDI spectra of the five precursors produced using single-column DGE at 350 °C and the pressures noted above. The arrows show the trends with increasing extraction pressure.

Here we see a continuous change in the spectra with increasing DGE pressure, the dimer peak being dominant in the spectra of the 750psig precursor, and the trimer peak dominant in the 830psig precursor. The arrows on the figure show the trend in spectra with increasing extraction pressure.

3.1.3 Mesophase Content

The precursors produced by DGE were also analyzed for mesophase content. Although the mother M-50 pitch is isotropic, the removal of lower mol wt species during the fractionation process can result in the development of molecular order (anisotropy) Larger, higher mol wt molecules are mobile in the liquid state and can orient themselves to form nematic discotic liquid crystals, which are also called mesophase (Brooks and Taylor, 1965). For this analysis, molten pitch samples collected at the end of MSP measurements were mounted in epoxy, polished, and then observed under cross-polarized light via optical microscopy (see Chapter 2 for details). Photomicrographs of the polished surfaces of the samples are given in **Fig. 3.4**, along with their mesophase percentages.
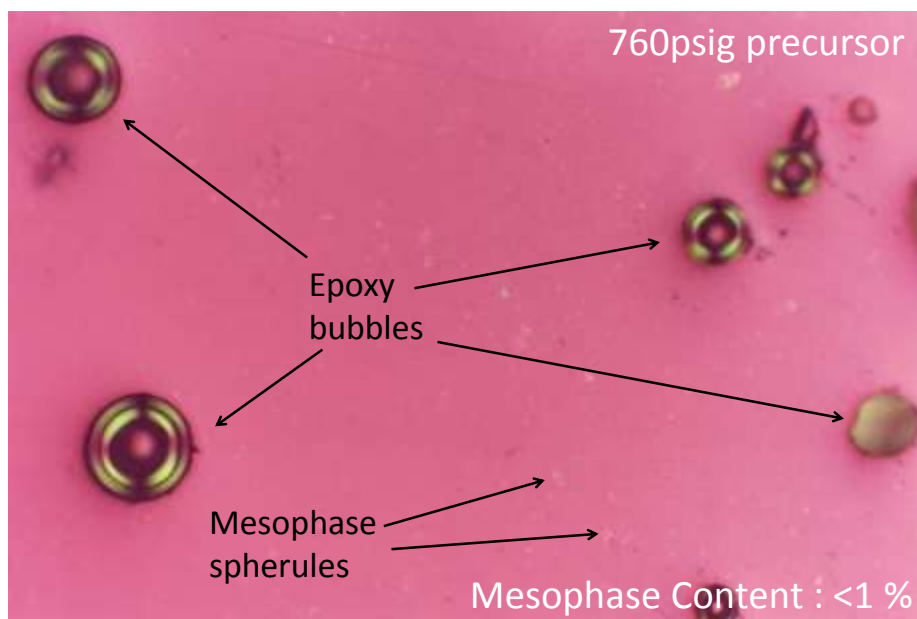
Fig. 3.4   Photomicrographs of the polished surfaces under polarized-light microscopy of the five precursors produced using single-column DGE at 350 ˚C. The mesophase content of each precursor is given on its micrograph in area %.
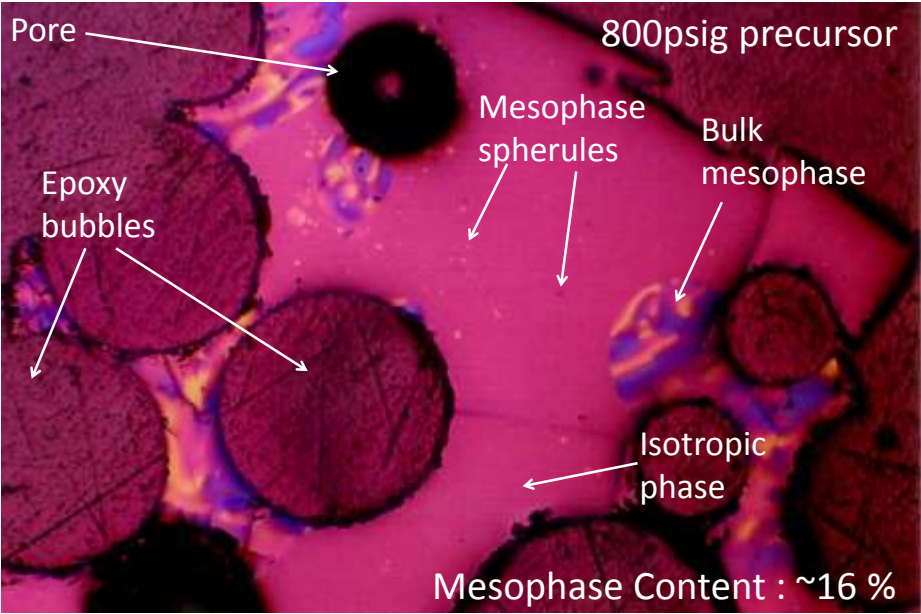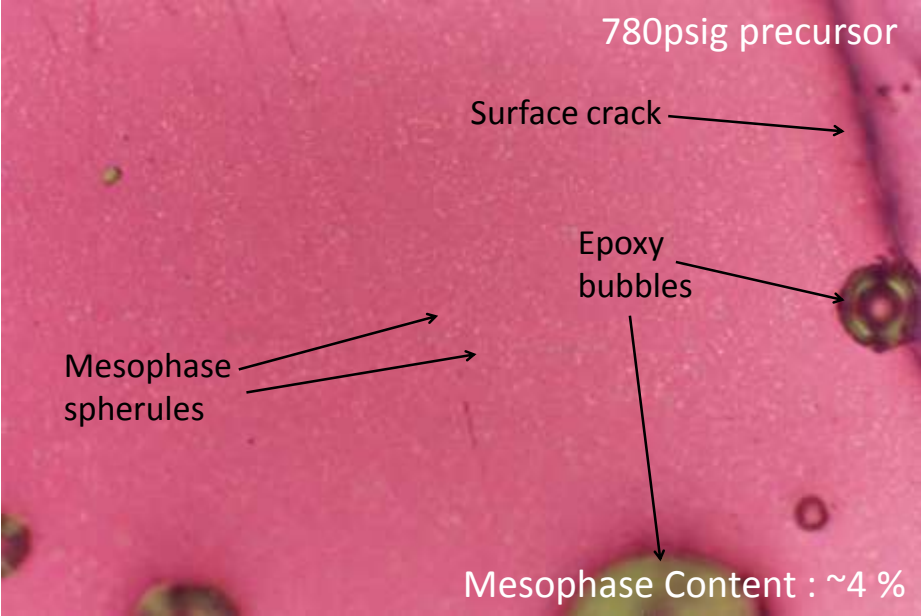
Fig. 3.4   Continued.
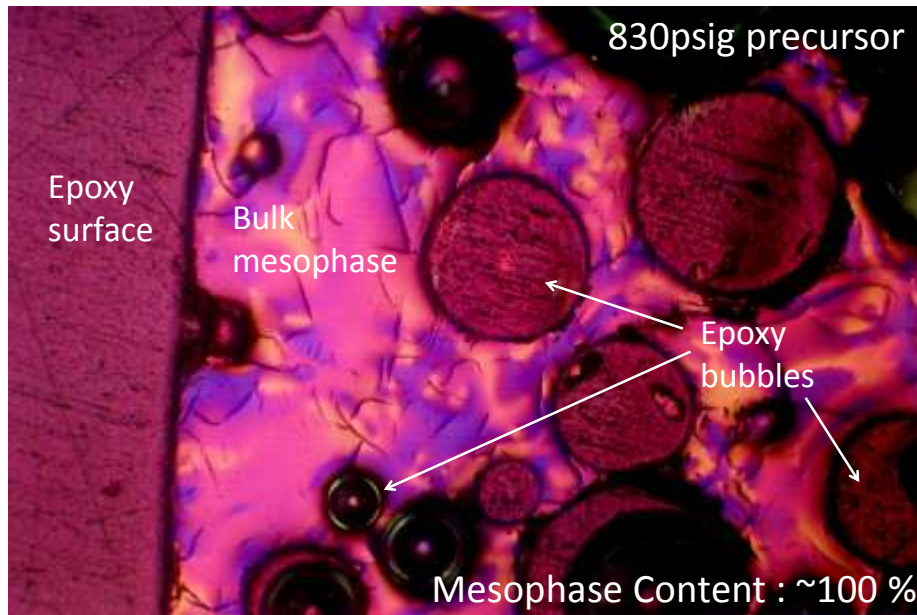
Fig. 3.4   Continued.

As seen from the micrographs (**Fig. 3.4**), only the 750psig precursor is fully isotropic, and the rest of the precursors have mesophase regions in various amounts. 760psig has few mesophase spherules, while 780psig precursor has many. On the other hand, for the 800psig precursor, the mesophase has coalesced into distinct regions, and the 830psig precursor consists of 100% mesophase (fully anisotropic).

3.2 Production of Dimer-1 and Dimer-2 Precursors

In general, activated carbons are non-graphitic (i.e., isotropic) and non-graphitizable carbons (Menendez-Diaz and Martin-Gullon, 2006), and many of the precursors discussed above had some level of anisotropy (i.e., mesophase content). Therefore, investigating only these five precursors would not have enabled us to

distinguish between the effects of molecular composition (i.e., mol wt distribution) and molecular order (anisotropy) with respect to activation rate and porosity formation. Thus, additional precursors that were fully isotropic (albeit with different molecular composition) were required. To this this end, two additional precursors, known as Dimer-1 and Dimer-2, were produced.

Because a single-column DGE process can only separate a feed into two streams, further processing was required in order to produce the middle cut, Dimer-1 and Dimer-2 products. As we discussed in Chapter 2, Dimer-1 was produced using a setup of two packed columns in series, with the first column, operating at DGE conditions, being used to extract monomer and dimer, and the second column, operating as a low pressure, high-temperature stripper, being used to recover the desired, dimer-rich (bottom) product. As with Dimer-1, the first step in producing Dimer-2 was the isolation of a monomer/dimer mixture from M-50 pitch via single-column DGE. The second step, on the other hand, was evaporation of the monomer species in a free-convention vacuum oven in order to produce the desired, dimer-rich product. Details of both procedures are given in Chapter 2.

The procedure for removal of the monomer from the Dimer-2 precursor was only established after some initial, less successful runs. In particular, when we tried to "dry" 200-g quantities of the monomer/dimer mixture in the vacuum oven at 350 ˚C and 2 mbar, vacuum had to be maintained for 2 hr in order to reach an acceptable level of monomer removal. The experiment was first performed for 30 min, and then an additional 30 min and then another 1 hr, while checking the MALDI spectra and yield

after each sequence. The product yield (as a percentage of the initial monomer/dimer "feed") with increasing time was 16.8%, 14.6% and 10.5%, respectively. Subsequent tests for drying the monomer/dimer mixture in the vacuum oven in 30-g (vs. 200-g) quantities for 30 min, using the same-sized tray, temperature, and vacuum, resulted in a product with the narrower, higher mol wt distribution shown in **Figs. 3.5** and **3.6**. We then concluded that the larger samples had been diffusion-limited, and subsequently limited sample sizes to 30 g.

3.2.1 Mettler Softening Points and Mesophase Content

Mettler softening points for all precursors used in the production of ACFs are summarized in **Table 3.2**. Note that MSPs for Dimer-1 and Dimer-2 are close to that of
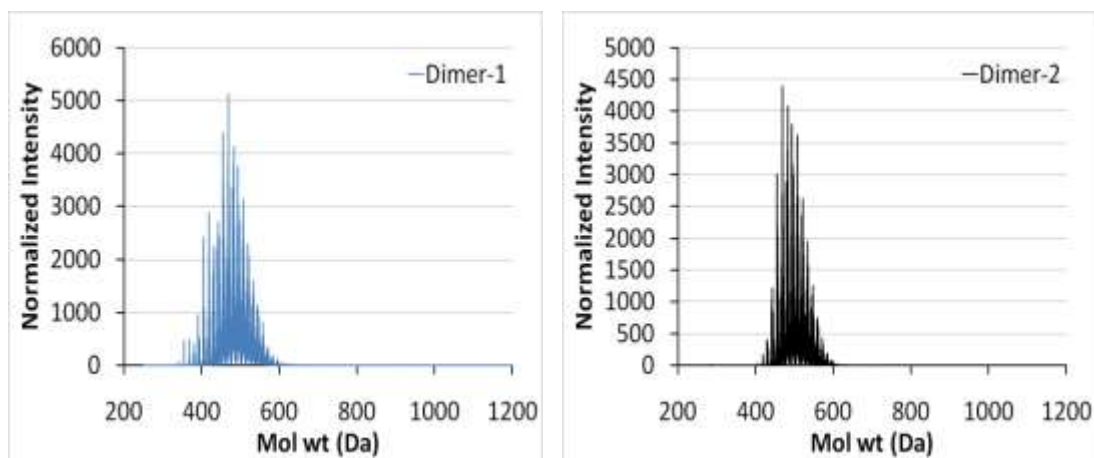
Fig. 3.5   Raw MALDI spectra for Dimer-1 and Dimer-2 precursors, analyzed on the same day as the precursors shown in **Fig. 3.2** to ensure consistency.
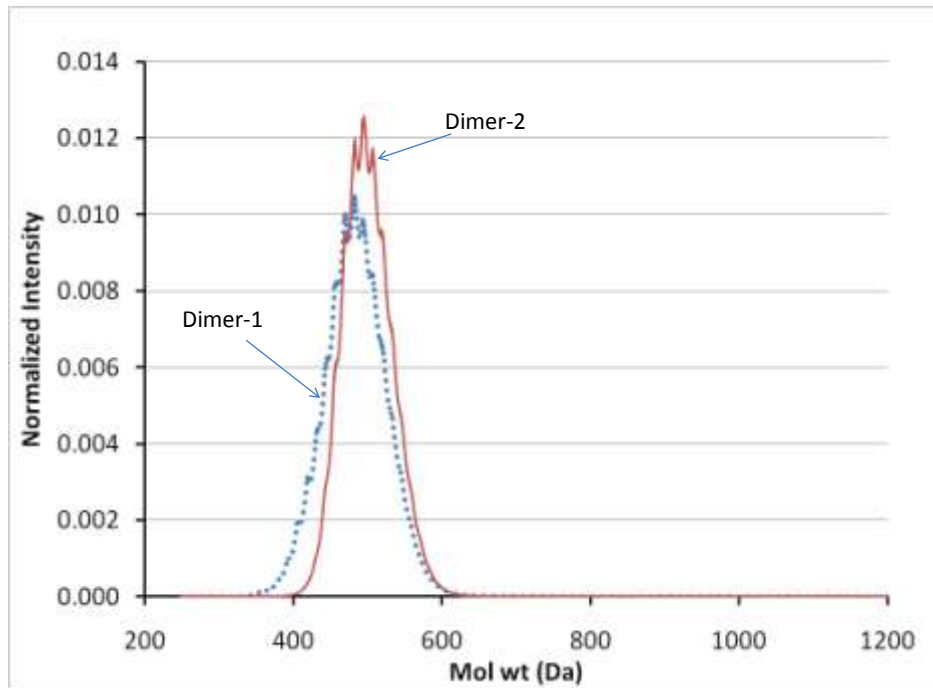
Fig. 3.6   Smoothed and normalized versions of the MALDI spectra shown above for Dimer-1 and Dimer-precursors.

the 750psig precursor, even though the mol wt distributions are quite different from each other. Cross-polarized light microscopy analysis of both of these samples indicated that they were both fully isotropic (see **Fig 3.7**).

Table 3.2   Mettler Softening Points of all precursors used for ACF production.

	MSP(˚C)[a]
M-50	116
Dimer-1	202
Dimer-2	212
750psig	210
760psig	257
780psig	297
800psig	312
830psig	339

[a] MSPs are accurate to ±2 ˚C.
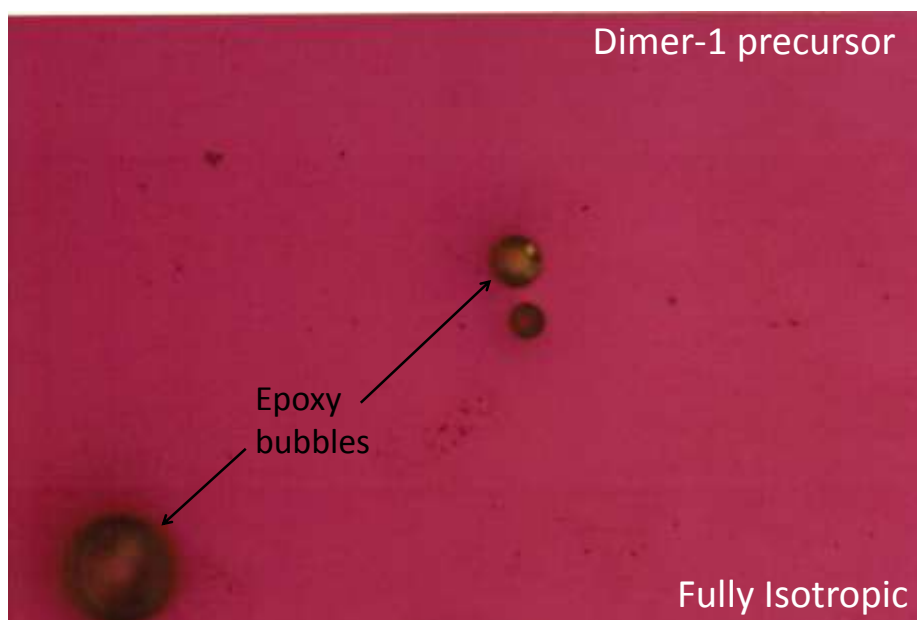
Fig. 3.7   Photomicrographs of the polished surfaces under polarized-light microscopy of Dimer-1 and Dimer-2 precursors. Both precursors were found to be fully isotropic.
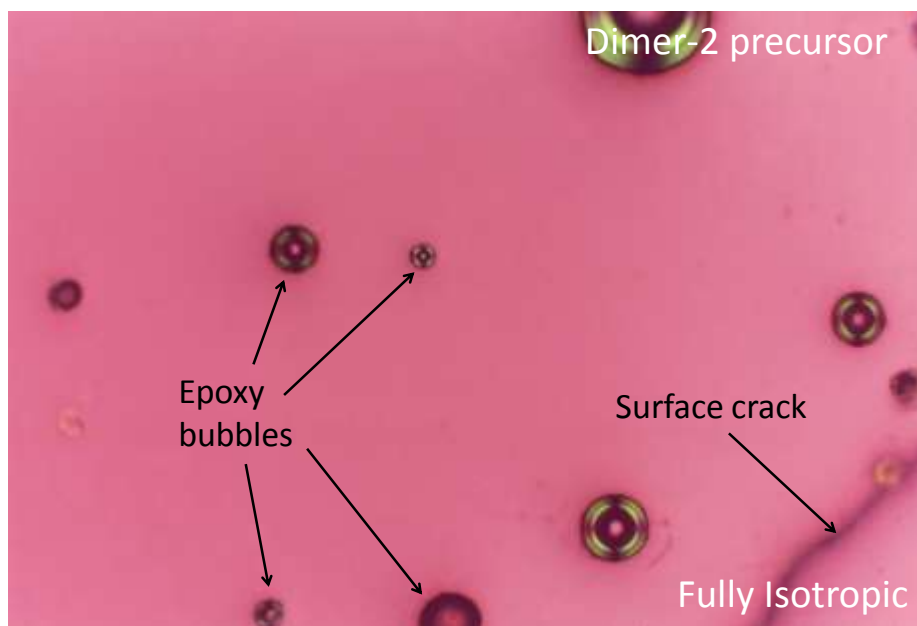
Fig. 3.7   Continued.

3.3 Normalized MALDI Spectra for all Precursors

MALDI spectra for all precursors and the M-50 mother pitch are presented together as smoothed, normalized spectra to facilitate comparison in **Fig. 3.8**. **Fig. 3.8a** contains the spectra for all isotropic samples and **Fig. 3.8b** for all samples that contained any amounts of mesophase. As 760psig was "on the border" between the two scenarios, its spectra is included in both figures.
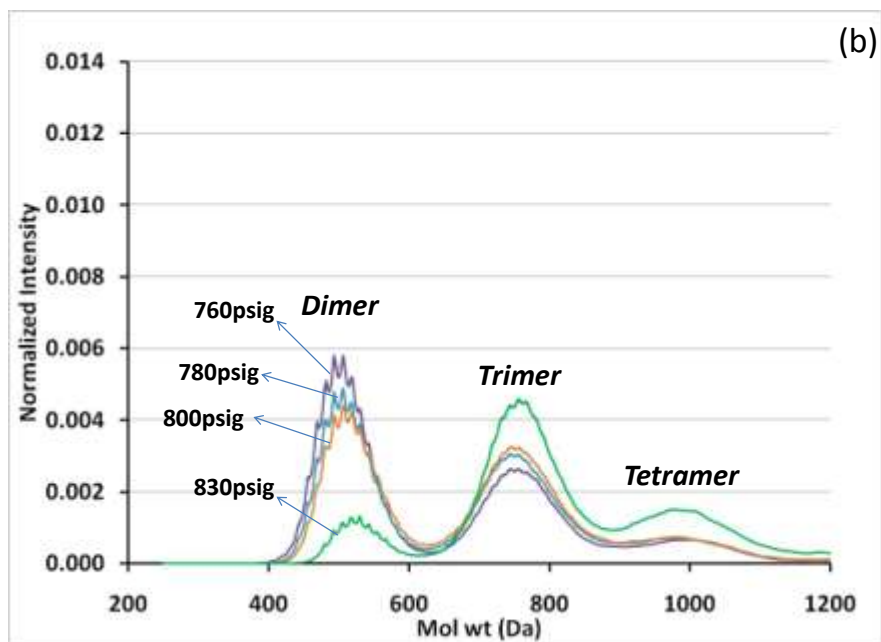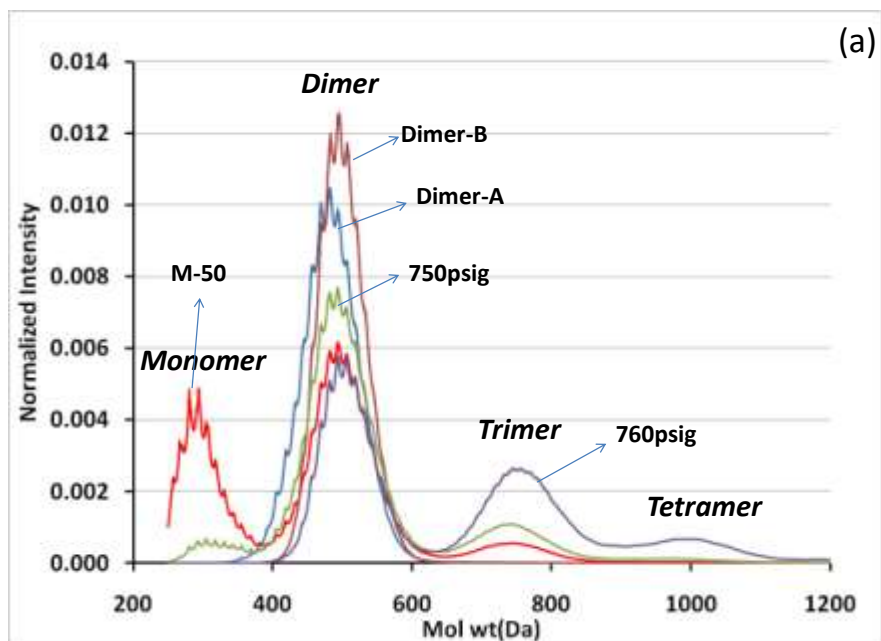
Fig. 3.8 Smoothed and normalized MALDI spectra of all precursors used for ACF production in addition to M-50: (a) 760psig and lower mol wt precursors; (b) 760psig and higher mol wt precursors. For consistency, all of the above spectra were obtained on the same day.

The area percent under each oligomeric peak (monomer, dimer, etc.) for each precursor was calculated from the spectra shown in **Fig. 3.8** and is given in **Table 3.3,** along with the mesophase content and average molecular weight (number-average (MW_n) and weight-average (MW_w)) of the precursor. As shown by Kulkarni et al. (2011), MALDI area percentages have been shown to be approximately equal to mol percentages, with monomer being somewhat underrepresented (due to its volatility) along with higher oligomers (due to their strong adsorption) (Kulkarni and Thies, 2009).

Table 3.3 Oligomer area percentages, mesophase content, and average molecular weight of all precursors used for ACF production in addition to M-50.

	MALDI-TOF Area Percentages [b]					Mesophase	Average Mol Wt	
	Monomer	Dimer	Trimer	Tetramer	Pentamer	Content (%)	MWn	MWw
M-50	33.0	59.9	6.7	0.3	0.0	0	430	470
Dimer-1	0.7	99.0	0.2	0.1	0.0	0	482	486
Dimer-2	0.0	99.9	0.0	0.0	0.0	0	500	502
750psig	5.2	78.7	14.0	1.8	0.2	0	521	549
760psig	0.0	52.3	35.2	11.0	1.4	<1	639	687
780psig	0.0	44.5	41.3	12.2	2.0	4	666	714
800psig	0.0	41.6	44.6	12.1	1.7	16	676	720
830psig	0.0	11.1	57.9	25.1	5.9	100	807	844

[b] The following mol wt range were used to define oligomers (Burgess and Thies, 2011): monomer 202-388, dimer 388-645, trimer 645-890, tetramer 890-1120, and pentamer 1120-1500 Da.

3.4 Heat Treatment Tests on the 780psig Precursor: Mesophase Transformation

Although the smoothed, normalized MALDI spectra for 760psig, 780psig and 800psig precursors (**Fig 3.8b**) are quite similar to each other, the difference between their

softening points (Table 3.2) is significant. Furthermore, a close inspection of the photomicrographs in Fig. 3.4 indicates that the 780psig precursor contains a large number of small mesophase spherules, indicating that incipient mesophase formation on a bulk scale may be possible. Räder and co-workers (Cristadoro et al., 2007) have shown that pure component PAH species that are prone to stacking in the solid state generate significantly less signal response in MALDI vs. those that are more random in their arrangement. Thus, the similar MALDI spectra observed for the above three precursors may very well be an indication of stacking of molecular species and formation of mesophase, with the stacked mesogens exhibiting low signal response and thus not being readily visible in the spectra.

Because the presence of mesophase (i.e., anisotropy) can have such a significant impact on the activation behavior (i.e., activation rate and final porosity) of ACFs (Menendez-Diaz and Martin-Gullon, 2006), a study was conducted in order to determine how easily our samples containing small amounts of mesophase could convert to bulk mesophase under conditions normally encountered during the processing of pitch to form ACFs. 360°C was chosen as the heat treatment temperature, on the high side of that which could be encountered in pitch melt-spinning. It is high enough to allow molecules to move to orient, but not so high as to cause formation of mesophase pitch via thermal polymerization reactions among the oligomers, which starts to occur around 380-440°C (McHenry, 1976).

Based on the discussion above, the 780psig precursor seemed to be the one most suitable candidate for the study. Thus, samples of the 780psig precursor were heat-treated

under nitrogen flow for 30 min, 1 hr, 3 hr and 5 hr, respectively. Additional details of the experimental procedure are given in Chapter 2. Weight loss (wt loss) and MSP of the 780psig precursor after heat treatment are summarized in **Table 3.4**.

Table 3.4   Heat Treatment of 780psig precursor at 360 ˚C under N_2 flow for investigation of mesophase transformation.

Heat Treatment Time	% Wt Loss	MSP(˚C) [a]
Before Heat Treatment	-	299
30min	1.5	304
1hr	2	304
3hr	4.4	310
5hr	5.4	313

[a] MSPs are accurate to ±2 ˚C.

The continuous increase in weight loss with time shows that the loss is not simply due to the loss of moisture adsorbed in the samples, but also the loss of some dimer species. Because the temperature was quite low, reaction between dimer molecules was thought to be unlikely. Normalized MALDI spectra of the heat-treated samples (**Fig. 3.9**) did not show significant differences from the initial, untreated 780psig precursor. Although the weight loss was only ~5% and the softening point increase was only ~13˚C after even 5 hr of heat treatment under inert atmosphere, **Fig. 3.10** shows that a significant increase in mesophase content was observed. That is, we see that the mesophase spherules grew and

were converted into bulk mesophase with increasing heat exposure time at a relatively low heat-treatment temperature.
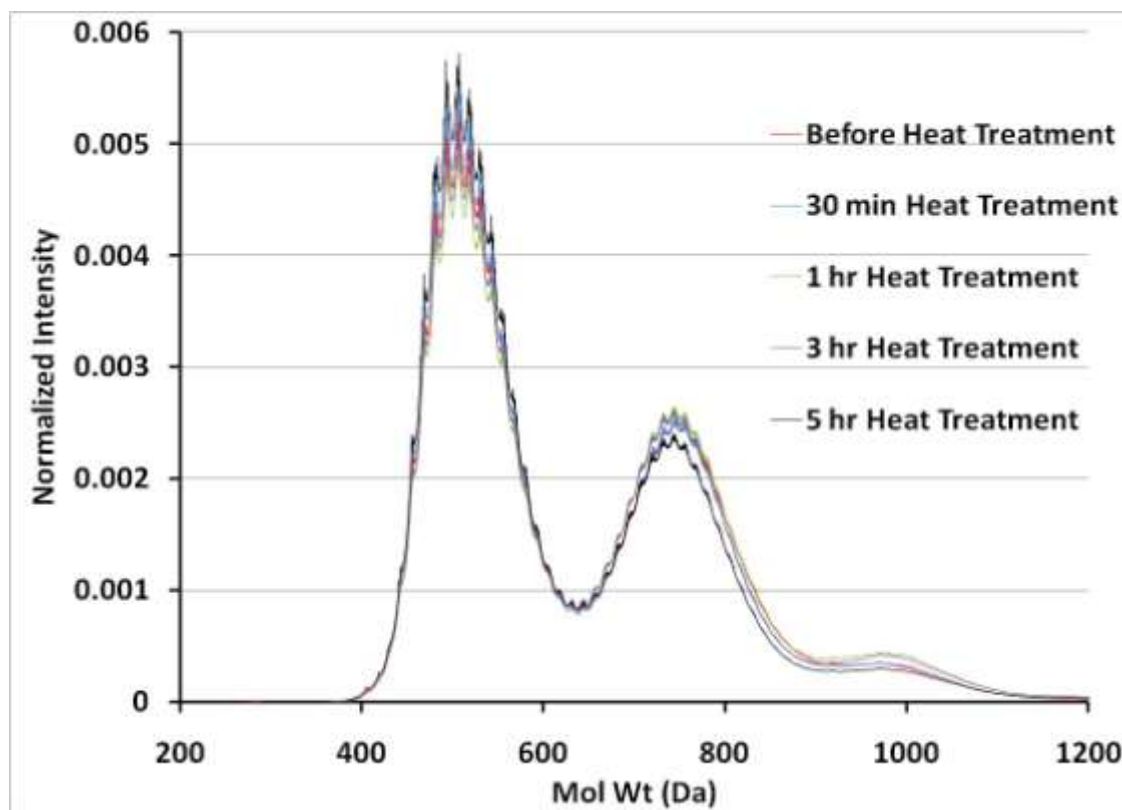
Fig. 3.9   Smoothed and normalized MALDI spectra of 780psig precursor before and after heat treatments at 360 ˚C. All spectra appear to be similar to each other, with no trend with increasing heat treatment time being observed. For consistency, all of the above spectra were obtained on the same day.

These results show that precursors containing small amounts of dispensed mesophase can form bulk mesophase, if sufficient time is allowed in the molten form. During ACF production, the pitch fibers are exposed to relatively high temperatures during spinning, but the spinning process typically takes only about 1 hr. Because the

750psig and 760psig samples were both spun well below 360 ˚C (see **Table 3.5**), such a change in mesophase content would not have been expected to occur.
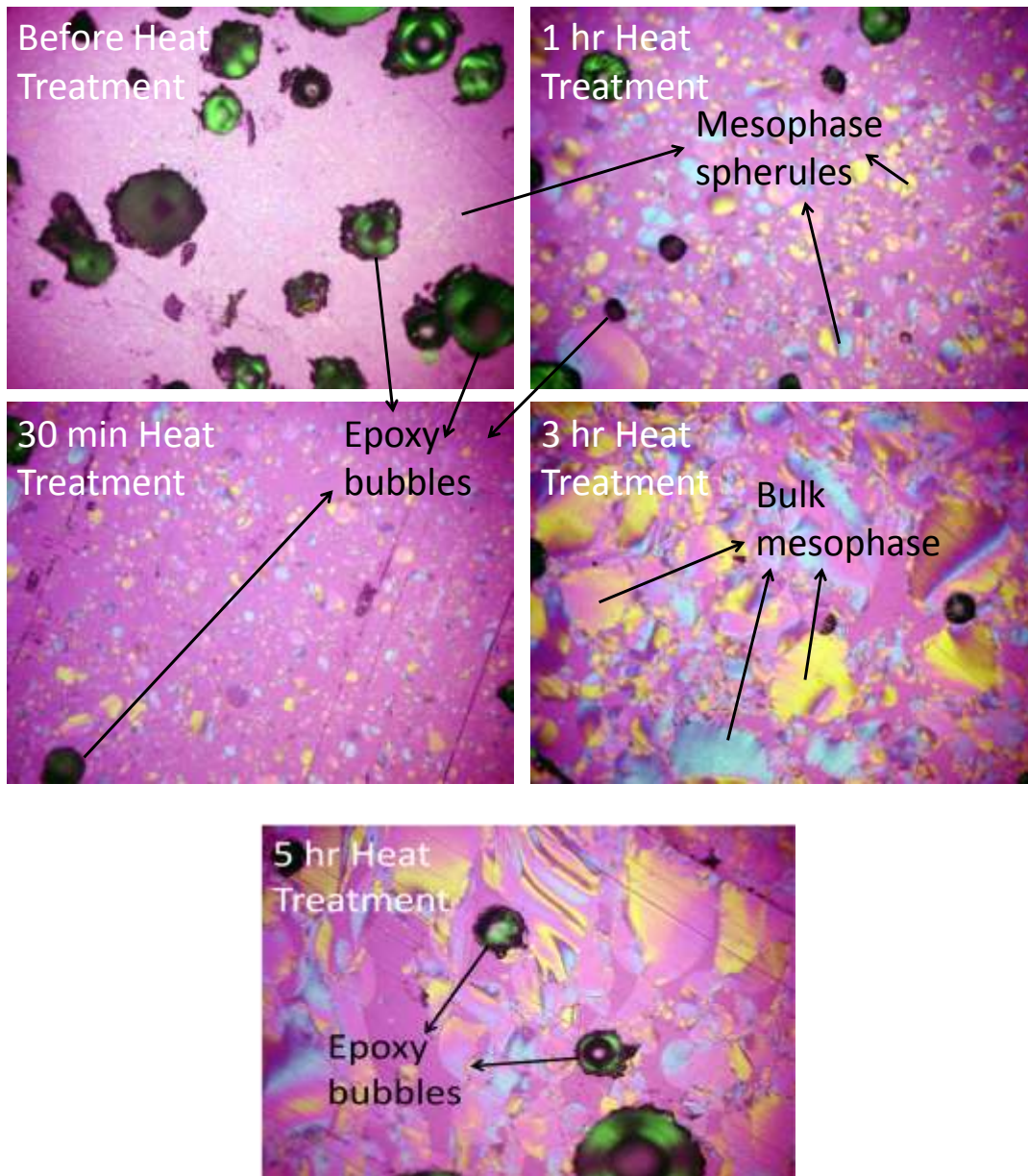
Fig. 3.10 Photomicrographs of polished surfaces under polarized-light microscopy of heat-treated 780psig precursors. Transformation of mesophase spherules into bulk mesophase and increase in mesophase is shown with increasing heat-treatment time.

3.5 Activated Carbon Fiber Production

3.5.1 Spinning

After the MSPs and mesophase content of the precursors were determined, they were spun into fibers using our batch melt-spinning equipment, as described in Chapter 2. In order to determine the appropriate spinning temperatures, MSP measurements were used as an initial guide. Based on our experience, the spinning temperature has been found to be approximately 20-25°C above the MSP of a given precursor. The actual spinning temperatures were then selected based on observations during the spinning process itself, in order to obtain the optimum amount of fibers. When fibers could be spun and collected as continuous filaments without breaking too often, the temperature was fixed at that point and the pressure reading was recorded. In general, the melt-spinning of pitch precursors can only be carried out over a limited temperature range. At too low a temperature, fibers will break because the precursor is not completely melted; at too high a temperature, the precursor will have too low a viscosity, and fibers will break as the winder pulls them down.

Molten pitch is essentially an incompressible fluid; therefore spinning pressure only has a negligible effect on the structure of the as-spun fibers. Because spinning is a temperature-sensitive process and we had only a limited amount of material, we focused on obtaining similar-sized fibers in sufficient amounts for further analysis. Pressure differences were as a result of differences in viscosity during spinning. Once continuous filaments started to be collected, the temperature was fixed at that point.

The spinning conditions that were used for each precursor are given in **Table 3.5**. It is important that all precursors be completely dry and free of any solvent, as any solvent left in the pitch will cause bubbling and therefore breakage of fibers during

Table 3.5   Spinning conditions (temperature and pressures) for all precursors used for ACF production. All fibers were collected at a ram speed of 2.0 cm^3/min and a winding speed of 177 m/min.

	Temp (˚C)	Press (psig)
Dimer-1	222	1050
Dimer-2	234	600
750psig	231	700
760psig	285	950
780psig	328	1150
800psig	341	1400
830psig	362	900

the spinning process. Fibers from all precursors were collected at the same ram speed (2.0 cm^3/min) and winding speed (177 m/min). Diameters of the fibers were between 20 and 30 μm.

3.5.2 Stabilization

Carbonization and activation of as-spun (green) fibers must be carried out at temperatures above 800˚C, well above the softening point of even the highest mol wt precursor that can be spun. Thus, as-spun fibers must be first stabilized in order to keep their fiber form. This process is also referred as "oxidation", or "oxidative stabilization", because during stabilization the fibers react with oxygen molecules in the gas phase.

For consistency, we desired to apply the same stabilization procedure to all precursors. As shown in **Table 3.2**, some of our precursors had low softening points, so the lowest stabilization temperature had to be applied to them all. Oxidation is a slow process at temperatures below 250 ˚C, so our stabilization process took about 6 days (the detailed procedure was given in Chapter 2).

As can be seen in **Fig. 3.11**, during the stabilization process fibers from all precursors followed a similar trend in terms of weight change, with all fibers gaining weight until some point and then starting to lose it thereafter. Weight change during this process results from several simultaneous mechanisms, including the uptake of oxygen, the loss of water, and the loss of some carbon in the form of carbon dioxide and carbon monoxide (Miura et al., 1995). All fibers had a weight gain of about 15-18% by weight, indicating that they were fully stabilized (Lin et al., 1991). Note that the samples started to lose weight near the end of the oxidative stabilization process, probably because of the completion of oxygen uptake and the continued loss of aromatic carbons as carbon dioxide and carbon monoxide. In a study of the stabilization of a naphthalene-derived, synthetic mesophase pitch, Drbohlav and Stevenson (1995) concluded that during the weight-gain period of oxidation, the aliphatic content of the pitch decreased while the oxygen content increased, with the oxygen forming mostly ester and anhydride groups. During the weight-loss period of the oxidation process, the aromatic carbon content decreased, being released as carbon monoxide and dioxide. Also, at low temperatures weight gain was more favored, while at higher temperatures weight loss dominated.
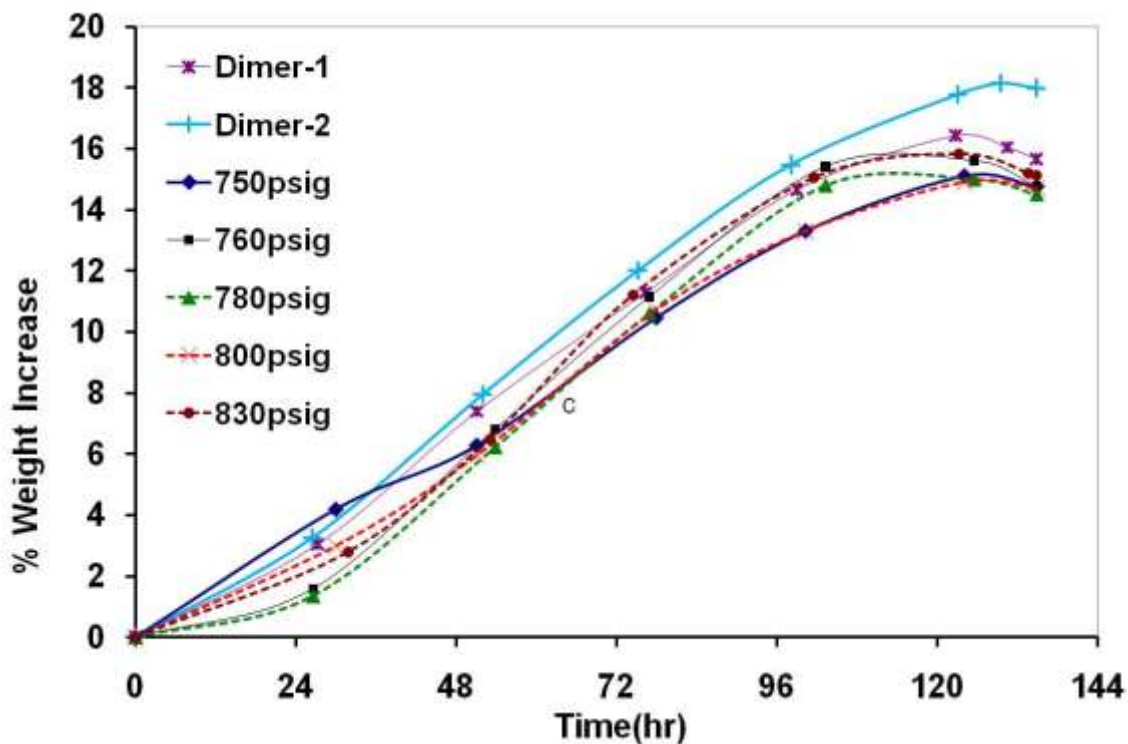
Fig. 3.11 Weight increase vs. stabilization time for as-spun fibers from each of our seven precursors during the oxidative-stabilization process.

Among the precursors studied, Dimer-2 was notable in gaining more weight compared to the others (see **Fig. 3.11**). Thus, based on the above study, one might assume that Dimer-2 has a higher alkyl content than the other precursors. However, Dimer-1 has a similar mol wt distribution to Dimer-2 (see **Fig. 3.8a**), so it is difficult to conclude from the molecular structures present in dimers (see **Fig. 3.12**) that Dimer-2, which is concentrated in higher mol wt dimer species, has a higher alkyl content than Dimer-1. In addition, no noticeable difference in the ratio of alkylated to aromatic protons for Dimer-1 vs. Dimer-2 was observed by solution ^{1}H-NMR (see **Fig. 3.13**). However, the ratio of

107

the 0.0-2.0 ppm peak to the 2.0-3.5 ppm peak (see **Fig. 3.13**) is higher for Dimer-1 than for Dimer-2, indicating that the alkyl groups in Dimer-1 are longer (i.e., more ethyl and propyl than methyl groups). These longer alkyl groups might be responsible for the less net oxidation gain of Dimer-1 compared to Dimer-2.
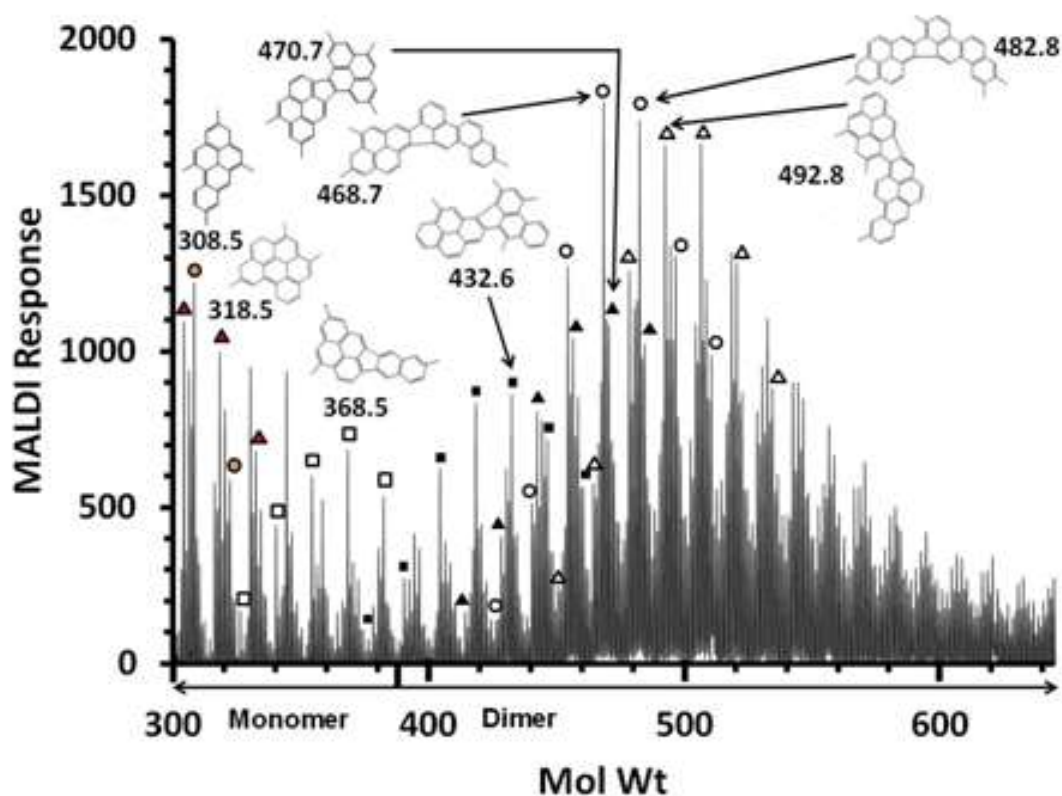
Fig. 3.12   MALDI spectra of M-50 pitch and proposed structures for monomer and dimer molecules. (Reprinted with permission from Burgess and Thies, 2011. Copyright 2011 Elsevier.)

MALDI analyses of the Dimer-1 and Dimer-2 precursors were also repeated using a solvent-based preparation method (see **Fig. 3.14a** and **b**), as this method elucidates higher mol wt species better than solid-based preparation method. As shown in **Fig. 3.14a**

and **b**, the Dimer-1 precursor does have more tetramer species than the Dimer-2 precursor, and this difference might have caused the difference in oxidation weight gain as we expect tetramer species to have relatively fewer alkyl groups than dimer species. In the next section, it is shown that carbonization results also support this possibility. Because the solvent-based preparation method might result in variations in signal response, the results can only be interpreted qualitatively. Nevertheless, The MALDI analyses were repeated at two different target spots for each precursor, and the results were consistent.

Finally, we caution the reader that in the above discussions, we have proposed several explanations for the oxidation weight gain differences between Dimer-1 and Dimer-2. However, the differences observed were not large, so it is possible that we are seeing nothing more than the effects of differences in fiber diameter.
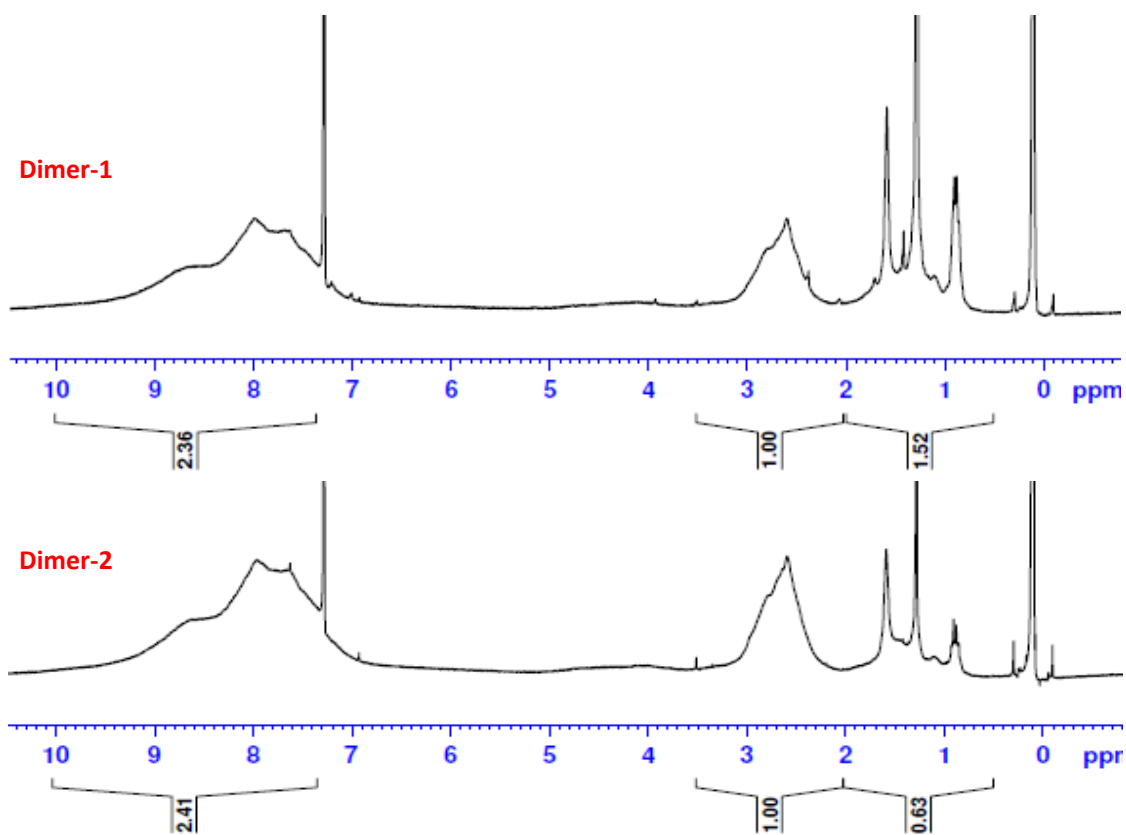
Fig. 3.13 ^{1}H-NMR spectra of Dimer-1 and Dimer-2 precursors. Normalized peak areas appear below the respective spectra and provide information about the relative abundance of aromatic (7.3-10.0 ppm), benzylic (2.0-3.5 ppm), and aliphatic (0.5-2.0 ppm) protons in the sample. Deuterated chloroform was used as the solvent.
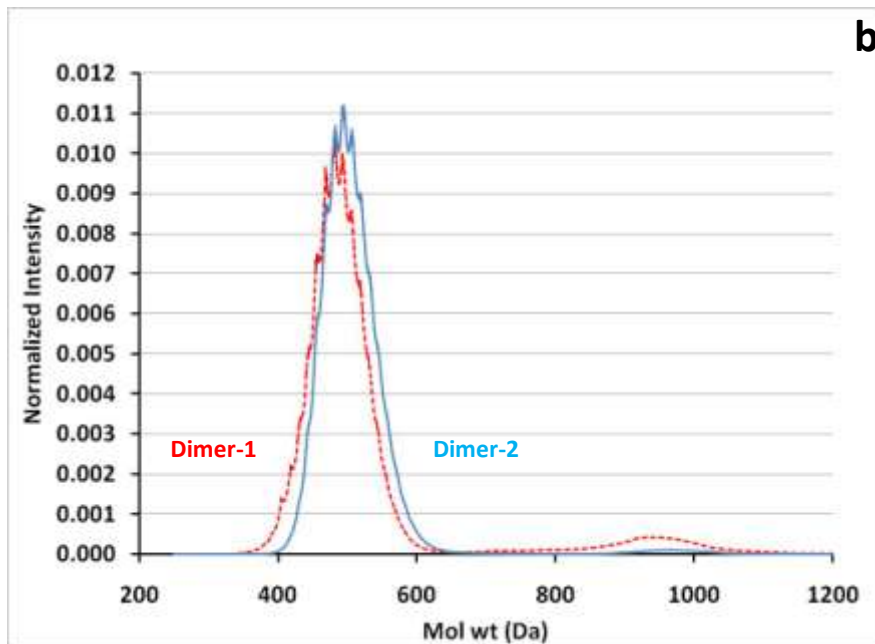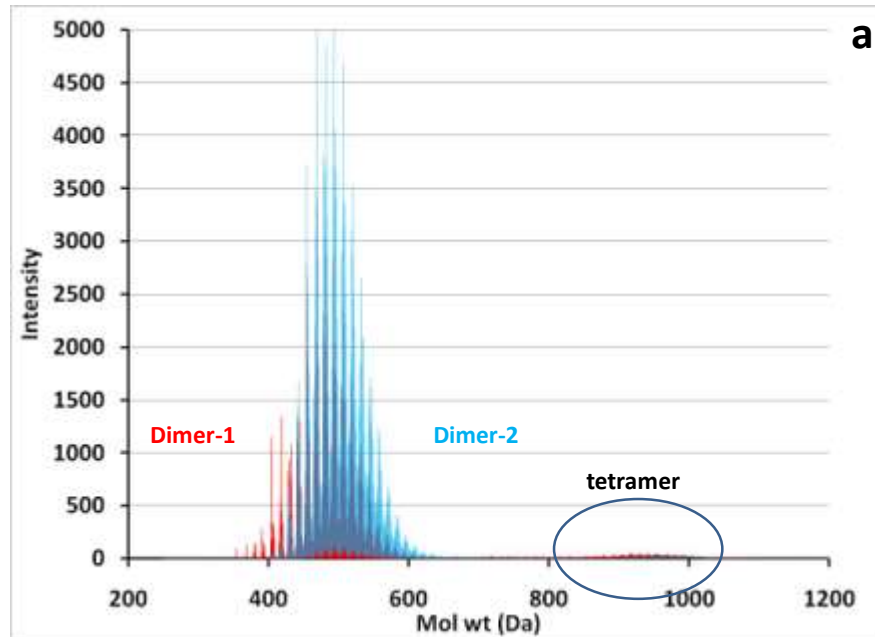
Fig. 3.14 (a) Raw, and (b) smoothed and normalized solvent-based MALDI spectra comparison of Dimer-1 and Dimer-2 precursors. Solvent-based method elucidates higher mol wt species better than solid-based preparation method.

111

3.5.3 Carbonization

Because our stabilized fibers were directly activated in a CO_2 environment, the separate contributions of carbonization and activation to the weight losses of our fibers had to be established by a separate set of carbonization experiments. Thus, a small portion (~100 mg) of the fibers stabilized above was treated to a "carbonization-only" step. This procedure is described in detail in Chapter 2.

The results of these carbonization experiments are given in **Figs 3.15**. Mol wt values referred to in **Fig. 3.15** and in the rest of the dissertation are MW_n and were calculated from MALDI spectra for each precursor using a Fortran code as explained elsewhere (Edwards, 2005, p191). The weight loss was found to be higher for precursors with a lower average molecular weight, that is, those consisting primarily of monomer and dimer species (Dimer-1, Dimer-2 and the 750psig precursors, see **Fig. 3.2** and **Table 3.3**). Because elimination of side chains is among the basic reactions that occur during carbonization (Lewis I.C., 1982), the higher alkyl and side chain (H) content of the smaller monomer and dimer molecules, as compared to the bigger trimer and tetramer molecules, could be the reason for the higher carbonization weight loss. Referring to **Fig. 3.12**, Burgess' MALDI results do not definitely establish that there are more alkyl groups/carbon atom for monomer and dimer vs. trimer and tetramer species. However, MALDI peak heights are not a reliable enough indicator of the amount of a given species present to make any definite statements in this regard.

Another trend of interest in **Fig. 3.15** is the fact that, for the 760psig precursor, carbonization % weight loss reaches a steady value with increasing average molecular weight.
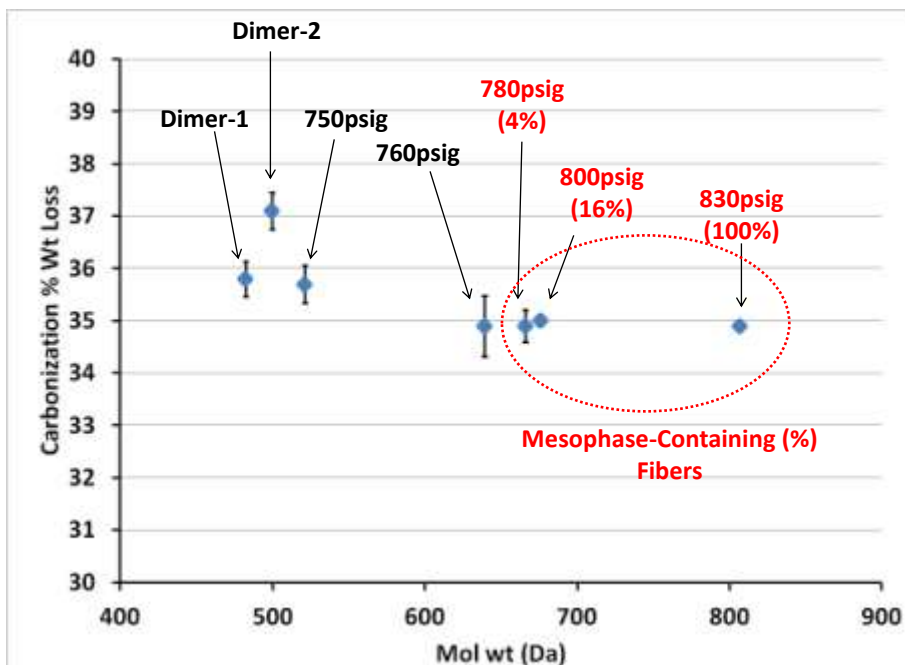
Fig. 3.15   Weight losses of stabilized fibers as a result of carbonization only are plotted vs. average molecular weight (error bars = ± 1 std dev).

Further increase in molecular weight has no further impact on carbonization % weight loss, even for the mesophase-containing precursors at 760psig and above. Thus we see that carbonization wt loss depends on the molecular weight of the precursor, with the presence of mesophase itself not being the determining factor.

3.5.3.1 Wide-Angle X-Ray Diffraction Analysis of Carbonized Fibers

Wide-angle x-ray diffraction (WAXD) analyses were carried out on carbonized fibers prepared from all seven precursors in order to determine the significance of the mesophase amount present in mesophase-containing fibers. Carbonized fibers were chosen for X-ray diffraction analyses, as fibers reach their final microstructure during the carbonization process, when they are exposed to the highest temperatures (up to 1000 °C) prior to the activation process.

WAXD analysis 2θ intensity profiles of all carbonized fiber samples are given in **Fig. 3.16**. Although the spectra are broad and the exact 002 peak locations are hard to determine, the difference between the locations of the 002 peaks for the isotropic vs. the mesophase-containing fibers can be clearly observed. The azimuthal intensity distribution for the approximate 002 peak location for each precursor is given in **Fig. 3.17**. This comparison clearly shows that the spectra for the 760psig sample is similar to those for isotropic precursors, and do not show any peak, whereas the spectra for 780psig and other two mesophase-containing fibers show clear peaks. Thus, the small amounts of mesophase detected in the 760psig precursor by polarized-light microscopy are seen to have a negligible impact on the extend of molecular order in this precursor, and it can be considered to be a fully isotropic precursor. **Fig. 3.17** also shows that the azimuthal intensity peak for 830psig fibers is narrower than 800psig and 780psig fibers, showing a higher degree of orientation with increasing mesophase percentage.

The tests were carried out on 2 sets of fiber samples prepared from each precursor to ensure reproducibility and similar results were obtained. WAXD analysis 2θ intensity

114

profiles and the azimuthal intensity distributions for the second set of samples are given

in Appendix C.
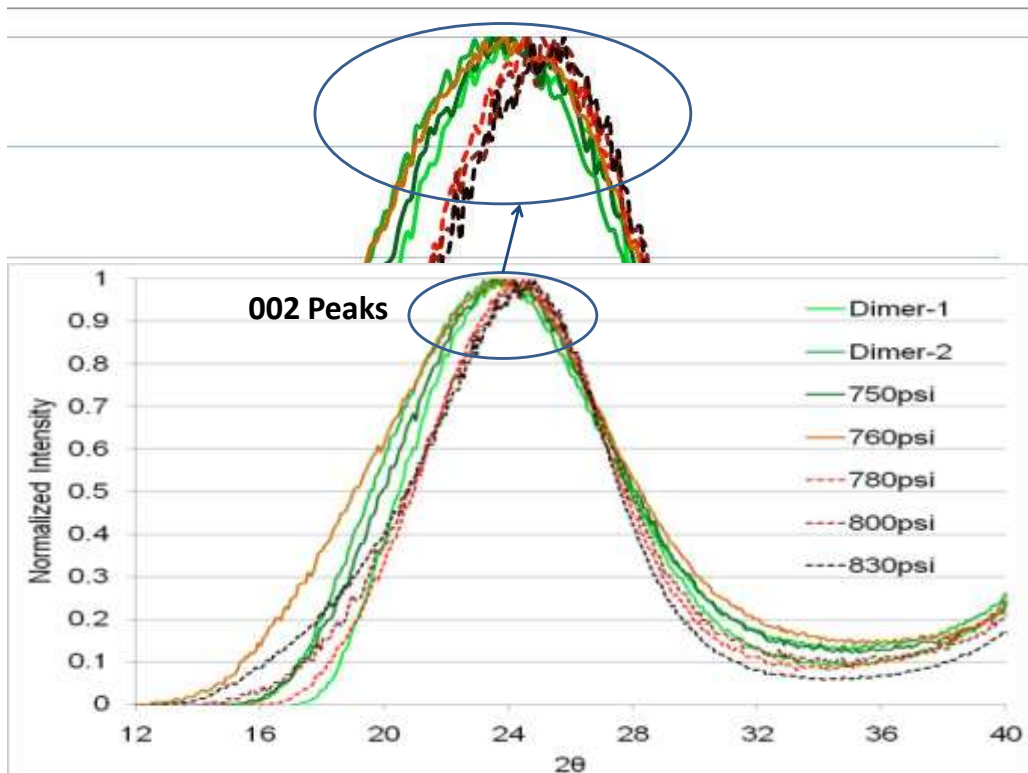
Fig. 3.16   WAXD analysis 2θ intensity profiles of the carbonized fibers prepared from all seven precursors. Note that the 002 peaks of the 780, 800, and 830psig (dotted curves) fibers are located at higher 2θ values than the 002 peaks of the 760psig and lower average mol wt precursors (solid curves).
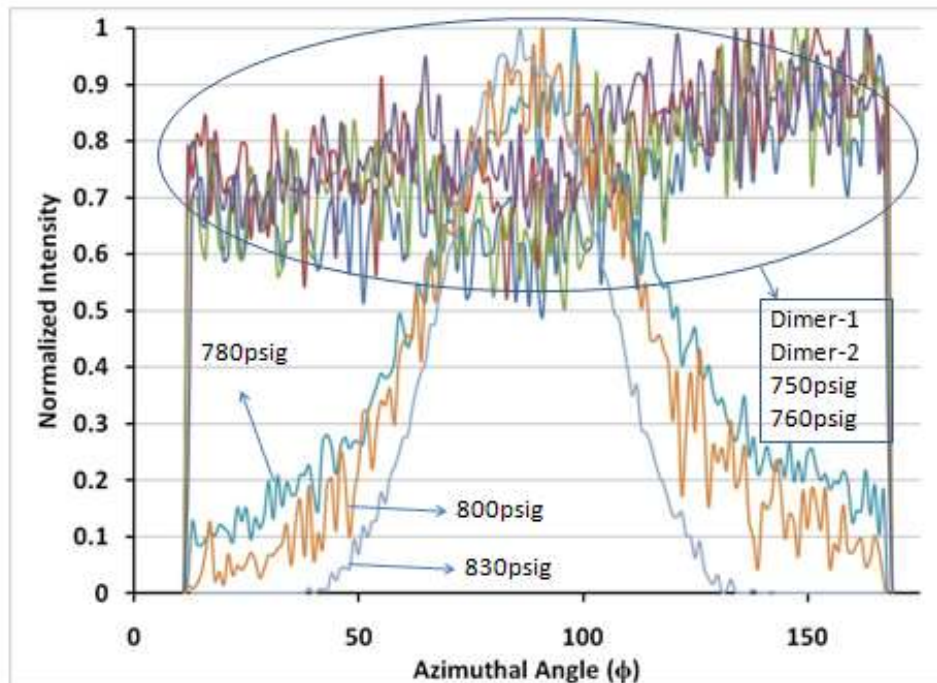
Fig. 3.17 WAXD analysis azimuthal intensity distributions at approximate 002 peak locations for carbonized fibers prepared from all seven precursors. Note that the azimuthal intensity distributions of the mesophase-containing fibers (780psig, 800psig and 800psig) are in the form of peaks, while those of the 760psig and other isotropic fibers are not.

3.5.4 Direct Activation

Following the above "carbonization-only" experiments, the remaining portion (~150 mg) of the stabilized fibers were subjected to direct activation for 6 hr at 840 ˚C using the procedure described in Chapter 2.

Initially during direct-activation experiments, industrial-grade CO_2 (National Welders Inc., item no. CD50) was used; however, after observing fluctuations in weight loss during the experiments, Coleman Grade CO_2 (National Welders Inc., item no.

114041) was used. Although the exact problem was not determined, water as an impurity in the industrial grade CO_2, or even as a separate phase present in the cylinder, was thought to be one of the most likely reasons, because water vapor is a much more aggressive activating agent than CO_2. After these initial problems, we also subsequently made sure that there was no dip tube inside the CO_2 cylinder being used. Direct-activation experiments using a CO_2 cylinder with a dip tube resulted in much higher weight losses; in some cases all of the fibers were degasified, leaving no samples at the end! Thus, all of the results shown herein are for direct-activation experiments using Coleman Grade CO_2 cylinders without a dip tube, repeated at least twice for consistency.

Comparison of total % wt loss and % burn-off (i.e., weight loss corresponding to activation only) of all precursors during direct-activation experiments are given in **Fig. 3.18**. The average weight losses measured for carbonization only for each precursor (see **Fig. 3.15**) were used to calculate by difference the % burn-off (weight loss corresponding to activation only) (see Appendix B). As seen in **Fig. 3.18**, both total % wt loss and % burn-off values were essentially constant for all isotropic samples, but were noticeably lower for mesophase-containing precursors, taking a significant drop even with a mesophase content of only 4%.

Because all fibers were direct-activated for the same amount of time (i.e., 6 hr), the % burn-off values can also be considered as a measure of activation rate. Unlike carbonization, there is a big drop off in the % burn-off as we move from isotropic to anisotropic (i.e., 780psig and higher) fibers, and the activation rate continues to decrease as the mesophase content increases (**Fig. 3.18**). Based on these results, we conclude that

(1) all isotropic fibers undergo the same activation mechanism because they all have the same activation rate, and (2) the presence of structural anisotropy, as caused by the presence of mesophase, interrupts the activation process.

Finally, we consider the cumulative % yield of the ACFs produced from each precursor, which is the net % yield of the direct-activated carbon fibers starting from the as-spun fibers (i.e., oxidation + carbonization + activation). Higher yields will lower the cost of ACFs and will be preferred, as long as the desired porosity is obtained. The cumulative % yield is essentially constant for the isotropic (760psig and below) precursor fibers, but then increases significantly for the anisotropic 780psig and higher mol wt precursor fibers (**Fig. 3.19**). Of course, we already know that the anisotropic fractions have a higher product yield because of their lower activation rate, which we expect will negatively affect pore structure formation.
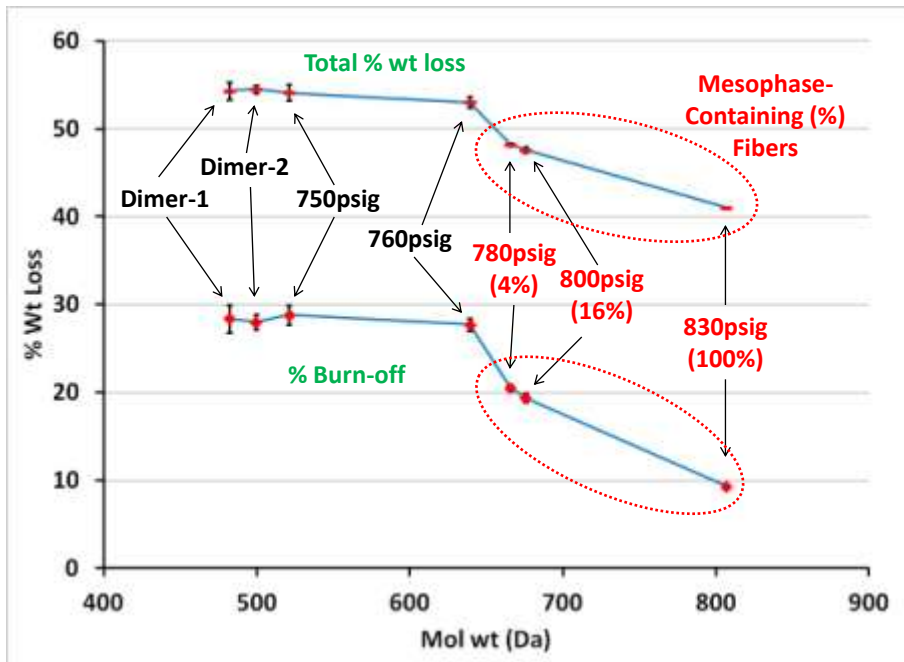
Fig. 3.18   Total % weight loss and % burn-off of stabilized fibers as a result of 6-hr, direct activation based on average molecular weight of each precursor (error bars = ± 1 std dev). The lines connecting the data are to guide the reader's eye only.
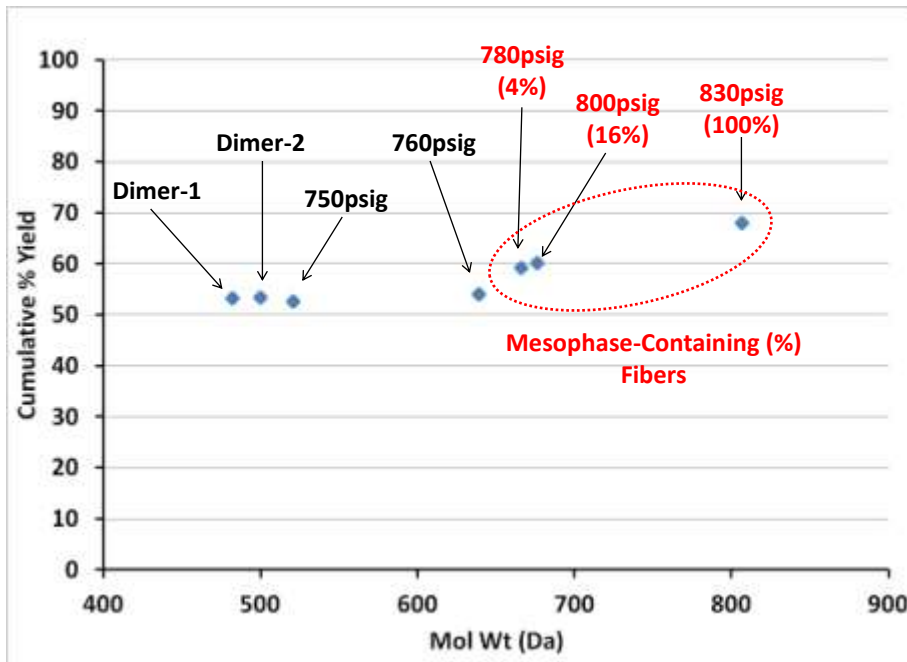
Fig. 3.19   Cumulative % yield of production of ACFs from as-spun fibers based on average molecular weight of each precursor.

3.6 Surface Characterization of Activated Carbon Fibers

In order to see the effect of the activation process and determine the final pore characteristics of the fibers, surface analyses were carried out on 6-hr, direct-activated fibers made from each precursor. The detailed procedure was described in Chapter 2. **Fig. 3.20** shows the nitrogen adsorption isotherms of the ACFs from 10^{-7} to 0.3 relative pressures. Adsorption measurements at such low relative pressures are required in order to obtain information about the ultramicropores (<7 Å). All isotherms are IUPAC Type I (Sing et al., 1985), and show microporous adsorption behavior. The results clearly show the differences among the nitrogen uptakes of the different fractions.
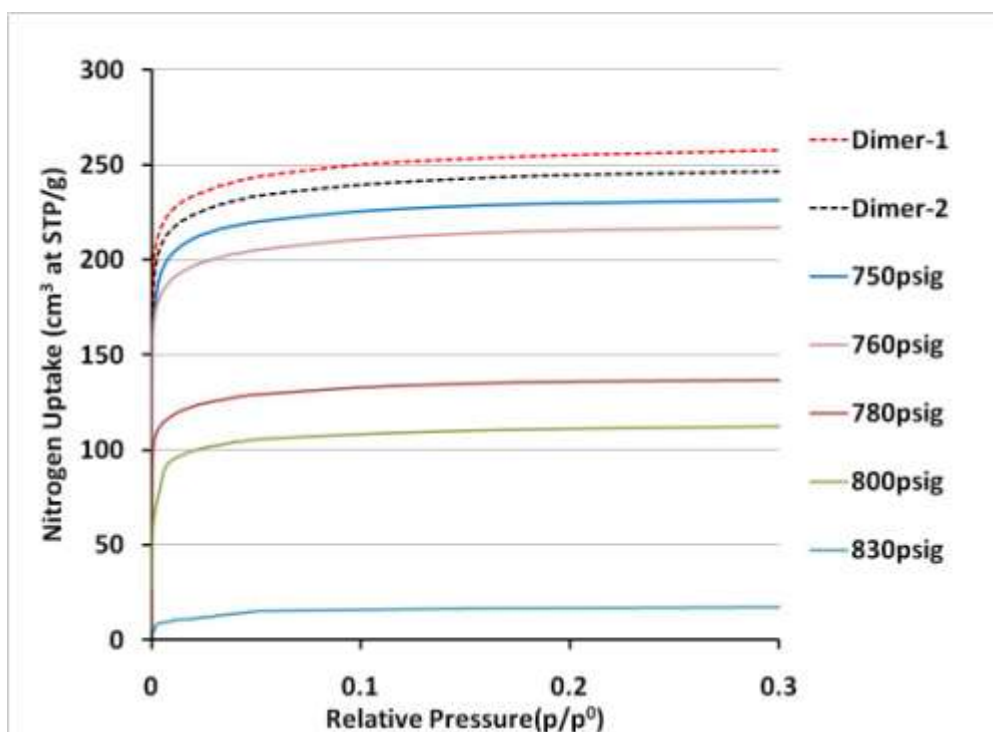
Fig. 3.20   Nitrogen isotherms of 6-hr, direct-activated carbon fibers from all seven precursors, showing the volume of N_2 adsorbed (cm^3 at standard temperature and pressure (STP)) per gram of ACFs at different relative pressures (p/p^0) from 10^{-7} to 0.3. (p^0: saturation pressure of the adsorbent at liquid nitrogen bath temperature (77 K)).

In order to see the significance of the differences in nitrogen adsorption behavior among the different precursors, total nitrogen-uptake values of all fractions at a constant relative pressure of 0.3 were compared; these results are given in **Fig. 3.21**. Although the values at a relative pressure of 0.3 were chosen because they had the highest uptake values, **Fig. 3.20** shows that all isotherms are essentially parallel to each other. Therefore, choosing another relative pressure would have given the same results. **Fig. 3.21** shows that even for the fully isotropic (Dimer-1, Dimer-2, 750psig, 760psig) ACFs, the nitrogen uptake decreases with increasing molecular weight. Thus, even if there is no molecular

121

order (brought about by mesophase content), the precursors that are composed of smaller (i.e., lower mol wt) molecules have a higher pore volume. Also of interest is the dramatic drop-off in nitrogen uptake that occurs when we undergo the transition from isotropic (760psig) to anisotropic (780psig) behavior, even though the increase in molecular weight (see **Fig. 3.21**) is quite modest. Note how this behavior corresponds well with the drop in % burn-off observed in **Fig. 3.18**, when we move from isotropic (760psig) to anisotropic (780psig) fibers. According to Marsh and Reinoso (2006), this phenomenon occurs because of stacking of the long micrographene layers forming the mesophase
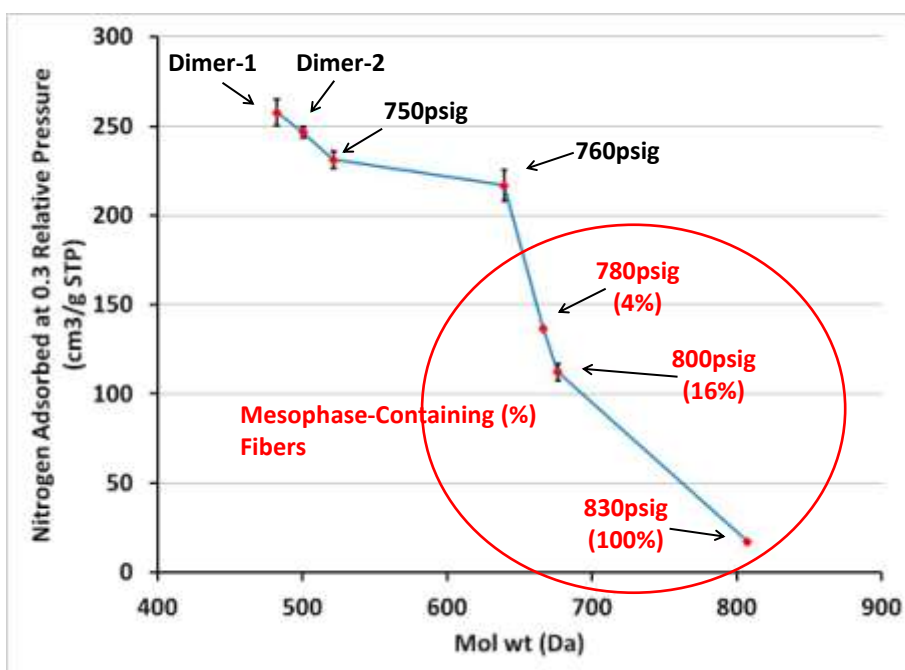
Fig. 3.21   Nitrogen-uptake values of 6-hr, direct-activated fibers at a relative pressure of 0.3 (from **Fig. 3.20**) based on average molecular weight (error bars = ± 1 std dev). The lines connecting the data are to guide the reader's eye only.

regions, so that the activating gas (i.e., carbon dioxide) cannot gain access to the inner carbon atoms of the mesophase regions of the fibers during activation, preventing the formation of micropores.

Density Functional Theory (DFT) was used through preinstalled software (Micromeritics Inc., DFT Plus) to interpret the adsorption isotherm data and to obtain pore size distributions. To briefly explain (Webb and Orr, 1997), DFT predicts the distribution of adsorbate molecules from the wall of the pores for a specific, assumed pore geometry (slit-shaped in our case) and pore size at a specific temperature and pressure by minimizing the free energy of the system. For each pore size, the distribution is predicted over a range of pressures at a specific temperature, and an adsorption isotherm specific to that pore size is obtained. Then, the experimental adsorption isotherm is fitted using a deconvolution method, assuming the isotherm is the sum of individual contributions of each pore of a different size.

Figs 3.22 and **3.23** show the cumulative and incremental pore size distributions of the direct-activated, precursor carbon fibers, respectively. All pore volume values are specific pore volumes, i.e., volume per gram of ACF sample. As shown by comparing **Fig. 3.23a** to **Fig. 3.23b**, the higher nitrogen uptake of the fibers made from lower mol wt isotropic precursors is not because they have larger pores, but because they have more pores, both ultramicropores (<7 Å) and larger-sized ones. We believe the reason for this is that the smaller molecules form shorter, defective-micrographene layers, which allow easier access of the gasifying agent (CO_2) to the inner carbon atoms, and thus their easier removal from the microstructure. In other words, because the micrographene layers are

shorter, it is easier for the activating gas cut a pore (channel) from one micrographene layer to the next. A similar trend was observed for those ACFs containing partial amounts of mesophase (780psig and 800psig) (see **Fig. 3.23b**); however, for 830psig (100% mesophase) ACFs almost no pores smaller than 13 Å were observed, showing that CO_2 activation is insufficient for the activation of mesophase fibers.
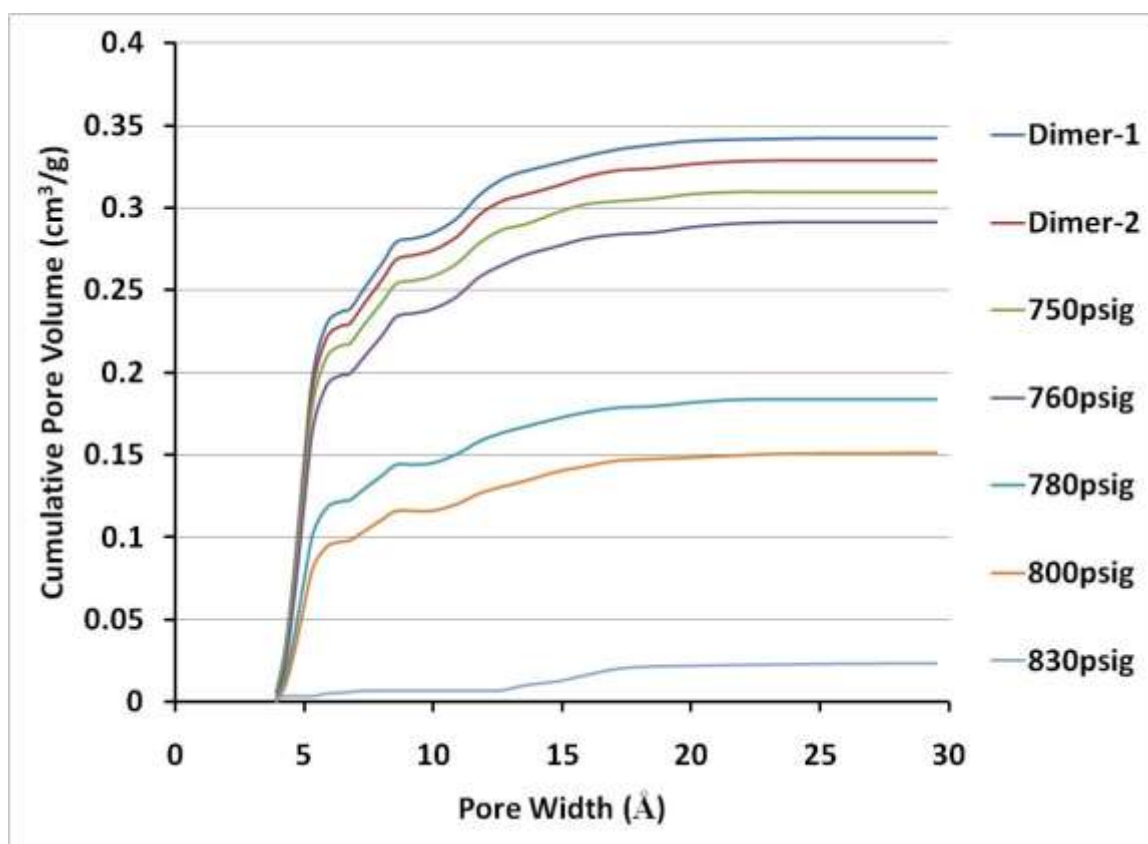
Fig. 3.22   Cumulative pore size distributions of 6-hr, direct-activated carbon fibers prepared from all seven precursors. Data was obtained using the preinstalled software (DFT Plus, Micromeritics Inc.) based on interpretation of nitrogen adsorption data via Density Functional Theory, assuming slit-shaped pores.
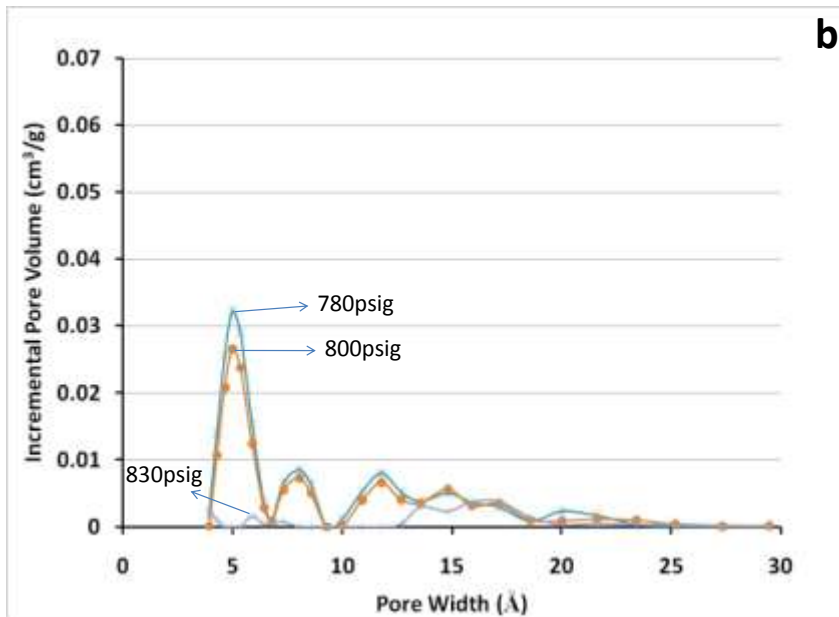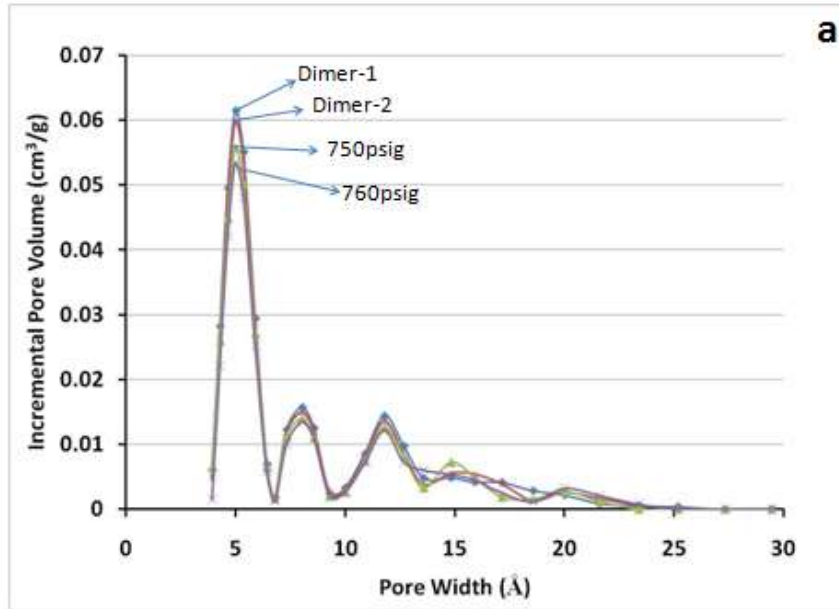
Fig. 3.23 Incremental Pore size distribution of 6-hr, direct-activated carbon fibers prepared from all seven precursors. Data was obtained using the preinstalled software (DFT Plus, Micromeritics Inc.) based on interpretation of nitrogen adsorption data via Density Functional Theory, assuming slit-shaped pores. For clarity, (a) isotropic and (b) mesophase-containing fibers were plotted in separate graphs.

125

Both preliminary molecular modeling studies conducted at Oak Ridge National Laboratory (ORNL) and the study of Cabria et al. (2007) have shown that the optimum pore size for hydrogen storage would be 6-7 Å. Therefore, the volume of the 1st peak (representing ultramicropores) in the incremental pore distribution graphs (**Fig. 3.23**) is the one of primary interest for hydrogen-storage purposes.

In **Fig. 3.24**, we have plotted both the total pore volume and the volume of the major peak of interest in **Fig. 3.23a** (i.e., the ultramicropores, or 1st peak) vs. precursor type and precursor molecular weight. "1st peak" volumes were taken from cumulative pore volume data (i.e., **Fig. 3.22**) at a pore width of 6.8 Å, while total pore volumes were taken at a cumulative pore volume of 30 Å. Analogous to the N_2 uptake plots in **Fig. 3.21**, we see a steady drop in both 1st peak and total pore volume with increasing molecular weight for the isotropic precursors, and then a transition to an even steeper drop off in pore volume with the onset of molecular order and anisotropy.

Additional insights are obtained by plotting the ratio of the 1st peak volume to the total pore volume (**Fig. 3.25**). Thus, we see that this ratio is virtually constant for the isotropic fibers, starts to decrease with increasing mesophase content, and then plummets as the mesophase content approaches 100%.
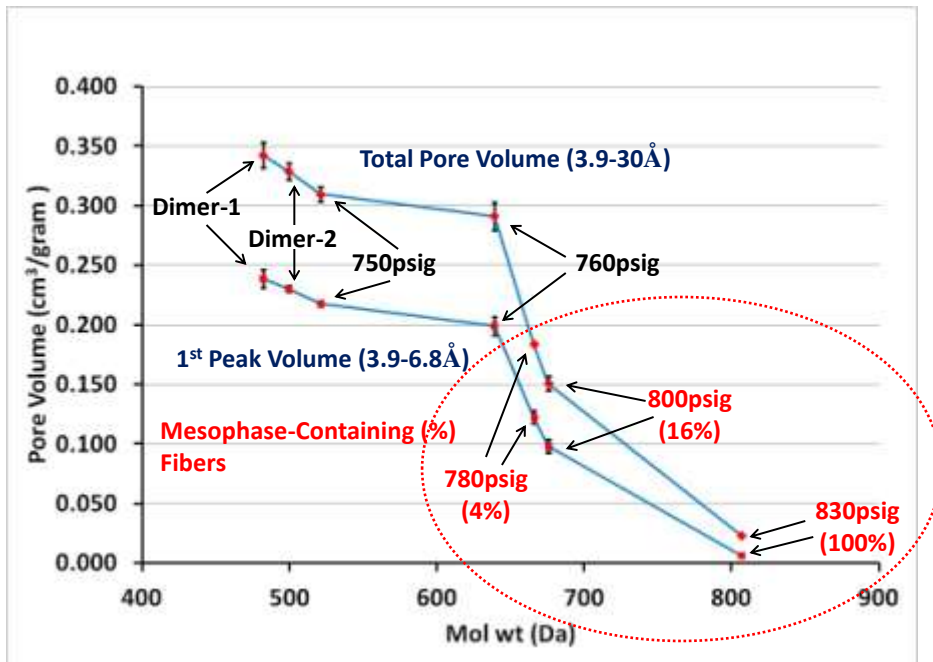
Fig. 3.24   Pore volume of 6-hr direct-activated fibers. Pore volumes were taken from cumulative pore volume data (**Fig. 3.22**) and plotted based on average molecular weight (error bars = ± 1 std dev). The lines connecting the data are to guide the reader's eye only.
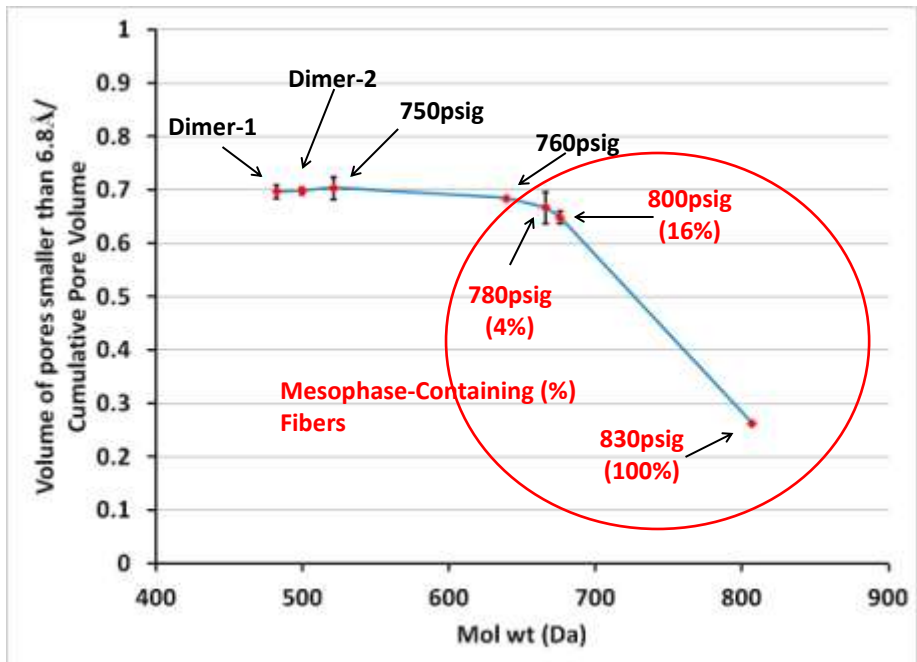
Fig. 3.25   Ratio of the volume of the pores smaller than 7 Å to the total pore volume (<30Å) of the 6-hr, direct-activated fibers based on average molecular weight (error bars = ± 1 std dev). The lines connecting the data are to guide the reader's eye only.

Although the above results clearly indicate that the effects of mol wt distribution and molecular order (anisotropy) are both important in understanding the adsorption behavior of ACFs, but it would be helpful to be able to separate out these effects from each other. For this purpose, as an approximation, mesophase regions of all mesophase-containing fibers were assumed to activate in the same way and have the same specific pore volume (pore volume per gram of mesophase region). In other words, the specific pore volumes (both 1st peak volume and total pore volume) of the mesophase regions for

the mesophase-containing fibers (i.e., the 780psig and 800psig fibers) were assumed to be the same as the specific pore volumes of the 100% mesophase 830psig precursor. (The 830psig fibers were chosen because, being 100% mesophase, their specific pore volumes are entirely those of the mesophase region.) As the pore volumes of the mesophase regions are significantly less than those of the isotropic regions, assuming that the specific pore volumes of all mesophase regions are the same should be a reasonable approximation.

Using the above approximation and knowing the mesophase percentages of the 780psig and 800psig precursors, the specific pore volumes in these precursors corresponding to their isotropic regions were then calculated. In a similar manner, the activation rates of all mesophase regions were assumed to be the same, and based on this assumption % burn-off values corresponding to the isotropic regions were calculated. Then, the isotropic-phase specific pore volumes of 780psig and 800psig ACFs calculated above were divided by the isotropic-phase % burn-off and multiplied by 100 in order to eliminate the differences between the burn-off levels (see Appendices B for details).

Results are shown in **Fig. 3.26** and indicate that the trend of decreasing pore volume with increasing molecular weight is better-behaved when the mesophase regions are factored out. However, the higher slope of the curve above the 760psig precursor shows that to some extent, the mesophase regions are probably limiting the access of activating gas (CO_2) molecules to the isotropic regions closer to the center of the fibers.
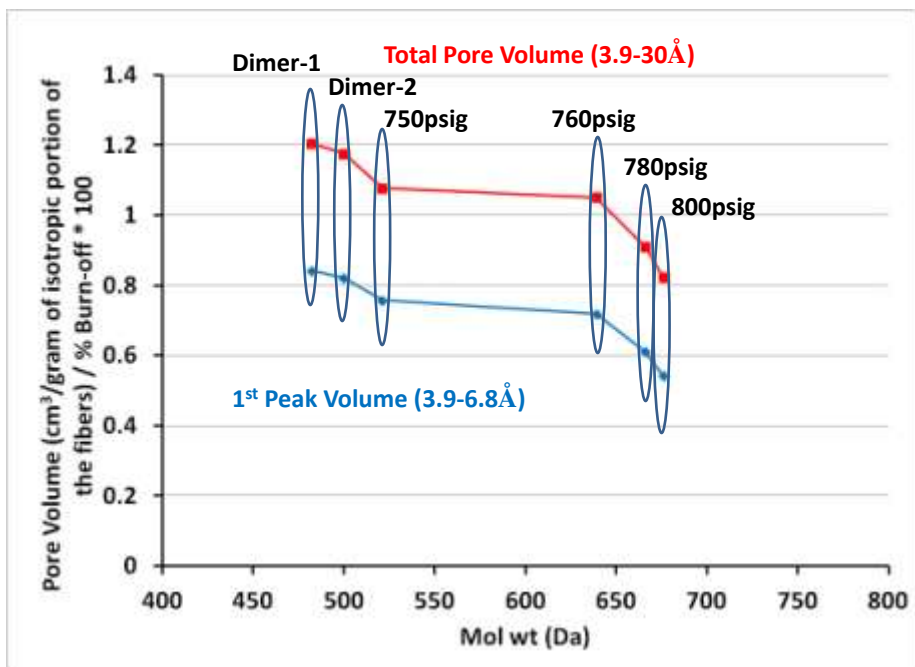
Fig. 3.26   Specific pore volumes per burn-off of the isotropic phase of the ACFs based on average molecular weight. For mesophase-containing fibers (780psig and 800psig) an approximate specific pore volume for isotropic phase was calculated using their mesophase area % and the pore volume of 100% mesophase (830psig) fibers. Details can be found in Appendix B. The lines connecting the data are to guide the reader's eye only.

3.7 The Effect of Direct-Activation Time on Burn-off and Final Porosity of Dimer-1 Activated Carbon Fibers

In the work discussed above, all precursor fibers were direct-activated at the same set of conditions, that is, for 6 hr at 840 ˚C. Thus, in order to determine how pore development varied with the degree of burn-off, Dimer-1 fibers were also direct-activated for 3 hr, 9 hr and 12 hr. (Dimer-1 fibers were chosen because they had the highest nitrogen uptake and pore volume after the 6-hr direct activation time period.) Percent

burn-off vs. direct-activation time results for Dimer-1 samples are given in **Fig. 3.27**. The higher initial slope (see **Fig. 3.27**) shows that the activation rate was higher at the initial stages of the activation process, while it was essentially constant at the latter stages of the activation process.

While **Fig. 3.28a** shows the nitrogen adsorption isotherms at relative pressures (p/p^0) of 10^{-7} to 0.3 for all Dimer-1 samples, **Fig. 3.28b** shows the nitrogen-uptake values only at the highest relative pressure (0.3) measured (for an easier comparison). As expected, as the degree of burn-off increased, the total nitrogen uptake also increased. The linear relationship between the nitrogen uptake and burn-off level was maintained, indicating a similar pore formation mechanism in all Dimer-1 fibers. Also, the incremental pore distribution plot (**Fig. 3.29**) shows that there is a significant increase in the 1st-peak volume (3.9 - 6.8 Å pores) as we increase from 3 hr to 6 hr of direct activation, but the increases in 1st-peak volumes for 9 and 12 hrs are somewhat smaller.

In order to investigate the pore formation mechanism more closely, formation rates of different sizes of pores (i.e., the increase in volume of a specified size of pores per hour) were plotted in **Fig. 3.30**. As shown there, the rate of formation of 3.9 - 6.8 Å pores was initially almost an order of magnitude higher than the rate of formation of larger pores (i.e., 6.8 - 30 Å pores). However, the rate of formation of 3.9 - 6.8 Å pores decreased dramatically, while that of larger pores (i.e., 6.8 - 30 Å pores) slowly increased with increasing activation time (thus, burn-off). Until about 6 hr of direct activation time, the rate of formation of 3.9 - 6.8 Å pores was still higher than for the larger *pores*. Thus,

131

these results show that as part of the initial activation mechanism, new pore formation is much more dominant than pore enlargement.

Recall the non-graphitizable (i.e., isotropic) carbon model of Franklin (**Fig. 1.2**) to help us understand the activation mechanism. Based on her model, non-graphitizable carbon material is composed of groups of short graphene layers. Within each group, the graphene layers are unidirectional; however, each group has different, random directions. Although her model is conceptually correct, one must note that the graphene layers forming the groups are not perfectly planar or well-ordered, instead they are defective, bent, and not perfectly parallel to each other.

Therefore, based on our results and our basic understanding of isotropic precursors and activated carbon structure, new pore formation can be expressed as the selective removal of one of the defective micrographene layers within a group of several micrographene layers, and pore enlargement can be expressed as the removal of additional defective micrographene layers from the same group that are adjacent to the first removed layer. These micrographene layers are most probably the PAH molecules that constitute the pitch precursor, that is, the dimer molecules in our case. As all micrographene layers forming a group are not identical and will also be in different positions, they will have different reactivities at the edge plane of the group. Once the activating agent (i.e., CO_2) reaches and reacts with a carbon atom (with a relatively higher reactivity than the other carbon atoms on the same group edge plane) from a given defective micrographene layer and extracts that carbon atom, that micrographene layer (i.e., molecule) now becomes more reactive. Therefore, the gasification reaction is

expected to continue until this molecule (i.e., layer) is completely gasified and removed. Therefore, based on the pore formation rate results (**Fig. 3.30**) and discussions in the above paragraphs, we may conclude that the activation mechanism is governed first by the removal of a single defective micrographene layer from a group of defective micrographene layers, and at latter stages of activation second or further layers are also removed. The peaks in the incremental pore size distribution graph of Dimer-1 ACFs (see **Fig. 3.29)** can be used to further elucidate their structure. The fact that the first two peaks are completely isolated and that the peaks overlap beginning with the third peak may be interpreted as each micrographene group being composed of at least four dimer molecules (i.e., layers).
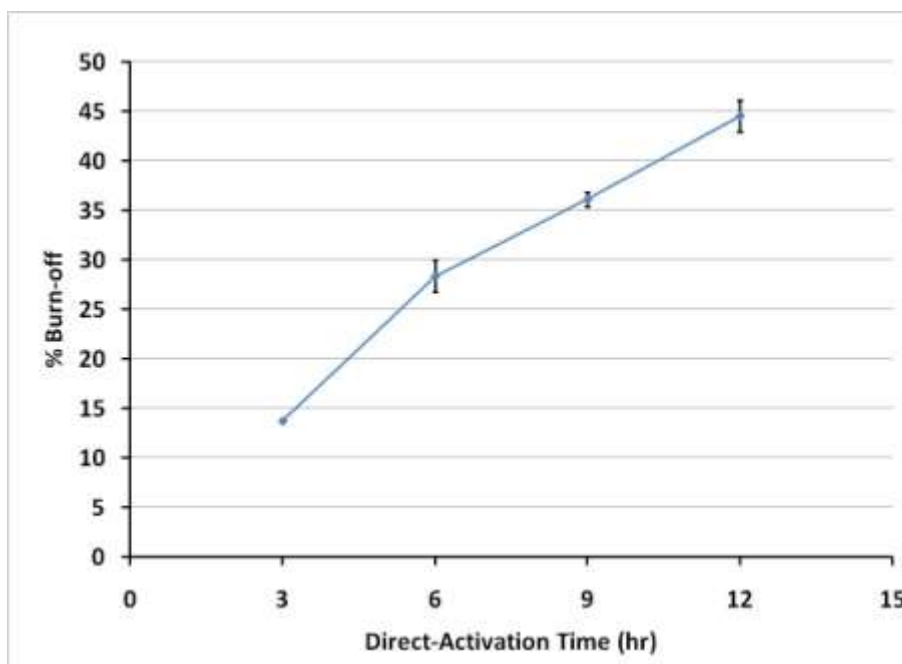
Fig. 3.27   % Burn-off (direct-activation weight loss excluding carbonization) of Dimer-1 fibers as a result of direct-activation experiments over time intervals of 3, 6, 9, and 12 hr (error bars = ± 1 std dev).
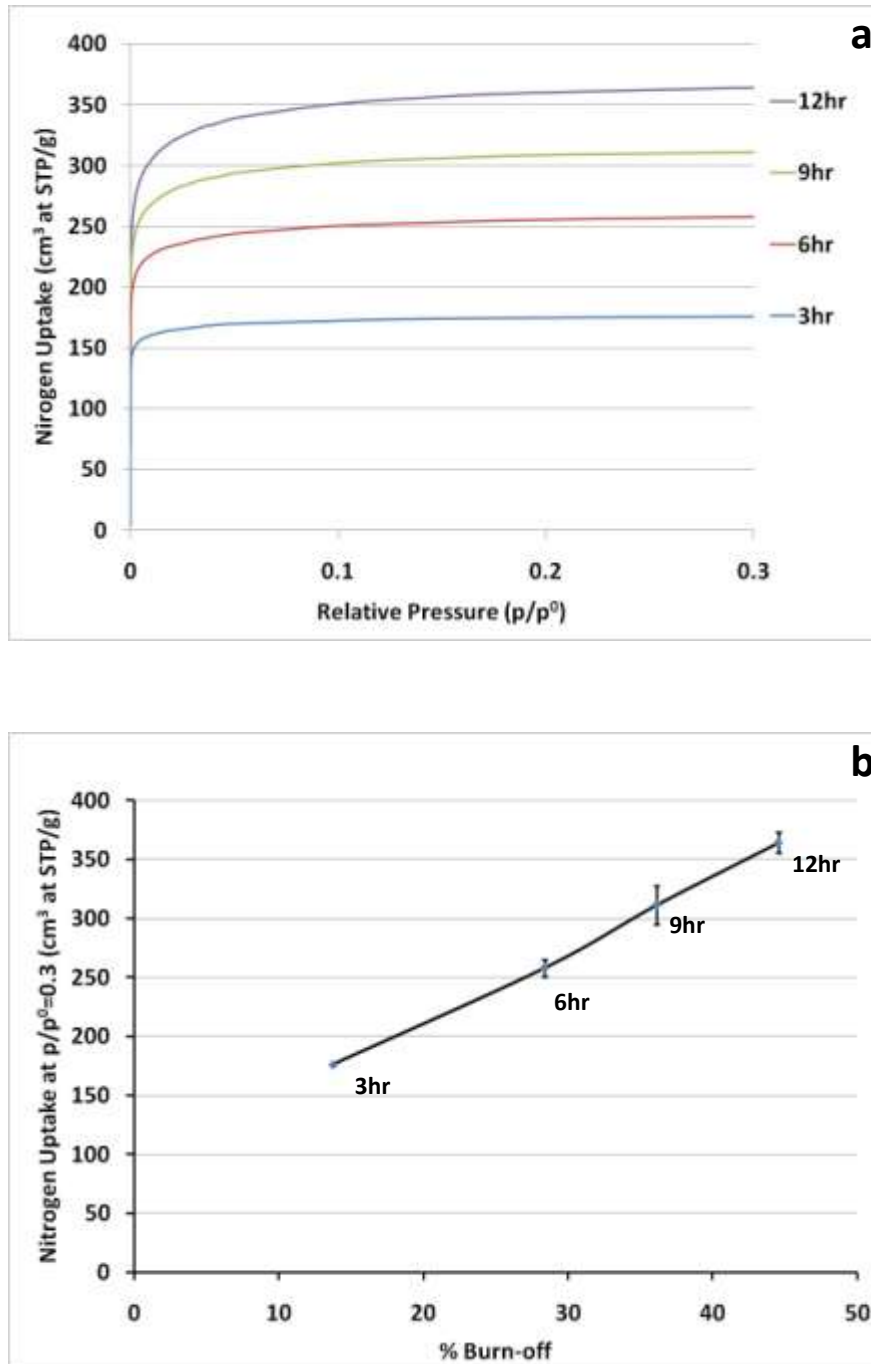
Fig. 3.28   Nitrogen-uptake values of Dimer-1 fibers as a result of direct-activation experiments over time intervals of 3, 6, 9, and 12 hr. (a) Nitrogen isotherm at p/p^0 of 10^{-7} to 0.3, and (b) nitrogen-uptake values at p/p^0 of 0.3 vs. % burn-off (error bars = ± 1 std dev).

Referring to **Fig. 3.30**, it is also important to note that the volume of pores larger than 6.8 Å increases relative to the pores smaller than 6.8 Å after 6 hr of direct-activation time. Thus, these results support the use of 6-hr direct activation, both for the development of pores smaller than 6.8 Å and for optimum yield.
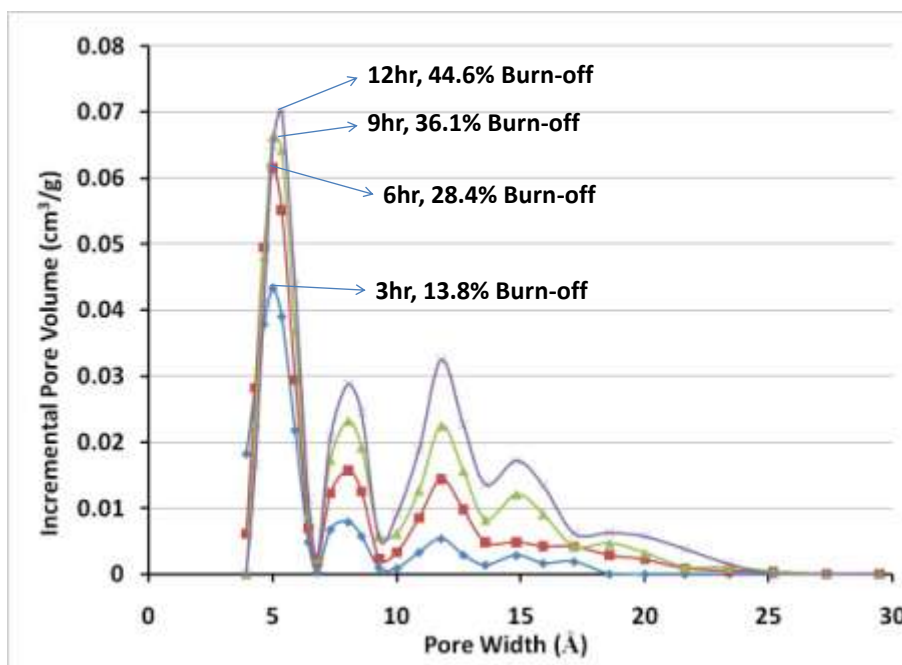
Fig. 3.29   Incremental pore size distributions of direct-activated Dimer-1 fibers for direct-activation times ranging from 3 to 12 hrs. Data was obtained using the preinstalled software (DFT Plus, Micromeritics Inc.) based on interpretation of nitrogen adsorption data via Density Functional Theory, assuming slit-shaped pores.

Finally, we note that the increase obtained in the 1st-peak volume of 6-hr direct-activated fibers when comparing 760psig precursor to Dimer-1 precursor (see **Fig. 3.23a**) is essentially the same as the increase obtained when comparing 6-hr, direct-activated

Dimer-1 fibers to those activated for 12 hours (**Fig. 3.29**). This shows how much of a difference the composition of the precursor can make in the volume of the ultramicropores available in ACFs.
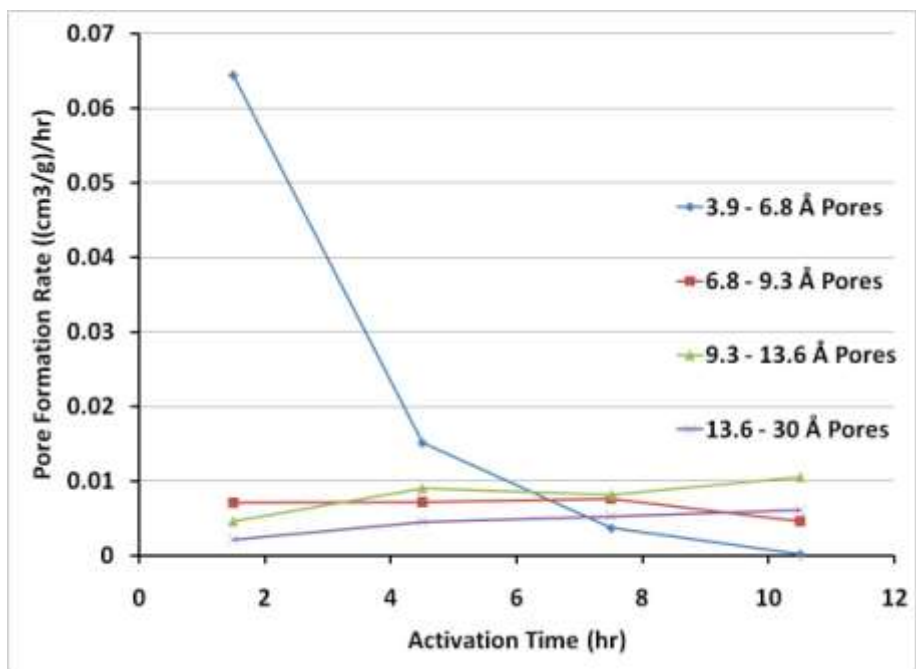
Fig. 3.30   Pore formation rate of direct-activated Dimer-1 fibers for direct-activation times ranging from 3 to 12 hrs. Pore size ranges are taken from the incremental pore size distribution peaks given in **Fig. 3.29**.

4. CONCLUSIONS AND RECOMMENDATIONS

4.1 Conclusions

Although researchers have previously investigated the effect of precursor composition on the final pore structure of activated carbon fibers (ACFs), the precursors compared in those studies were from different origins (e.g. coal-tar pitch vs. petroleum pitch), and the constituents of the precursors were not well-defined. In this study, the pore structure of ACFs was successfully controlled by manipulating the molecular weight distribution of precursor pitch fractions prepared from the same mother pitch. Results were used to obtain a better understanding of the effect of precursor composition on the properties and performance of ACFs. Conclusions of this study are given below.

4.1.1 Precursor Production

Seven precursors with different mol wt distributions were produced by fractionation of the mother pitch M-50. For the production of these precursors, dense-gas/supercritical extraction, low-pressure/high-temperature stripping, and vacuum evaporation processes were all used.

By means of a single, dense-gas extraction (DGE) column operating at 350 ˚C and at various pressures (i.e., 750-830 psig, or 51.7-57.2 bar), five precursors were produced as bottom products. The average mol wt of the pitch cuts increased with increasing operating pressure. In addition, two additional precursors representing middle cuts of the mother pitch M-50 were produced via combinations of DGE with low-pressure/high-temperature stripping (Dimer-1) and vacuum evaporation (Dimer-2). In both cases a

monomer/dimer mixture was collected as the top product of a DGE process operating under a positive temperature gradient from column bottom to top (330-380 ˚C for the production of Dimer-1; 350-400 ˚C for the production of Dimer-2) and at a pressure of 1000 psig, or 68.9 bar. Each mixture was then further processed to obtain the desired dimer-rich fraction. In particular, Dimer-1 was collected as the bottom product of a second packed column operating as a stripper at atmospheric pressure and high-temperature (380 ˚C), while Dimer-2 was produced in a vacuum oven, evaporating away all of the monomer and some of the low mol wt dimer molecules from the monomer/dimer mixture at 350 ˚C and 2 mbar.

4.1.2 Mesophase Analysis

Because the presence of mesophase is known to interrupt the activation process, three precursors with varying amounts of mesophase were produced in addition to four fully isotropic precursors, in order to isolate the effects of molecular weight from the effects of molecular order. Mesophase analyses of all precursors were carried out using polarized-light microscopy, and their photomicrographs were taken using a digital camera. The mesophase analyses of the precursors via polarized-light microscopy were carried out at UCSD by Dr. Fathollahi and co-workers, because the photomicrographs initially obtained at Clemson University were not clear. However, the procedure for obtaining micrographs was subsequently modified, and clear photomicrographs were obtained during our heat-treatment study of the 780psig samples (see below).

Furthermore, the color enhancement obtained using the "Auto-level" function in "Photoshop 6.0" has improved the quality of the photomicrographs significantly.

In addition to polarized-light microscopy, the carbonized fibers prepared from all precursors were analyzed via wide-angle X-ray diffraction (WAXD) as an independent, alternative analysis of molecular order. Azimuthal intensity spectra obtained at the 002 peak clearly distinguish between the isotropic and the anisotropic (i.e., mesophase-containing) fibers. The spectra of all mesophase-containing fibers formed a peak, while the spectra of the isotropic fibers were randomly scattered. These WAXD results were a significant help to our study, as they definitely established that the amount of the mesophase present in the 760psig precursor (<1% by polarized-light microscopy) had no effect on molecular order, and that the precursor could be considered as essentially isotropic in our analysis.

4.1.3 Heat Treatment of 780psig Precursor

In order to determine how easily the mesophase spherules present in a given precursor could be converted into bulk mesophase during processing, heat-treatment tests at a relatively low temperature (360 ˚C) were carried out on the 780psig precursor, which contained a significant percentage (4%) of mesophase in the form of spherules. These heat treatments, ranging from 30 min to 5 hr, resulted in a significant increase in the size of the mesophase spherules and the formation of mosaic/bulk mesophase. Interestingly, the mol wt distribution as measured by MALDI remained practically the same; furthermore, the Mettler softening point (MSP) of the precursor only increased from 299

˚C to 313 ˚C as a result of the 5-hr heat treatment. Additional evidence suggests that minimal change in the molecular composition of the pitch occurred as a result of the heat treatment conditions as follows: (1) The heat treatment temperature (360 ˚C) was below that suggested by McHenry (1976) for the formation of mesophase pitch via thermal polymerization (380-440 ˚C); (2) in our laboratory, the reaction of dimer species to form tetramer molecules was not observed to be significant until around 400 ˚C; (3) Cervo et al. (2008) reported a similar increase in the mesophase content of an extracted petroleum pitch with a mild heat treatment at 330 ˚C to what we observed; and (4) Diefendorf and Riggs (1980) reported that a solvent-extracted isotropic pitch can be converted into a mesophase pitch by heating to a temperature between 230 and 400 ˚C. In summary, the body of these results indicates that pitch precursors can require a nontrivial time in the molten state in order for the necessary molecular motion to occur such that they can reach their potential level of mesophase formation.

4.1.4 Fiber Spinning and Stabilization

One of the most critical steps of the ACF production in this study was the conversion of the pitch precursor into fibers. Because each spinning trial requires at least 45-50 g of precursor, a failure to obtain fibers during this trial results in the loss of all precursor, and additional material must be produced, which is a time-consuming task. Thus, proper estimation of the approximate spinning temperature was crucial for the success of the spinning process. Fortunately, a good correlation between the MSPs and

the spinning temperatures of the precursors (i.e., spinning temperatures were 20-25 ˚C above the MSPs) was observed.

4.1.5 Direct Activation

The initial motivation of this dissertation was to study the storage of hydrogen in pitch-based ACFs. In order to enhance the hydrogen storage capability of the ACFs, a Pd(acac)$_2$ metal complex was added to the precursor prior to the spinning process, and ACFs were prepared. It was observed that Pd particles migrated and agglomerated at the elevated temperatures of the carbonization and activation processes. Therefore, in order to minimize the agglomeration of the Pd particles, the separate carbonization process was omitted and the stabilized fibers were directly activated under CO_2 flow. Furthermore, the activation temperature was lowered from 900 ˚C to 840 ˚C for the same reason. Although Pd-containing ACFs were not part of the focus of this dissertation (but were the focus of an associated project with ORNL), the direct activation procedure at 840 ˚C was nonetheless adopted. All fiber used in this study were prepared using the direct-activation procedure, and ACFs with narrow, high-volume porosity were obtained as in the traditional activation process, where a separate carbonization process is used.

4.1.6 The Impact of Precursor Molecular Weight Distribution and Molecular Composition

Mol wt distributions (i.e., MALDI spectra) and MSPs of all precursors were determined. As a main focus of this dissertation, ACFs were prepared from all seven

precursors, and the effect of the mol wt and composition differences among the precursors on the overall activation process (including oxidation, carbonization, direct activation, and porosity) was investigated.

The differences between the MSPs of the 760psig and the 780psig precursors were found to be significant, considering the fact that their mol wt distributions (as observed by MALDI) were so close to each other. Räder and co-workers (Cristadoro et al., 2007) have reported that the MALDI signal response of pure component PAH species which are prone to stacking in the solid state is significantly less than that of PAH species that are in more random arrangement. Thus, the similarity between the MALDI spectra of these two precursors is likely due to the fact that the higher mol wt molecules present in the 780psig precursor are prone to stacking, and thus their MALDI signal response is significantly less than that of the lower mol wt molecules present in 780psig precursor. The results of the mild heat-treatment tests on the 780psig precursor also showed that some of the molecules present in the 780psig precursor are highly prone to the formation of bulk mesophase.

As-spun fibers prepared from all precursors were oxidized in an air convection oven, and the weight change of the fibers during the process was recorded at each temperature set point. Also, in order to determine the carbonization yield, all stabilized fibers were separately carbonized under nitrogen flow, and the carbonization weight losses were measured for each precursor. As a result of oxidative stabilization, all fibers gained 15-16% of their initial weight, except Dimer-2 fibers, which gained slightly higher weight (~18%) than the rest of the fibers. Also, weight losses during carbonization were

found to be slightly higher (36-37%) for the lower mol wt precursors (Dimer-1, Dimer-2, and 750psig), while they were almost the same for the rest of the precursors (~35%). Because of these results, we have suggested that the lower average mol wt fibers, especially the Dimer-2 fibers, have higher alkyl (aliphatic) content than the other fibers, even though there is inadequate evidence to support this conclusion. For example, ^{1}H-NMR runs have shown no significant difference between the ratio of aliphatic to aromatic protons for Dimer-1 and Dimer-2 precursors, although Dimer-2 fibers gained more weight during oxidation and lost more weight during carbonization than Dimer-1 fibers. However, it should be noted that the differences in oxidation weight gains and the carbonization weight losses were only 1-2 wt %. Also, solvent-based MALDI results showed that Dimer-1 precursor contains more tetramer species than Dimer-2 precursor, and this difference might help us explain the differences between the oxidation and carbonization weight changes of Dimer-1 and Dimer-2 fibers, assuming that the above conclusion about the lower mol wt species having higher alkyl content is true.

Stabilized fibers produced from all precursors were direct-activated for 6 hr, and % burn-off values were calculated for each sample using the difference between the total weight loss and the average carbonization weight loss measured during carbonization tests. Because all fibers were activated for the same amount of time (i.e., 6 hr), the burn-off levels were also considered as a measure of the activation rate. The burn-off values (i.e., ~28% burn-off), and therefore the activation rates, of all isotropic fibers were found to be essentially constant, while the presence of the mesophase spherules and the bulk mesophase caused a significant drop in activation rate (i.e., ~20% burn-off for 780psig

143

and 800psig precursors, and ~9% burn-off for 830psig precursor). These results show that a similar activation mechanism occurred for all isotropic fibers, and that the activating gas gained access to the inner regions of the fibers. On the other hand, the mesophase spherules and the bulk mesophase regions did not activate and probably limited the access of the activating gas to the inner isotropic regions.

The specific pore volume of ACFs direct-activated for 6 hrs was found to increase as the average mol wt of their precursor decreases. Also, the mesophase content of the precursor was found to cause a further decrease in specific pore volume and interrupt the formation of micropores. The ratio of the pores smaller than 7 Å (i.e., the desired pore size) to the total pore volume (3.9-30 Å) was found to be the same for all isotropic precursors, whereas it significantly dropped for mesophase-containing precursors. These results support the conclusions in the previous paragraph, and show that in the case of isotropic fibers the formation of ultramicropores continues as the activating gas reaches to the inner regions of the fiber at higher burn-off levels, while widening of the previously formed narrow pores also continues. In the case of fibers containing mesophase and thus having a significant degree of anisotropy, at higher burn-off levels pore widening dominates over the formation of new pores, as the activating gas cannot gain access to inner, unreacted regions of the fiber core.

In addition to the 6-hr direct activation performed on all seven precursors, the effect of direct-activation time on fiber properties was also studied, albeit only with the Dimer-1 precursor. Results indicated that the % burn-off increased essentially linearly with activation time up to the maximum measured activation time of 12 hr with 45%

144

burn-off. In other words, the activation rate was constant up to 45% burn-off. Also, the nitrogen uptake of all Dimer-1 ACFs at the same conditions also increased linearly with % burn-off, showing that a similar activation mechanism was in force throughout the activation process.

4.2 Recommendations

4.2.1 Heat Treatment

Heat-treatment tests were carried out on the 780psig precursor in order to observe the change in mesophase content and the mesophase development. Although the results were not presented in this dissertation (see Appendix C), heat-treatment tests were also carried out on fractions of mother M-50 pitch other than those used in this study. During these tests, the dimer peak of the smoothed, normalized MALDI spectra of some of the samples was observed to *increase* as a result of 1-hr heat treatment at 360 ˚C under nitrogen flow. Because none of the fractions tested contained any monomer molecules that could react to form dimer molecules, and the heat-treatment temperature was too low to cause a decomposition of any higher mol wt species, the observed incident was likely to be artificial. One possible explanation is that the stacking of the higher mol wt species to form mesophase makes the desorption of those species harder during MALDI analysis and causes a decrease in their MALDI signal response relative to the MALDI signal response of the dimer species. Because the samples were possibly inhomogeneous after heat treatment, the MALDI spectra for different samples were not consistent.

In order to eliminate the possible inhomogeneity issue, a mini-ball mill (Thermo Electron Corp., model Wig-L-Bug) can be used to homogenize the sample after heat treatment and prior to MALDI sample preparation. Therefore, it is recommended that the heat-treatment tests should be repeated using a mini-ball mill, using an organized set of experiments in order to see how mesophase formation/development affects the MALDI signal response of the precursor. The above work should be considered as a first step into the development of MALDI as a more effective tool for analyzing fractions containing mesophase, which should be a long-term goal in the Thies research group. Finally, application of heat-treatment tests on various additional fractions of M-50 mother pitch with different mol wt distributions is recommended, as they can help us better understand the effect of mol wt distribution on mesophase development.

4.2.2 Alternative M-50 Fractions

Although the primary focus in this study was to obtain pores with a size of 6-7 Å for hydrogen storage, different pore size distributions might be preferred for other applications. Furthermore, as shown in Chapter 3, in order to maximize the number of pores with a size of 6-7 Å, lower mol wt (and therefore lower MSP) precursors are preferred. Thus, a longer oxidative stabilization procedure at lower temperatures has to be applied. Unfortunately, this would slow down the whole ACF production. Therefore, we recommend that isotropic precursors of different molecular compositions with higher MSPs be used to prepare ACFs in order to further investigate the effect of composition on pore formation. Other precursors that are recommended are (a) a high-MSP, isotropic,

trimer-rich M-50 fraction (our colleague David Esguerra obtained an isotropic trimer-rich fraction with a MSP of ~300 °C); (b) an M-50 fraction with a bimodal mol wt distribution, such as dimer/tetramer, which can be produced by the reaction of dimer species. As these fractions will have relatively higher MSPs than the isotropic precursors used in the study of this dissertation, a much faster oxidative stabilization procedure can be employed in order to see if the oxidation rate affects the activation behavior of the fibers and the final pore structure.

4.2.3 Alternative Activation Methods

As mentioned in Chapter 1, there are alternative activation methods, such as steam activation and chemical activation, that can be used to produce ACFs. Depending on the activation method, different porosity profiles can be achieved. Also, these alternative methods may have other advantages. For example, steam activation creates larger pores compared to CO_2 activation; however, the tensile strength of the fibers is preserved in steam activation, while it significantly decreases in CO_2 activation. Also, via chemical activation, better activation of the mesophase precursors can be achieved than via physical activation with CO_2 or steam. Furthermore, some researchers have reported that ACFs with narrower microporosity can be obtained via chemical activation than by CO_2 activation. As mentioned earlier in this chapter, different specific pore sizes could also be of interest for different applications. Therefore, an evaluation of these two alternative activation methods is recommended with precursors of well-defined molecular

weight and composition, analogous to the work done herein. In particular, chemical activation might be preferred as it can also activate the mesophase regions.

4.2.4 Alternative Mother Pitch

The precursors used in this study were fractions of the same mother petroleum pitch, M-50. Although all these precursors had different mol wt distributions than M-50 itself, they still had relatively broad mol wt distributions, and they were all composed of a range of PAH backbone structures and their alkylated derivatives. Therefore, the use of another well-defined pitch of known chemical composition and a different chemical nature as a mother pitch, and using its fractions to prepare ACFs, could help us further understand the effect of the precursor composition on the activation mechanism and the porosity of ACFs. Choosing a mother pitch with a narrow mol wt distribution should make it easier to define its constituents, as there will be fewer species. As an example of such a pitch, anthracene pitch has far fewer species than the M-50 petroleum pitch used in this study (Burgess, 2010, p149).

Burgess and Thies (2011) have shown that oligomeric species that constitute the M-50 pitch are formed by the combination of the monomeric species via the formation of five-membered rings. These five-membered rings cause a strain on the molecules, and thus a bending of the molecules. Although this bending is relatively small, it could affect the arrangement of the precursor molecules. Therefore, conducting a similar study on a mother pitch that has been prepared using M-50 monomeric molecules similar to M-50, but with the molecules combined via six-membered rings to form oligomers, might help

us better understand the effect of precursor composition on the properties of final product. Six-membered ring connections might cause an increase in molecular order and stacking of the molecules, which is a disadvantage in terms of CO_2 activation; however, the study would still be useful for understanding the effect of composition on mesophase formation. Fractionation of such a mother pitch might result in pitch fractions with higher mesophase content at a lower average mol wt than M-50 fractions, and thus with lower softening points, as softening point would be expected to be lower for lower average mol wt fractions. Therefore, we may recommend the production of M-50-like pitch with six-membered ring connections from M-50 monomeric molecules, and use it as a mother pitch to fractionate and make ACFs. Catalytic polymerization is recommended, as it results in formation of six-membered ring connections.

4.2.5 Additional Recommendations

Anisotropy of the precursors was determined using polarized-light microscopy. In order to obtain clear photomicrographs, it is important that the sample surface is well polished. In order to improve the polishing, Kundu's procedure (2006) was modified by adding grinding steps and minimizing the force applied to the sample surface. However, if the sample is soft and deep scratches cannot be avoided, then it is recommended to slightly oxidize the sample surface after the grinding step with 400-grit SiC paper. 200 ˚C can be used as an oxidation temperature, as suggested by Fathollahi and White (1994). This process will help to harden the surface and improve the scratch resistance of the sample surface.

MALDI analysis is one of the most important characterization methods used by Thies and co-workers. Samples to be analyzed are mixed with matrix material at a predefined proportion using a mini-ball mill (Thermo Electron Corp., model Wig-L-Bug). The homogeneity of this mixture is important for consistency, as the matrix/sample ratio also has an effect on the spectra obtained. In this regard, our group had problems during MALDI sample preparation of monomer-rich M-50 fraction, because the material was sticky. An attempt towards the solution of this problem was the solidification of the material prior to being put into the mini-ball mill by pouring liquid nitrogen on it; however, during mixing/shaking the material melts down and becomes sticky again, preventing homogenous mixing. To improve this process and to prevent the melting of the material during mixing, use of a cryogun (Brymill Corp., model no. BRY-B-700), which is a type of liquid nitrogen spray, is recommended. Spraying liquid nitrogen during mixing/shaking to the mini-ball mill intermittently will help to keep the material solid during the entire process.

As a final comment, it is recommended that extra attention be paid to the residence time of a pitch during the DGE processes, especially when higher temperatures (i.e., approaching 400 ˚C) are employed. At these temperatures, higher residence times could result in a more ordered product. Therefore, fluctuations in the residence time during the DGE process could result in products with different mesophase content even at the same extraction conditions (i.e., the same temperature, pressure and solvent/pitch ratio).

APPENDICES

<center>**Appendix A:**</center>

<center>**Instruments and Materials**</center>

<center>**A.1 Instruments for Activated Carbon Fiber Production**</center>

Precursor production

- DGE apparatus **(Earle 222)**

    o Stainless steel column with an i.d. of 1.8 cm and a height of 2.0 m

    o Stainless steel packing, Cannon Instrument Co., part no. 3947-A20

    o Single-screw extruder, Alex James and Assoc., model no. AJA 58

    o Metering pump, Zenith Pumps, Model HPB, 0.160 ml/rev

    o HPLC pump,

- Vacuum oven evaporation

    o Vacuum Atmospheres Model VTW Vacuum Oven, connected to a Model Dri-Lab-08/85 nitrogen glove box **(Earle 31)**

- Precursor drying

    o Vacuum oven, Fisher Scientific, model no. 285A **(Earle 116)**

ACF preparation

- Spinning **(Earle B15)**

- o Batch-spinning cartridge, piston, spinneret, nitrogen purge extender, temperature and pressure probes, pressure cap, bolts; Alex James and Assoc.

- o Batch spinning instrument, Alex and James Inc.

- o Spinning Mesh filter, Alex and James Inc., part no. RBD3040148.51

- o Graphite tape, Teadit Inc., part no. 2550

- o Anti-seize lubricant, Permatex, item no. 80078

- Antechamber attached to the nitrogen glove box (Vacuum Atmosphere Inc., model no. Dri-Lab-08/85) **(Earle 31)**

- Oxidation **(Earle 202)**

  - o Fisher Scientific air convection oven, model: 825F

  - o Ohaus Corporation lab scale, model no. AR2140

- Carbonization and direct activation **(Earle 202)**

  - o Custom-made Lindberg tubular furnace, General Signal, project no. 9305198

  - o Quartz boat, or sample holder, Sigma-Aldrich, model no. Z406627

A.2 Analytical Instruments

- Molecular weight (mol wt) analysis

- o Bruker Daltonics Autoflex MALDI-TOF mass spectrometer equipped with a 337 nm nitrogen laser **(Earle 116)**

- o Mini-ball mill, Thermo Electron Corp., model no. Wig-L-Bug **(Earle 222)**

- Softening point measurement

  - o Temperature-monitored hot plate (Melting Point Apparatus), Fisher-Johns, serial no.1833 **(Earle 222)**

  - o Mettler Dropping Point Cell instrument, model no. FP83HT **(Earle B17)**

- Sample polishing **(Earle B15)**

  - o Mounting cup with an i.d. of 1.25", Allied High Tech Products Inc., part no. 197-10005

  - o GCA Precision mechanical convection oven, Precision Scientific Inc., model no. STM135

  - o Buehler AutoMet sample holder (holds 6 samples), part no. 60-2483

  - o Buehler AutoMet 2000 powerhead / EcoMet 3000 variable speed grinder-polisher

  - o 240-grit SiC grinding paper, Buehler Carbimet, part no. 50-10015

  - o 320-grit SiC grinding paper, Buehler Carbimet, part no. 30-5108-320-100

  - o 400-grit SiC grinding paper, Buehler Carbimet, part no. 30-5108-400-100

  - o 600-grit SiC grinding paper, Buehler Carbimet, part no. 50-10030

  - o 1200-grit SiC grinding paper, Buehler Carbimet, part no. 50-10077

- White label polishing paper, Allied High Tech Products Inc., part no. 90-150-500

- Chem-Pol Black polishing cloth, Allied High Tech Products Inc., part no. 180-10050

- Canned compressed air, Miller-Stephenson Allied High Tech Products Inc.

- Polarized-light microscopy **(Earle 212)**
  - Olympus BX60 Microscope with cross-polarized light and a first-order red plate
  - soft clay, microscope slide, sample flattener
  - Sony DSC-S70 digital camera with a camera adaptor, Martin Microscope Company, model no. MM3XS

- ^{1}H –NMR analysis **(Hunter Hall 225, Clemson University)**
  - 300 MHz Bruker Avance System, ^{1}H-NMR spectrometer

- Wide angle x-ray diffraction (WAXD) **(Rhodes Hall 305, Clemson University)**
  - An osmic Micromax CuK_α X-Ray source
  - Collimator with a pinhole size of 0.5mm,
  - 2D image plates
  - Fuji BAS 1800 scanner

- Surface Characterization **(Earle 220)**

    o Micromeritics Accelerated Surface and Porosity Analyzer, Micromeritics Instrument Corporation, model no. 2020

    o Test tube with a ½ inch i.d., Micromeritics Inc., part no. 240-61003-00

    o Seal frit assembly, Micromeritics Inc., part no. 260-25890-00

    o Antistatic gun, Bellex International Corp., model no. Milty Zerostat 3

    o Isothermal jacket, Micromeritics Inc., part no. 202-25903-00

A.3 Materials

- Isotropic petroleum pitch, M-50, Marathon Petroleum Company LLC, CAS 68187-58-6 **(Earle 222)**

- HPLC-grade toluene, Fisher Scientific, CAS 108-88-3 **(Earle 222)**

- 7,7,8,8- tetracyanoquinodimethane (TCNQ), TCI America, CAS 1518-16-7 **(Earle 222)**

- $Pd(acac)_2$ (Palladium(II) 2,4 – pentanedionate, Pd 34.7%), Alfa Aesar, CAS 14024-61-4 **(Earle 202)**

- Coleman Grade carbon dioxide gas, National Welders, UN1013, 114041 **(Earle 202)**

- UHP Helium gas, National Welders **(Earle 220)**

- Liquid nitrogen (99.99% purity) in a central unit, National Welders **(Earle Hall)**

- Epoxy resin, Buehler, item number: 20-8120-009 **(Earle B15)**

156

- Epoxy hardener, Leco Corporation, item no. 811-164 **(Earle B15)**

- 1μm diamond suspension, Allied High Tech Products Inc., part no. 90-33015 **(Earle B15)**

- 0.05 μm alumina suspension, High Tech Products Inc., part no. 90-187505 **(Earle B15)**

- Micro Organic Soap, Allied High Tech Products Inc., part no. 148-10000 **(Earle B15)**

- CDC_{l3} (99.8% atom D), Acros Organics **(Earle 220)**

Appendix B:

B. Weight Loss, Burn-off and Isotropic Specific Pore Volume Calculations

B.1 Direct Activation total % Weight Loss and % Burn-off Calculation

$$\text{TWL} = (1 - w_f / w_i) * 100 \qquad\qquad (B.1)$$

$$w_i' = w_i * (1 - C_{loss} / 100) \qquad\qquad (B.2)$$

and

$$\text{BO} = (1 - w_f / w_i') * 100 \qquad\qquad (B.3)$$

Where

w_i : weight of fibers before direct activation

w_f : weight of fibers after direct activation

w_i' : weight of fibers after approximate carbonization weight loss is subtracted

C_{loss} : Average % carbonization weight loss of fibers measured by previous carbonization tests

TWL: Total % weight loss

BO : % Burn-off

Sample Calculation

Direct activation total % weight loss and % burn-off calculation for Dimer-1 fibers is given below.

w_i : 731 g

w_f : 330 g

C_{loss} : 35.8 %

$$\textbf{TWL} = (1 - 330 / 731) * 100 = 54.9\ \%$$

$$w_i' = 731 * (1 - 35.8 / 100) = 469.3$$

and

$$\textbf{BO} = (1 - 330/ 469.3) * 100 = 29.7\ \%$$

B.2 Isotropic Phase Specific Pore Volume Calculation for Mesophase-Containing Fibers

Specific pore volume of the mesophase containing fibers is equal to the summation of the partial specific pore volume of the mesophase portion of the fibers and the partial specific pore volume of the isotropic portion of the fibers.

$$\tilde{V} = m * \tilde{V}_m + (1 - m) * \tilde{V}_{iso} \tag{B.4}$$

Equation B.4 was rearranged to give equation B.5 as follows

$$\tilde{V}_{iso} = (\tilde{V} - m * \tilde{V}_m) / (1 - m) \tag{B.5}$$

Where

$\tilde{V}_{iso}$: specific pore volume of isotropic phase of the mesophase-containing fibers

$\tilde{V}$: specific pore volume of the mesophase-containing fibers

m : mesophase %

$\tilde{V}_m$: specific pore volume of 100 % mesophase fibers (830psig)

Note that all mesophase regions were assumed to have the same specific pore volume as 830psig fibers

$$BO_{iso} = (BO - m * BO_m) / (1 - m) \tag{B.6}$$

Where

BO_{iso} : % burn-off of isotropic phase of the mesophase-containing fibers

BO : % burn-off of the mesophase-containing fibers

m : mesophase fraction

BO$_m$: % burn-off of 100 % mesophase fibers (830psig)

Note that all mesophase regions were assumed to activate at the same rate as 830psig

fibers

In order to eliminate the differences in activation rate, isotropic specific pore volumes of the fibers were compared after being divided by the isotropic % burn-off ($\tilde{V}_{iso}$ / **BO$_{iso}$**) for each precursor. Note that the isotropic specific pore volume for 830psig fibers is unidentified as it is 100% mesophase, and the isotropic specific pore volume for isotropic fibers is equal to their specific pore volume as they are 100% isotropic.

Sample Calculation

Isotropic phase specific pore volume calculation for 780psig fibers is given below. The sample calculation is given here for only the total pore volume of the 780psig fibers. The same calculation was repeated for the 1st peak volume of the fibers, too.

$\tilde{V}$: 0.184 cm^3/g

m : 0.04

$\tilde{V}_m$: 0.023 cm^3/g

$$\tilde{V}_{iso} = (0.184 - 0.04 * 0.023) / (1 - 0.04) = 0.191 \text{ cm}^3/\text{g}$$

BO : 20.5 %

m : 0.04

BO$_m$: 9.3 %

$$\textbf{BO}_{\textbf{iso}} = (20.5 - 0.04 * 9.3) / (1 - 0.04) = 21.0 \text{ \%}$$

Appendix C:

C. Additional WAXD Results on Carbonized Fibers

As mentioned in Chapter 3, wide-angle X-ray tests were carried out on a second set of carbonized fibers prepared from all seven precursors for reproducibility; as can be seen below, similar results were obtained (see **Figs C.1** and **C.2**).
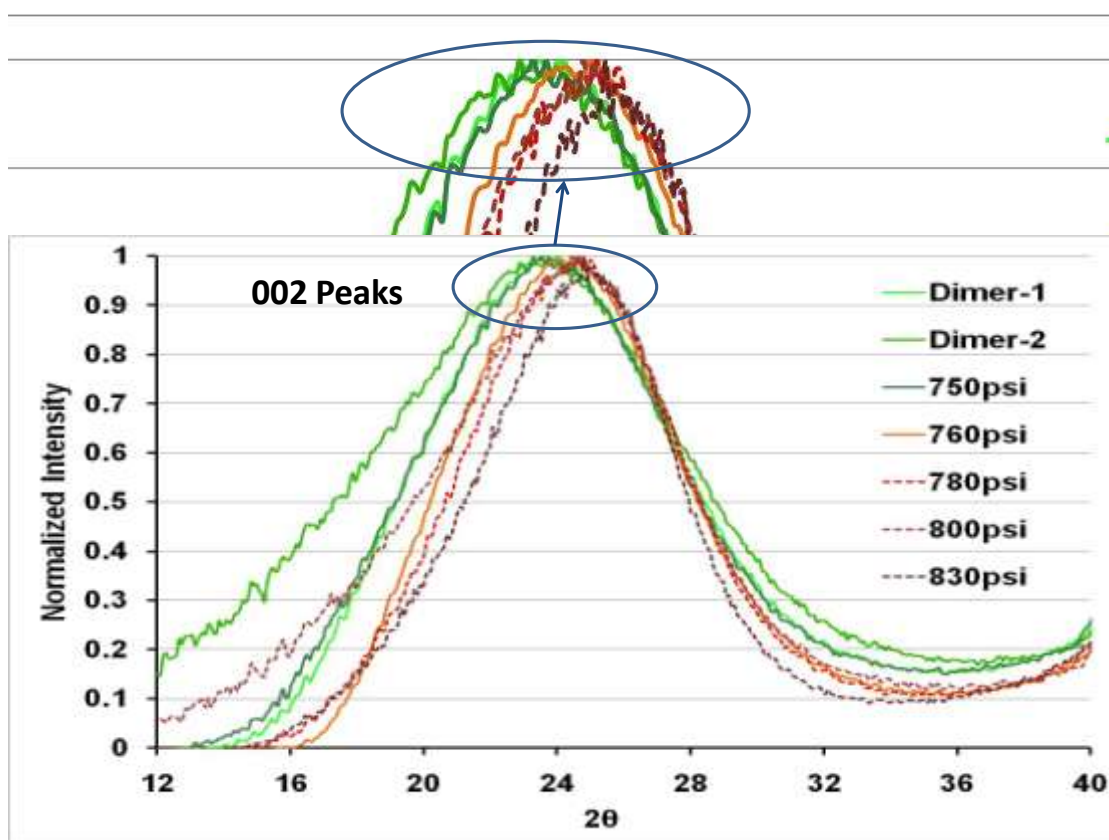
Figure C.1   WAXD analysis 2θ intensity profiles of the carbonized fibers prepared from all seven precursors. Note that the 002 peaks of the 780, 800, and 830psig (dotted curves) fibers are located at higher 2θ values than the 002 peaks of the 760psig and lower average mol wt precursors (solid curves).
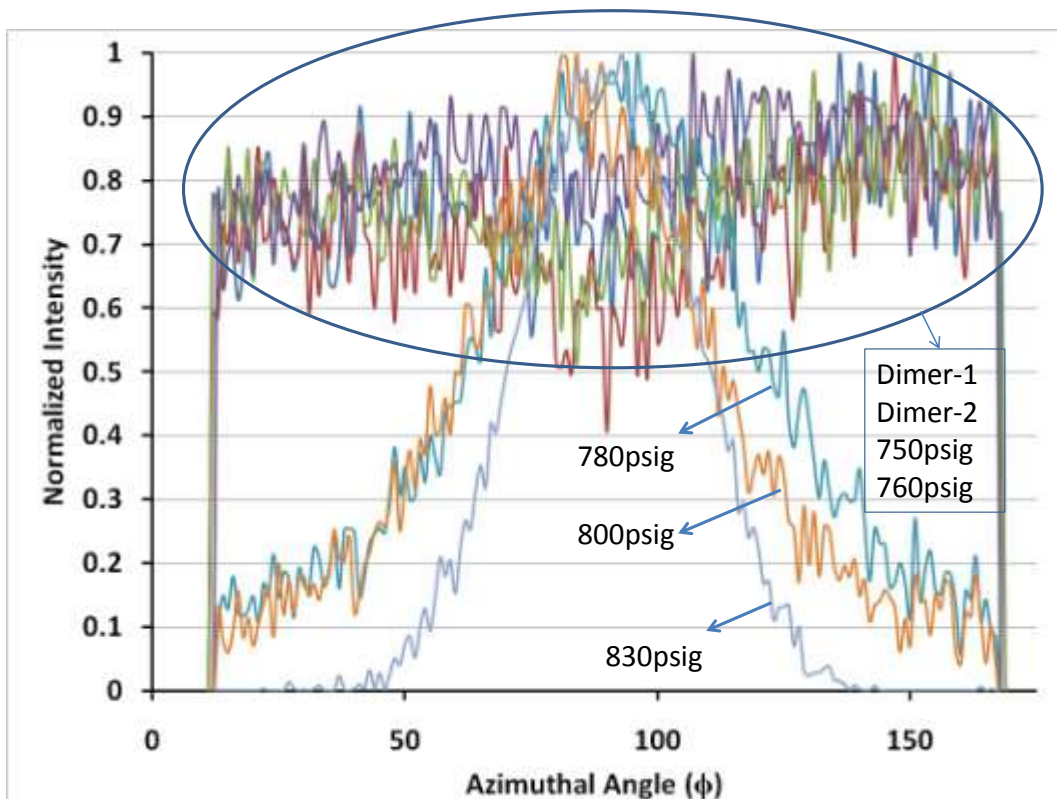
Figure C.2 WAXD analysis azimuthal intensity distributions at approximate 002 peak locations for carbonized fibers prepared from all seven precursors. Note that the azimuthal intensity distributions of the mesophase-containing fibers (780psig, 800psig and 800psig) are in the form of peaks, while those of the 760psig and other isotropic fibers are not.

Appendix D:

D. Additional Heat-Treatment Tests

Heat-treatment tests similar to the ones performed on 780psig samples were carried out on four other samples that were readily available for further observation of mesophase formation. First three of these samples were prepared by David Esguerra, a PhD candidate in Chemical Engineering at Clemson University, using two-column DGE operation, in which the top stream from the first column was fed to the second column. In particular, first column was operated at 1000 psig and a S/P ratio of 8.0/1 under a positive temperature gradient (ΔT), with the bottom of the column at 330 ˚C, the middle at 350 ˚C, and the top at 380 ˚C. The second column was operated at a S/P ratio of 17.8/1 under a positive temperature gradient (ΔT), with the bottom of the column at 350 ˚C, and the top at 400 ˚C and at 875psig, 900psig, and 925psig in order to produce-190 D2C2B, E-190 D2C3B, and E-190 D2C4B, respectively. The last sample for heat-treatment tests was produced using single-column DGE. In particular, the column was operated at 1000 psig and a S/P ratio of 5.1/1 under a positive temperature gradient (ΔT), with the bottom of the column at 330 ˚C, the middle at 350 ˚C, and the top at 380 ˚C, and bottom product was collected as E-136 D1C3B.

During these heat-treatment tests, some interesting results were observed. As a result of 1-hr heat treatments at 360 ℃ and under 1 L/min nitrogen flow, dimer peaks of the heat-treated samples at normalized MALDI spectra were found to increase (see **Figs D.1a**, **D.2a**, **D.3a**, and **D.4a**), while there was no consistent trend in MALDI peak

intensity spectra (see **Figs D.1b**, **D.2b**, **D.3b**, and **D.4b**). Because the amounts of samples were not sufficient, softening-point measurements could not be done for each sample. However, in general, as a result of 1-hr heat treatment the weight loss was only few percent, and the increase in softening point was less than 2℃. Also, **Fig. D.5a** and **b** show that the molecular weight distribution of the Dimer-1 precursor does not change at all as a result of the 1-hr heat treatment. If there was any significant loss of dimer species, we would have expected it to happen from the lower mol wt dimer species, so that the MALDI spectra of Dimer-1 precursor would have gotten narrower from the left-hand side. These results indicate that the observed changes in normalized MALDI spectra are artificial, and that the compositions of the samples actually do not change as a result of heat treatment.

There can be two possible explanations that might cause these changes in MALDI spectra: One is the inhomogeneity of the heat-treated samples, and the other one is the decreased relative MALDI signal response of mesophase-forming species as a result of heat treatment. Since these tests were only preliminary tests, for a better understanding these tests need to be carried out on new samples with a controlled set of experiments, using the Wig-l Bug as recommended in Chapter 4, in order to eliminate the possibility of inhomogeneity. In all figures, photomicrographs of the samples before and after heat treatment are also given in order to show the change in mesophase content.

Figure D.1 E-190 D2C2B before and after 1-hr heat treatment at 360 ℃ under nitrogen flow (a) Smoothed and normalized MALDI spectra, (b) maximum peak outline MALDI spectra, and (c) Photomicrographs showing change in mesophase content.

170
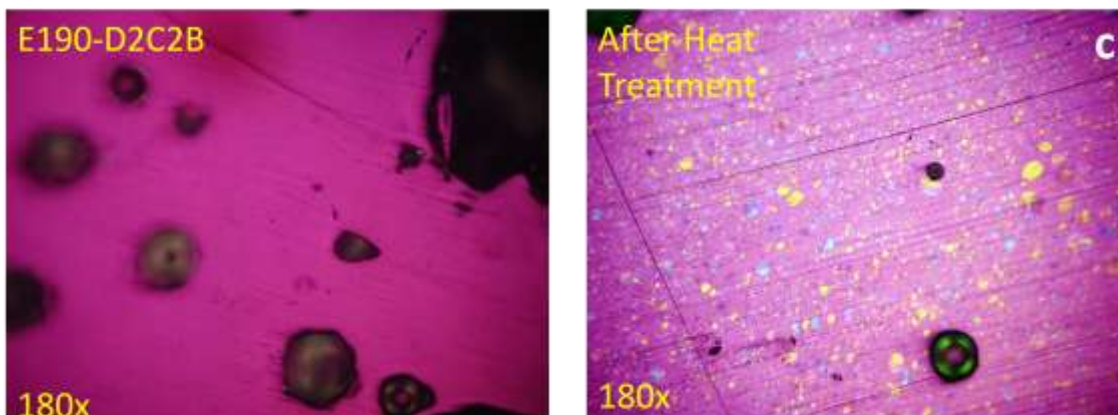
Figure D.1   Continued.
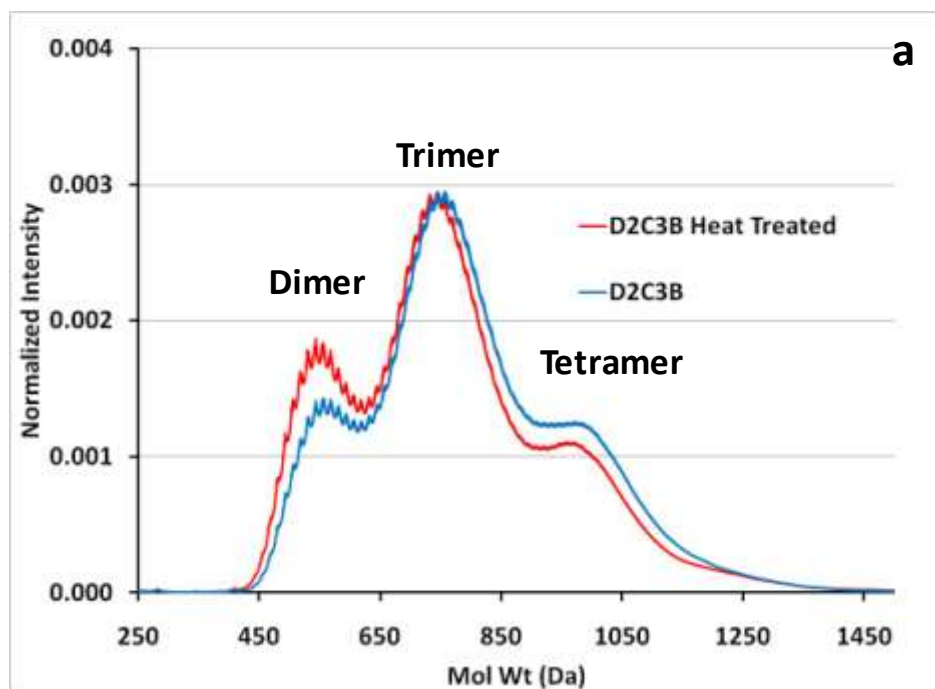
Figure D.2   E-190 D2C3B before and after 1-hr heat treatment at 360 °C under nitrogen flow (a) Smoothed and normalized MALDI spectra, (b) maximum peak outline MALDI spectra, and (c) Photomicrographs showing change in mesophase content.

171
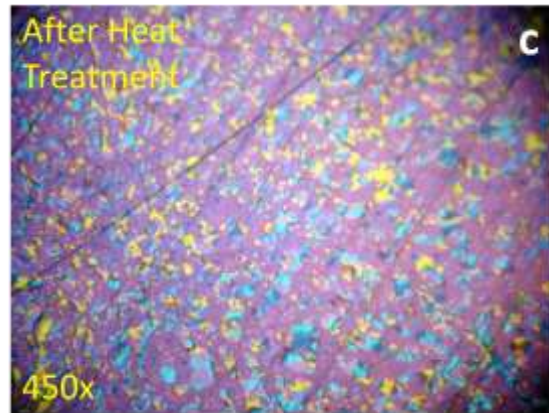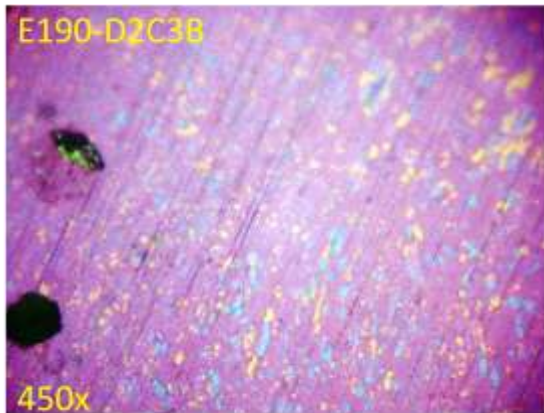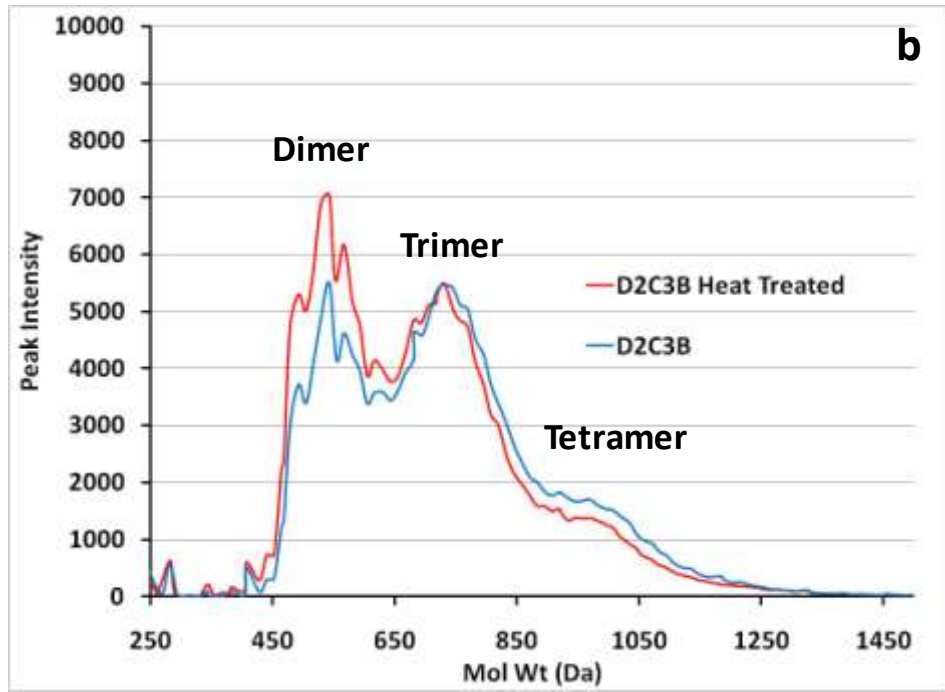
Figure D.2   Continued.

172
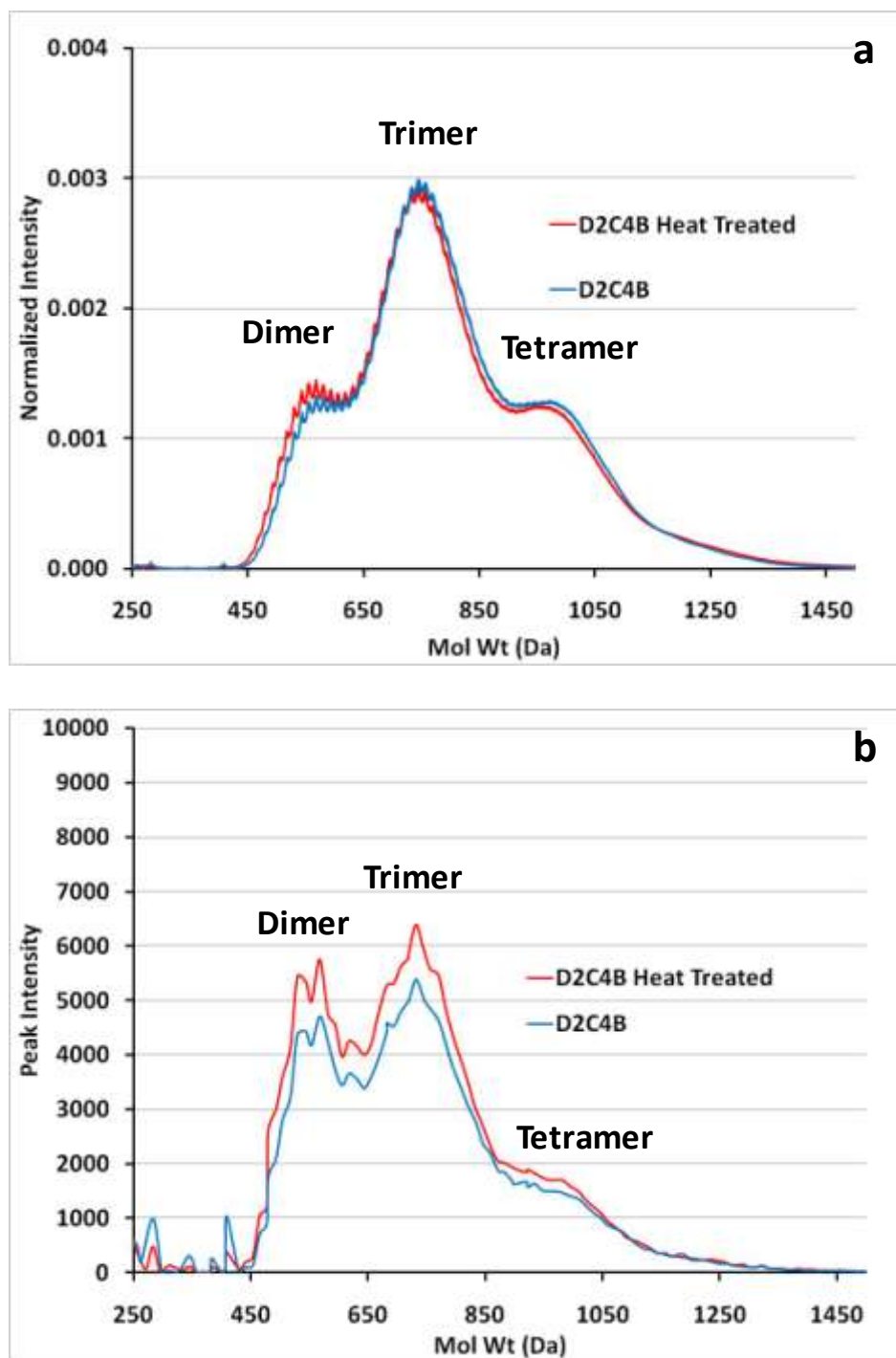
Figure D.3 E-190 D2C4B before and after 1-hr heat treatment at 360 °C under nitrogen flow (a) Smoothed and normalized MALDI spectra, (b) maximum peak outline MALDI spectra, and (c) Photomicrographs showing change in mesophase content.
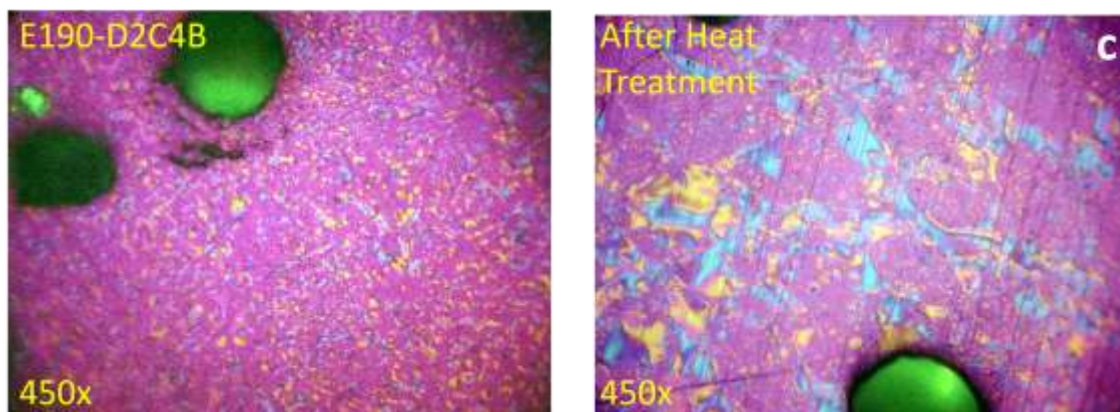
Figure D.3   Continued.
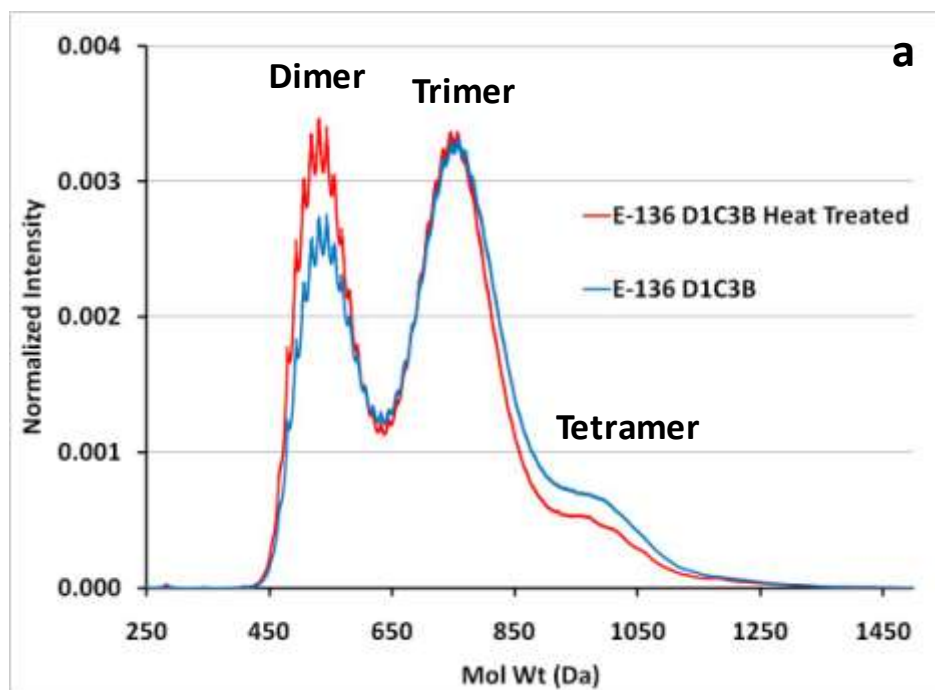
Figure D.4   E-136 D1C3B before and after 1-hr heat treatment at 360 ℃ under nitrogen flow (a) Smoothed and normalized MALDI spectra, (b) maximum peak outline MALDI spectra, and (c) Photomicrographs showing change in mesophase content.
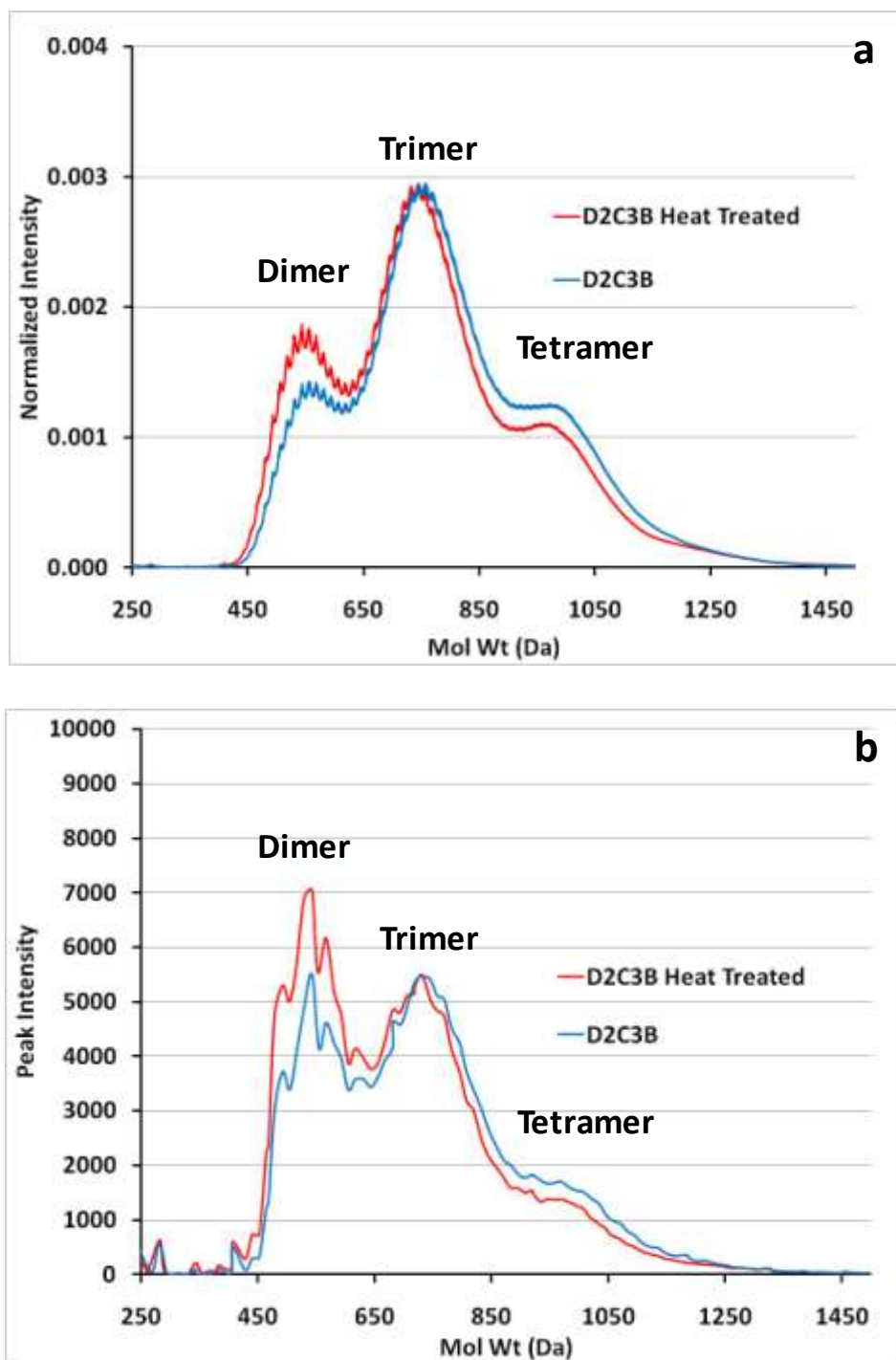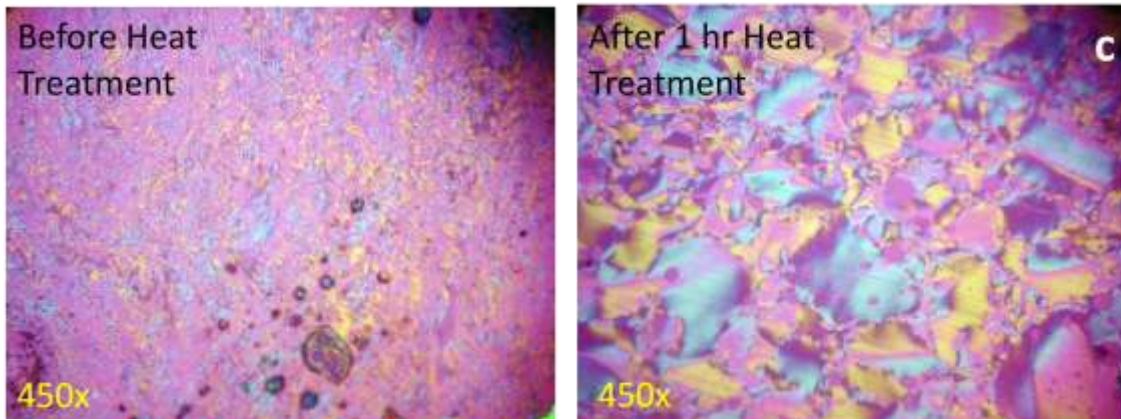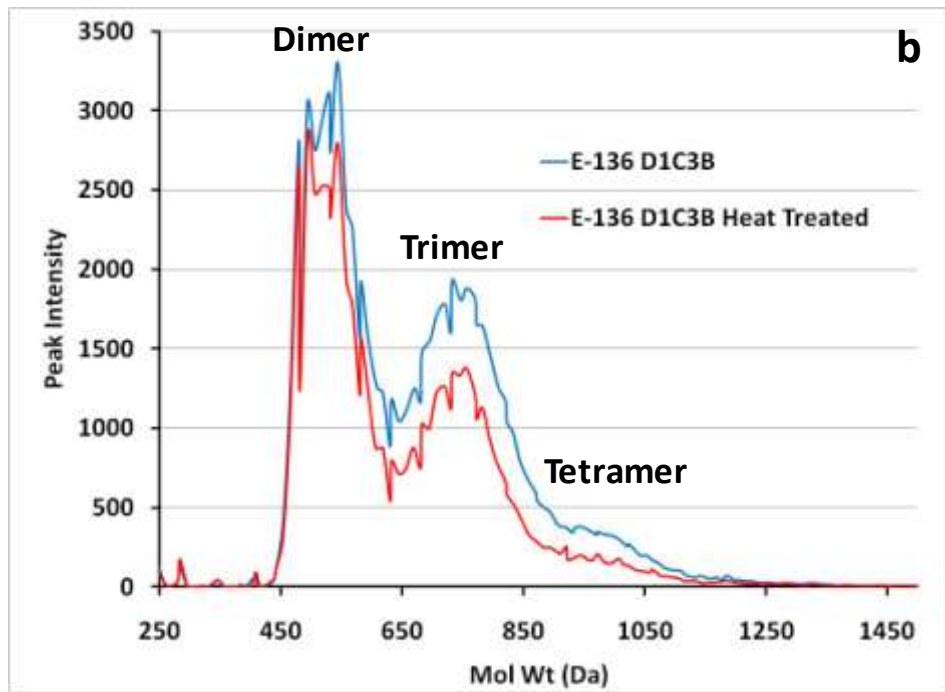
Figure D.4   Continued.
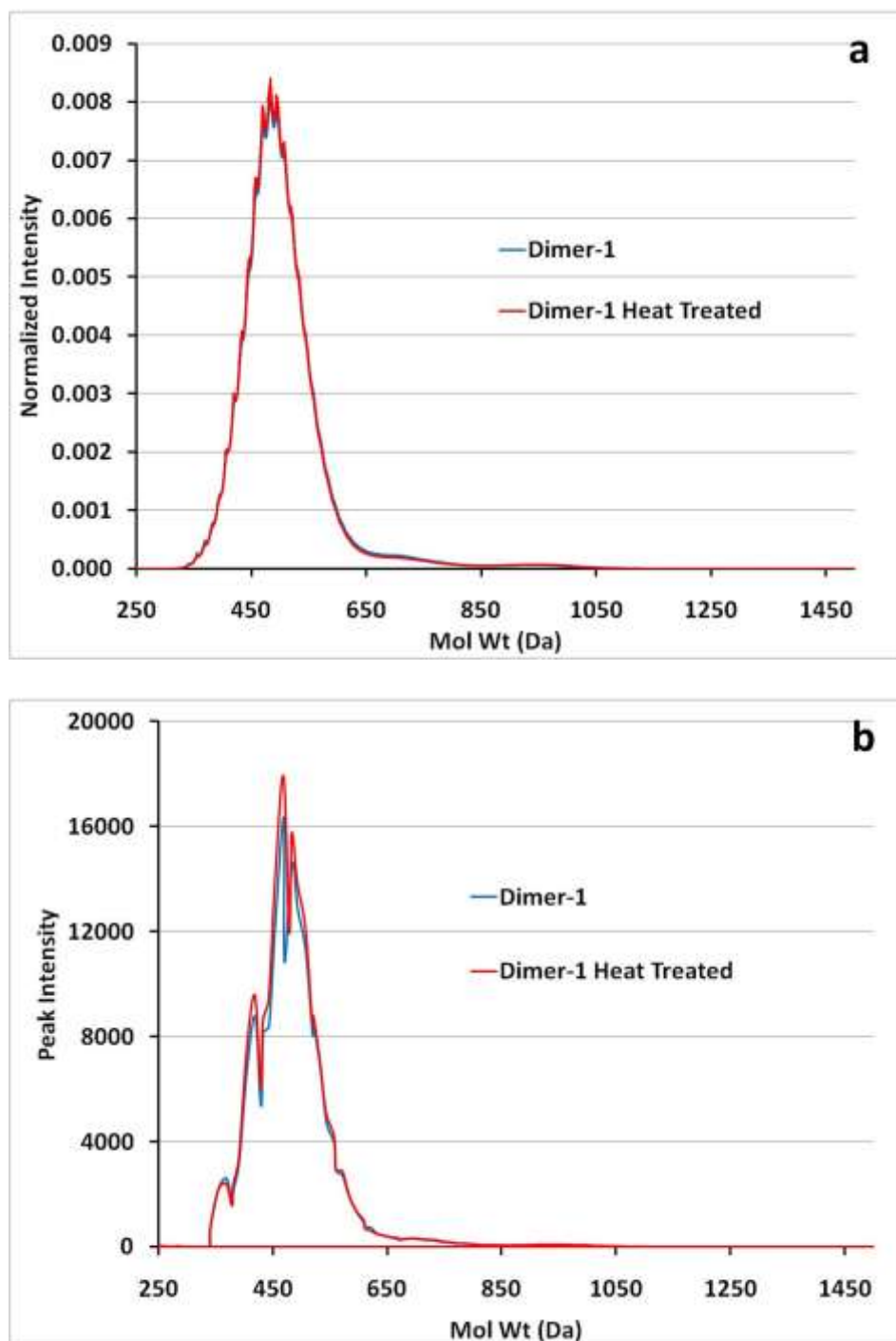
Figure D.5   Dimer-1 precursor before and after 1-hr heat treatment at 360℃ under nitrogen flow (a) Smoothed and normalized MALDI spectra, (b) peak MALDI spectra, (c) Photomicrographs showing change in mesophase content.
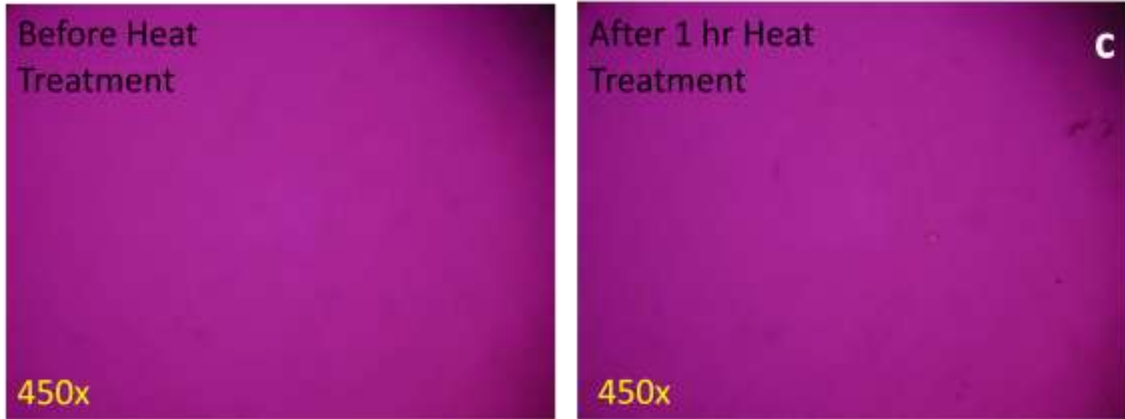
Figure D.5   Continued

Appendix E:

D. Copyright Permission Documentation

Figure (s): Fig. 1.1a
Permission Request Submitted

Your request is now under review.
You will be notified of the decision via email.
Please print this request for your records.

Order Number	500642220
Order Date	Nov 27, 2011
Licensed content publisher	Elsevier
Licensed content publication	Elsevier Books
Licensed content title	Carbon AlloysNovel Concepts to Develop Carbon Science and Technology
Licensed content author	Ei-ichi Yasuda,Michio Inagaki
Licensed content date	2003
Number of pages	9
Type of Use	reuse in a thesis/dissertation
Portion	figures/tables/illustrations
Number of figures/tables/illustrations	1
Format	both print and electronic
Are you the author of this Elsevier chapter?	No
Will you be translating?	No
Order reference number	
Title of your thesis/dissertation	Pitch-Based Activated Carbon Fibers: The Effect of Precursor Composition on Pore Structure
Expected completion date	Dec 2011
Estimated size (number of pages)	180
Elsevier VAT number	GB 494 6272 12
Permissions price	Not Available
VAT/Local Sales Tax	Not Available
Total	Not Available

Figure (s): Fig. 1.1b, Fig. 1.3, Fig. 1.4, Fig. 1.5, Fig. 1.6, Fig. 1.7, and Fig. 1.13

Order Completed

This is a License Agreement between Halil L Tekinalp ("You") and Elsevier ("Elsevier"). The license consists of your order details, the terms and conditions provided by Elsevier, and the payment terms and conditions.

License Number	2797341287182
License date	Nov 27, 2011
Licensed content publisher	Elsevier
Licensed content publication	Elsevier Books
Licensed content title	Activated Carbon
Licensed content author	Harry Marsh,Francisco Rodríguez-Reinoso
Licensed content date	2006
Number of pages	56
Type of Use	reuse in a thesis/dissertation
Portion	figures/tables/illustrations
Number of figures/tables/illustrations	7
Format	both print and electronic
Are you the author of this Elsevier chapter?	No
Will you be translating?	No
Order reference number	
Title of your thesis/dissertation	Pitch-Based Activated Carbon Fibers: The Effect of Precursor Composition on Pore Structure
Expected completion date	Dec 2011
Estimated size (number of pages)	180
Elsevier VAT number	GB 494 6272 12
Permissions price	0.00 USD
VAT/Local Sales Tax	0.0 USD / 0.0 GBP
Total	0.00 USD

Figure (s): Fig. 1.2

Dear Halil

RE: Franklin 209 (1097): 196
Journal:Proceedings of the Royal Society A: Mathematical, Physical and Engineering Sciences

The Royal Society is pleased to grant permission for use of the above material, subject to the following conditions:
1. Full acknowledgement is given to the original source, with full details of the author(s), title, figure/page numbers, year of publication and the publisher.
2. The permission of the author(s) or the author's estate is obtained where practical.
3. The material is to be used only as described in your email and this permission is granted for one-time use only.

Yours sincerely

Jennifer Kren
Editorial Administrator

Citation:Franklin 209 (1097): 196
Journal:Proceedings of the Royal Society A: Mathematical, Physical and Engineering Sciences
Requester information:
Firstname: Halil
Lastname: Tekinalp
Telephone: 1 (864) 633-6842
Email: ltekinalp@hotmail.com
Address:

14059 E Camelia Ln
Seneca, SC, 29678
Organization: PhD Student

Figure (s): Fig. 1.8a
Order Completed

This is a License Agreement between Halil L Tekinalp ("You") and Elsevier ("Elsevier"). The license consists of your order details, the terms and conditions provided by Elsevier, and the payment terms and conditions.

License Number	2797260764052
License date	Nov 27, 2011
Licensed content publisher	Elsevier
Licensed content publication	Carbon
Licensed content title	Carbons of high surface area. A study by adsorption and high resolution electron microscopy
Licensed content author	H Marsh,D Crawford,T.M O'Grady,A Wennerberg
Licensed content date	1982
Licensed content volume number	20
Licensed content issue number	5
Number of pages	8
Type of Use	reuse in a thesis/dissertation
Portion	figures/tables/illustrations
Number of figures/tables/illustrations	1
Format	both print and electronic
Are you the author of this Elsevier article?	No
Will you be translating?	No
Order reference number	
Title of your thesis/dissertation	Pitch-Based Activated Carbon Fibers: The Effect of Precursor Composition on Pore Structure
Expected completion date	Dec 2011
Estimated size (number of pages)	180
Elsevier VAT number	GB 494 6272 12
Permissions price	0.00 USD
VAT/Local Sales Tax	0.0 USD / 0.0 GBP
Total	0.00 USD

Figure (s): Fig. 1.8b and c

This is a License Agreement between Halil L Tekinalp ("You") and Elsevier ("Elsevier"). The license consists of your order details, the terms and conditions provided by Elsevier, and the payment terms and conditions.

License Number	2797270173684
License date	Nov 27, 2011
Licensed content publisher	Elsevier
Licensed content publication	Fuel Processing Technology
Licensed content title	Quantitative high-resolution transmission electron microscopy: a promising tool for carbon materials characterization
Licensed content author	Jean-Noël Rouzaud,Christian Clinard
Licensed content date	20 June 2002
Licensed content volume number	77-78
Number of pages	7
Type of Use	reuse in a thesis/dissertation
Portion	figures/tables/illustrations
Number of figures/tables/illustrations	2
Format	both print and electronic
Are you the author of this Elsevier article?	No
Will you be translating?	No
Order reference number	
Title of your thesis/dissertation	Pitch-Based Activated Carbon Fibers: The Effect of Precursor Composition on Pore Structure
Expected completion date	Dec 2011
Estimated size (number of pages)	180
Elsevier VAT number	GB 494 6272 12
Permissions price	0.00 USD
VAT/Local Sales Tax	0.0 USD / 0.0 GBP
Total	0.00 USD

Figure (s): Fig. 1.9
Order Completed

This is a License Agreement between Halil L Tekinalp ("You") and Elsevier ("Elsevier"). The license consists of your order details, the terms and conditions provided by Elsevier, and the payment terms and conditions.

License Number	2797270487489
License date	Nov 27, 2011
Licensed content publisher	Elsevier
Licensed content publication	Carbon
Licensed content title	Microtexture and magnetoresistance of glass-like carbons
Licensed content author	Akira Yoshida,Yutaka Kaburagi,Yoshihiro Hishiyama
Licensed content date	1991
Licensed content volume number	29
Licensed content issue number	8
Number of pages	5
Type of Use	reuse in a thesis/dissertation
Portion	figures/tables/illustrations
Number of figures/tables/illustrations	1
Format	both print and electronic
Are you the author of this Elsevier article?	No
Will you be translating?	No
Order reference number	
Title of your thesis/dissertation	Pitch-Based Activated Carbon Fibers: The Effect of Precursor Composition on Pore Structure
Expected completion date	Dec 2011
Estimated size (number of pages)	180
Elsevier VAT number	GB 494 6272 12
Permissions price	0.00 USD
VAT/Local Sales Tax	0.0 USD / 0.0 GBP
Total	0.00 USD

Figure (s): Fig. 1.10

assocpub@aps.org

AMERICAN PHYSICAL SOCIETY

One Physics Ellipse, College Park, MD 20740 · http://www.aps.org

December 1, 2011

Halil L. Tekinalp
htekina@clemson.edu

Ref # 10866

Thank you for your permission request dated on November 29, 2011. We are pleased to grant you a non-exclusive, non-transferable permission, English and German rights, limited to **print and electronic format**, provided you meet the criteria outlined below. Permission is for a one-time use and does not include permission for future editions, updates, databases, translations, or any other matters. Permission must be sought for each additional use. This permission does not include the right to modify APS material.

Please print the required copyright credit line on the first page that the material appears: "Reprinted (abstract/excerpt/figure) with permission from [FULL REFERENCE CITATION] as follows: authors names, journal title, volume number, page number and year of publication. Copyright (YEAR) by the American Physical Society.

The following language must appear somewhere on the website: "Readers may view, browse, and/or download material for temporary copying purposes only, provided these uses are for noncommercial personal purposes. Except as provided by law this material may not be further reproduced, distributed, transmitted, modified, adapted, performed, displayed, published, or sold in whole or part, without prior written permission from the American Physical Society."

Provide a hyperlink from the reprinted APS material (the hyperlink may be embedded in the copyright credit line). APS's link manager technology makes it convenient and easy to provide links to individual articles in APS journals. For information, see: http://link.aps.org/

You must also obtain permission from at least one of the authors for each separate work, if you haven't done so already. The author's name and address can be found on the first page of the published Article.

Use of the APS material must not imply any endorsement by the American Physical Society.

Permission is granted for use of the following APS material only
Fig. 9, Phys. Rev. B Vol. 57, 14148 (1998)

Permission is limited to the single title specified or single edition of the publication as follows:
A PhD dissertation entitled "Pitch-based activated carbon fibers: The effect of precursor composition on pore structure" to be published by Halil L Tekinalp.

If you have any questions, please refer to the Copyright FAQ at: http://publish.aps.org/copyrightFAQ.html or send an email to assocpub@aps.org

Sincerely,

Eileen LaManca

Eileen LaManca
Publications Marketing Coordinator

Figure (s): Fig. 1.11
Permission Request Submitted

Your request is now under review.
You will be notified of the decision via email.
Please print this request for your records.

Order Number	500642784
Order Date	Nov 29, 2011
Licensed content publisher	Elsevier
Licensed content publication	Elsevier Books
Licensed content title	Activated Carbon
Licensed content author	Harry Marsh,Francisco Rodríguez-Reinoso
Licensed content date	2006
Number of pages	56
Type of Use	reuse in a thesis/dissertation
Portion	figures/tables/illustrations
Number of figures/tables/illustrations	2
Format	both print and electronic
Are you the author of this Elsevier chapter?	No
Will you be translating?	No
Order reference number	Request for 2 additional figures
Title of your thesis/dissertation	Pitch-Based Activated Carbon Fibers: The Effect of Precursor Composition on Pore Structure
Expected completion date	Dec 2011
Estimated size (number of pages)	180
Elsevier VAT number	GB 494 6272 12
Permissions price	Not Available
VAT/Local Sales Tax	Not Available
Total	Not Available

Figure (s): Fig. 1.12
Order Completed

This is a License Agreement between Halil L Tekinalp ("You") and Elsevier ("Elsevier"). The license consists of your order details, the terms and conditions provided by Elsevier, and the payment terms and conditions.

License Number	2797281436488
License date	Nov 27, 2011
Licensed content publisher	Elsevier
Licensed content publication	Carbon
Licensed content title	Structural analysis of carbonaceous solids using an adapted reverse Monte Carlo algorithm
Licensed content author	Tim Petersen,Irene Yarovsky,Ian Snook,Dougal G McCulloch,George Opletal
Licensed content date	2003
Licensed content volume number	41
Licensed content issue number	12
Number of pages	9
Type of Use	reuse in a thesis/dissertation
Portion	figures/tables/illustrations
Number of figures/tables/illustrations	1
Format	both print and electronic
Are you the author of this Elsevier article?	No
Will you be translating?	No
Order reference number	
Title of your thesis/dissertation	Pitch-Based Activated Carbon Fibers: The Effect of Precursor Composition on Pore Structure
Expected completion date	Dec 2011
Estimated size (number of pages)	180
Elsevier VAT number	GB 494 6272 12
Permissions price	0.00 USD
VAT/Local Sales Tax	0.0 USD / 0.0 GBP

Figure (s): Fig. 1.14, Fig. 2.1, Fig. 2.2

Cervo, 2010a
Permission obtained from the author(i.e., Dr. Eduardo G. Cervo) in person.

Figure (s): Fig. 3.12
Order Completed

This is a License Agreement between Halil L Tekinalp ("You") and Elsevier ("Elsevier"). The license consists of your order details, the terms and conditions provided by Elsevier, and the payment terms and conditions.

License Number	2797300302221
License date	Nov 27, 2011
Licensed content publisher	Elsevier
Licensed content publication	Carbon
Licensed content title	Molecular structures for the oligomeric constituents of petroleum pitch
Licensed content author	Ward A. Burgess,Mark C. Thies
Licensed content date	February 2011
Licensed content volume number	49
Licensed content issue number	2
Number of pages	16
Type of Use	reuse in a thesis/dissertation
Portion	figures/tables/illustrations
Number of figures/tables/illustrations	4
Format	both print and electronic
Are you the author of this Elsevier article?	No
Will you be translating?	No
Order reference number	
Title of your thesis/dissertation	Pitch-Based Activated Carbon Fibers: The Effect of Precursor Composition on Pore Structure
Expected completion date	Dec 2011
Estimated size (number of pages)	180
Elsevier VAT number	GB 494 6272 12
Permissions price	0.00 USD
VAT/Local Sales Tax	0.0 USD / 0.0 GBP

REFERENCES

Acharya, M.; Strano, M. S.; Mathews, J. P.; Billinges, S. J. L.; Petkov, V.; Subramoney, S.; Foley, H. C. Simulation of Nanoporous Carbons: A Chemically Constrained Structure. *Philosaphical Magazine B* **1999**, 79(10), 1499.

Alcaniz-Monge, J.;Cazorla-Amoros, D.; Linares-Solano, A. Effect of the Activating Gas on Tensile Sstrength and Pore Structure of Pitch-Based Carbon Fibres. *Carbon* **1994**, 32(7), 1277.

Alcaniz-Monge, J.; Cazorla-Amoros, D.; Linares-Solano, A.; Oya, A.; Sakamoto, A.; Hosm, K. Preparation of General Purpose Carbon Fibers from Coal Tar Pitches with Low Softening Point. *Carbon* **1997**, 35, 1079.

Basova, Y. V.; Edie, D. D.; Lee, Y. S.; Reid, L. K.; Ryu, S. K. Effect of Precursor Composition on the Activation of Pitchbased Carbon Fibers. Carbon **2004**, 42, 485.

Beauharnois, M. E.; Edie, D. D.; Thies, M. C. Carbon fibers from mixtures of AR and supercritically extracted mesophases. *Carbon* **2001**, 39(14), 2101.

Brooks, J. D.; Taylor, G. H. The Formation of Graphitizing Carbons from the Liquid Phase. *Carbon* **1965**, 3, 185.

Burgess, W. A.; Pittman, J. J.; Marcus, R. K.; Thies, M. C. Structural Identification of the Monomeric Constituents of Petroleum Pitch. *Energy Fuels* **2010**, 24, 4301.

Burgess, W. A.; Thies, M. C. Molecular Structures for the Oligomeric Constituents of Petroleum Pitch, *Carbon* **2011**, 49, 636.

Cabria, I.; Lopez, M. J.; Alonso, J. A. The Optimum Average nanopore Size for Hydrogen Storage in Carbon Nanoporous Materials. *Carbon* **2007**, 45, 2649.

Cervo, E. G.; Thies, M. C. Control of the Molecular Weight Distribution of Petroleum Pitches via Dense-Gas Extraction. *Chem Eng Technol* **2007**, 30(6), 742.

Cervo, E. G.; Thies, M. C.; Fathollahi, B. Controlling the Oligomeric Composition of Carbon-Fiber Precursors by Dense-Gas Extraction. *J Am Ceram Soc* **2008**, 91(5), 1416.

Cervo, E. G. Isolating Petroleum Pitch Oligomers via Multistage Supercritical Extraction. Ph.D. Dissertation, Clemson University, Clemson, SC, **2010a**.

Cervo, E. G.; Thies, M. C. Control of Molecular Weight Distribution of Petroleum Pitches via Multistage Supercritical Extraction. *Journal of Supercritical Fluids* **2010b**, 51(3), 345.

Chung, D. D. L. *Carbon Fiber Composites*. Butterwood-Heinemann, Elsevier: MA, USA, 1994.

Cristadoro, A.; Rader, H. J.; Mullen, K. Clustering of Polycyclic Aromatic Hydrocarbons in Matrix-Assisted Laser Desorption/Ionization and Laser Desorption Mass Spectrometry. *Rapid Commun Mass Spectrom* **2007**, 21, 2621.

Daguerre, E.; Guillot, A.; Py, X. Microporosity of Activated Carbons Produced from Heat-Treated and Fractionated Pitches. *Carbon* **2000**, 38, 59.

Derbyshire, F.; Andrews, R.; Jacques, D.; Jagtoyen, M.; Kimber, G.; Rantell, T. Synthesis of Isotropic Carbon Fibers and Activated Carbin Fibers from Pitch Precursors. *Fuel* **2001**, 80, 345.

Diefendorf, R. J.; Riggs, D. N. Forming Optically Anisotropic Pitches. U.S. Patent 4,208,267, June 17, 1980.

Doying, E. G. Activaton of Textile Forms of Carbon. U.S. Patent 3,256,206, June 14, 1966.

Drbohlav, J.; Stevenson, W. T. K. The Oxidative Stabilization and Carbonization of a Synthetic Mesophase Pitch, Part I: The Oxidative Stabilization Process. *Carbon* **1995**, 33(5), 693.

Drbohlav, J.; Stevenson, W. T. K. The Oxidative Stabilization and Carbonization of a Synthetic Mesophase Pitch, Part II: The Carbonization Process. *Carbon* **1995**, 33(5), 713.

Edie, D. D. The Effect of Processing on the Structure and Properties of Carbon Fibers. *Carbon* **1998**, 36(4), 345.

Edwards, W. F.; Jin, L. W.; Thies, M. C. MALDI-TOF Mass Spectrometry: Obtaining Reliable Mass Spectra for Insoluble Carbonaceous Pitches. *Carbon* **2003**, 41(14), 2761.

Edwards, W. F. Jr. Fractionation of Carbonaceous Pitches by Molecular Weight Using Dense-Gas Extraction. Ph.D. Dissertation, Clemson University, Clemson, 2005.

Ehrburger, P.; Pusset, N.; Dziedzinl, P. Active Surface Area of Microporous Carbons. *Carbon* **1992**, 30(7), 1105.

Fathollahi, B.; White, J. L. Polarized-Light Observations of Flow-Induced Microstructures in Mesaophase Pitch. *Journal of Rheology* **1994**, 38, 1591.

Franklin, R. E. Crystallite Growth in Graphitizing and Non-Graphitizing Carbons.,*Proc. Roy. Soc.* **1951**, 209A**,** 196.

Gonzales J. C.; Sepulveda-Escribano, A.; Molina-Sabio, M.; Rodrigues-Reinoso, F. Characterization of Porous Solids. The Royal Society of Chemistry: Cambridge, Great Britain, 1997; 4, 9.

Huidobro, A.; Pastor, A. C.; Rodrigues-Reinoso, F. Preparation of Activated Carbon Cloth from Viscous Rayon: Part IV. Chemical Activation. *Carbon* **2001**, 39, 389.

Kaneko, K.; Ishii, C.; Ruike, M.; Kuwabara, H. Origin of Superhigh Surface Area and Microcrystalline Graphitic Structures of Activated Carbons. *Carbon* **1992**, 30(7), 1075.

Kim, Y. J.; Horie, Y.; Matsuzawa, Y.; Ozaki, S.; Endo, M.; Dresselhaus, M. S. Structural Features Necessary to Obtain a High Specific Capacitance in Electric Double Layer Capacitors. *Carbon* **2004**, 42, 2423.

Koresh, J.; Soffer, A. Study of Molecular Sieve Carbons. Part 1. – Pore Structure, Gradual Pore Opening and Mechanism of Molecular Sieving. *J. Chem. Soc., Faraday Trans. 1* **1980**, 76, 2457.

Kulkarni, S. U.; Thies, M. C. Quantitative Analysis and Structural Characterization of Petroleum Pitches. *Abstracts of Papers, 237th ACS National Meeting, Salt Lake City, UT, United States, March 22-26* **2009.**

Kulkarni, S. U.; Raeder, H. J.;Thies, M. C. The Effects of Molecular Weight Distribution and Sample Preparation on MALDI Mass Spectrometry Analysis of Petroleum Macromolecules. *Rapid Commun Mass Spectrom* **2011**, Article in Press.

Lavin, J.G. Chemical Reactions in the Stabilization of Mesophase Pitch-Based Carbon Fiber. *Carbon* **1992**, 30(3), 351.

Lee, S.; Kim, M. S.; Naskar, A. K.; Ogale, A. A. Effect of Carbon Nanofibers on the Anisotropy of an Aromatic Thermotropic Liquid Crystalline Polymer. *Polymer* **2005**, 46, 2663.

Lewis, I.C. Chemistry of Carbonization. *Carbon* **1982**, 20(6), 519.

Lin, S.S. Oxidative Stabilization in Production of Pitch Based Carbon Fibers. *SAMPE Journal* **1991**, 27, 9.

Lopez, M. C. B.; Martinez-Alonso, A.; Tascon, J. M. D. N_2 and CO_2 Adsorption on Activated Carbon Fibres Prepared from Nomex Chars. *Carbon* **2000**, 38, 1177.

Lozano-Castello, D.; Raymundo-Pinero, E.; Cazorla-Amoros, D.; Linares-Solano, A.; Muller, M.; Riekel, C. Characterization of Pore Distribution in Activated Carbin Fibers by Microbeam Small Angle X-ray Scattering. *Carbon* **2002**, 40, 2727.

Lozano-Castello, D.; Macia-Agullo, J. A.; Cazorla-Amoros, D.; Linares-Solano, A.; Muller, M.; Burghammer, M.; Riekel, C. Isotropic and Anisotropic Microscopy Development Upon Chemical Activation of Carbon Fibers, Revealed by Microbeam Small-Angle X-ray Scattering. *Carbon* **2006**, 44, 1121.

Macia-Agullo, J. A.; Moore, B. C.; Cazorla-Amoros, D. Activation of Coal Tar Pitch Carbon Fibres: Physical Activation vs. Chemical Activation. *Carbon* **2004**, 42, 1367.

Marsh, H.; Crawford, D. Carbons of High Surface Area. A Study by Adsorption and High Resolution Electron Microscopy. *Carbon* **1982**, 20(5), 419.

Marsh, H.; Rodriguez-Reinoso F. *Activated Carbon*. Elsevier: London, Great Britain, 2006.

McHenry, E. R. Process for Producing Carbon Fibers from Mesophase Pitch. U.S Patent 3,974,264, Aug 10, 1976.

Menendez-Diaz, J. A..; Martin-Gullon, I. *Activated Carbon Surfaces in Environmental Remediation*. Elsevier: Amsterdam, Netherlands, 2006; Chapter 1. Types of Carbon Adsorbents and Their Production.

Miura, K.; Nakagawa, H.; Hashimoto, K. Examination of the Oxidative Stabilization Reaction of the Pitch-Based carbon Fiber Through Continuous Measurement of Oxygen Chemisorption and gas Formation Rate. *Carbon* **1995**, 33(3), 275.

Molin-Sabio, M.; Gonzales, M. T.; Rodrigues-Reinoso, F.; Sepulveda-Escribano, a. Effect of Steam and Carbon Dioxide Activation in the Micropore Size Distribution of Activated Carbon. **Carbon** *1996*, 34(4), 505.

O'Malley, B. O.; Snook, I.; McCulloch, D. Reverse Monte Carlo Analysis of the Structure of Glassy Carbon Using Electraon-Microscopy Data. *Physical Review B* **1998**, 57, 14148.

Park, S. H.; Kim, C.; Choi, Y. O.; Yang, K. S. Preparations of Pitch-Based CF/ACF Webs by Electrospinning. *Carbon* **2003**, 41, 2655.

Park, S. J.; Jang, Y. S.; Shim, J. W.; Ryu, S. K. Studies on Pore Structures and Surface Functional Groups of Pitch-Based Activated Carbon Fibers. *Journal of Colloid and Interface Science* **2003**, 260, 259.

Peters, E. M. Heat-Resistant Black Fibers and Fabrics Derived from Rayon. U.S. Patent 3,235,323, Feb 15, 1966.

Petersen, T.; Yarovsky, I.; Snook, I.; McCulloch, D. G.; Opletal, G. Structural Analysis of Carbonaceous Solids Using an Adaped Reverse Monte Carlo Algorithm. *Carbon* **2003**, 41, 2403.

Pierson, H. O. *Handbook of Carbon, Graphite, Diamond and Fullerenes - Properties, Processing and Applications*. William Andrew Publishing/Noyes: NJ, USA, 1993.

Pikunic, J.; Pellenq, R. J. M.; Thomson, K. T.; Rouzaud, J. N.; Levitz, P.; Gubbins, K. E. Improved Molecular Models for Porous Carbons. *Stud Surf Sci Catal* **2001**, 132, 647.

Rand, B.; Appleyard, S. P.; Yardim, M. F. *Design and Control of Structure of Advanced Carbon Materials for Enhanced Performance*. Kluwer Academic Publishers: Antalya, Turkey, 1998.

Rodgers, S.J.; Udavcak R.J.; Mausteller, J.W. Fission Product Release Transport Accident Conditions. *International Symp., Tennessee* **1965.**

Rodriguez-Reinoso, F.; Linares-Solano, A. *Chemistry and Physics of Carbon*. Marcel Dekker, Inc.: NY, USA, 1989; 21, 1.

Rodriguez-Reinoso F.; Garrido, J.; Martin-Martinez, J. M.; Molina-Sabio, M.; Torregrosa, R. The Combined Use of Different Approaches in the Characaterization of Microporous Carbons. *Carbon* **1989**, 27(1), 23.

Rouzaud, J. N.; Clinard, C. Quantitative high-resolution transmission electron microscopy: a promising tool for carbon materials characterization. *Fuel Processing Technology* **2002**, 77-78, 229

Sing, k. S. W.; Everett, D. H.; Haul, R. A. W.; Moscou, L.; Pierotti, R A.; Rouquerol, J.; Siemieniewska, T. Reporting IUPAC: Physisorption Data for Gas/Solid Systems with Special Reference to the Determination of Surface Area and Porosity. *Pure and Appl Chem* **1985**, 57(4), 603.

Stevens, W. C.; Diefendorf, R. J. Proceedings of Int. Conference on Carbon, Baden, Germany,37, 1986.

Suzuki, M. Activated Carbon Fiber: Fundamentals and Applications. *Carbon* **1994**, 32(4), 577.

Thwaites, M.W.; Stewart, M.L.; McNeese, B.E.; Sumner, M.B. Synthesis and Characterization of Activated Pitch-Based Carbon Fibers. *Fuel Processing Technology* **1994**, 34(2), 137.

Uraki, Y.; Nakatani, A.; Kubo, S. Preparation of Activated Carbon Fibers with Large Specific Surface Area from Softwood Acetic Acid Lignin. *J Wood Science* **2001**, 47, 465.

Vilaplana Ortego, E.; Alcaniz-Monge, J.; Cazorla-Amoros, D.; Linares-Solano, A. Stabilisation of Low Softening Point Petroleum Pitch Fibres by HNO_3. *Carbon* **2003**, 41, 1001.

Vilaplana Ortego, E.; Alcaniz-Monge, J.; Cazorla-Amoros, D.; Linares-Solano, A. Stabilisation of Low Softening Point Petroleum Pitch Fibres by Iodine Treatment. *Fuel Processing Technology* **2007**, 88, 265.

Vilaplana-Ortego, E.; Macia-Agullo, J. A.; Alcaniz-Monge, J.; Cazorla-Amoros, D.; Linares-Solano, A. Comparative Study of the Micropore Development on Physical Activation of Carbon Fibers from Coal Tar and Petroleum pitches. *Microporous and Mesoporous Materials* **2008**, 112, 125.

Walker, P. L. Production of Activated Carbons: use of CO_2 versus H_2O as Activating Agent. *Carbon* **1996**, 34(10), 1297.

Wheeler, A. *In Advances in Catalysis*. Academic Press; NY, USA, 1951; 3, 249.

Worasuwannarak, N.; Hatori, S.; Nakagawa, H.; Miura, K. Effect of Oxidation Pre-Treatment at 220 to 270 °C on the Carbonization and Activation Behavior of Phenolic Resin Fiber. *Carbon* **2003**, 41, 933.

Wu. X. X.; Gallego, N. C.; Contescu, C. I.; Tekinalp, H. L.; Bhat, V. V.; Baker, S.B.; Thies, M.C.; Edie D. D. The Effect of Processing Conditions on Microstructure of Pd-Containing Activated Carbon Fibers. *Carbon* **2008**, 46(1), 54.

Yang, C. Q.; Simms, J. R. Infrared Spectroscopy Studies of the Petroleum Pitch Carbon Fiber –I. The Raw Materials, the Stabilization, and Carbonization Processes. *Carbon* **1993**, 31(3), 451.

Yasuda, E.; Ingaki, M.; Kaneko, K.; Endo, M.; Oya, A.; Tanabe, Y. *Carbon Alloys: Novel Concepts to Develop Carbon Science and Technology*. Elsevier: Amsterdam, Netherlands, 2003.

Yehaskel A. *Activated Carbon: Manufacture and Regeneration*. Noyes Data Corp: NJ, USA, 1978.

Yoshida, A.; Kaburagi, Y.; Hishiyama, Y. Microtexture and Magnetoresistance of Glass-Like Carbons. *Carbon* **1991**, 29(8), 1107.